Twisted Single Photons and Their Applications in Quantum Information Processing

A thesis submitted in partial fulfilment of

the requirements for the degree of

Doctor of Philosophy

by

Nijil Lal C. K.

(Roll No. 14330006)

Under the supervision of

Prof. R. P. Singh

Professor

Atomic, Molecular and Optical Physics Division

Physical Research Laboratory, Ahmedabad, India

DISCIPLINE OF PHYSICS

INDIAN INSTITUTE OF TECHNOLOGY GANDHINAGAR

2019

To

My Family

Declaration

I declare that this written submission represents my ideas in my own words and where others' ideas or words have been included, I have adequately cited and referenced the original sources. I also declare that I have adhered to all principles of academic honesty and integrity and have not misrepresented or fabricated or falsified any idea/data/fact/source in my submission. I understand that any violation of the above will be cause for disciplinary action by the Institute and can also evoke penal action from the sources which have thus not been properly cited or from whom proper permission has not been taken when needed.

Signature

Name: Nijil Lal C. K.

(Roll No: 14330006)

Date:

CERTIFICATE

It is certified that the work contained in the thesis titled **"Twisted Single Photons and Their Applications in Quantum Information Processing"** by Mr. Nijil Lal C. K. (Roll No. 14330006), has been carried out under my supervision and that this work has not been submitted elsewhere for a degree.

Prof. R. P. Singh
Professor
Atomic, Molecular and Optical Physics Division,
Physical Research Laboratory,
Ahmedabad, India.

(Thesis Supervisor)

Date:

Thesis Approval

The thesis entitled

Twisted Single Photons and Their Applications in Quantum Information Processing

by

Nijil Lal C. K.

(Roll No. 14330006)

is approved for the degree of

Doctor of Philosophy

_____	_____
Examiner	Examiner
_____	_____
Supervisor	Chairman

Date: _____

Place: _____

Acknowledgments

Thanking is the most difficult task for we know that it will never be enough in most of the cases. My time in PRL is grateful to a number of people and the completion of my research would not have been possible without the contribution of each of them. I take this opportunity to extend my sincere gratitude to each of them.

First and foremost, I would like to acknowledge my sincere gratitude to my supervisor, Prof. R. P. Singh. I am afraid that words won't suffice to register my immense gratitude to him for being a constant source of support and encouragement throughout the past five years of my research work. He has inspired my curiosity towards newer fields of research and has shown that we should not be hesitant to try something new at any point of life. What I admire about him the most is that he believes in the student as well as respects their identity. He was always been there open to discussions and guidance, be it academic or personal. On occasions when I was stuck in experiments or felt guilty of not being able to raise up to the expectations, it was his calmness and encouragement that kept me moving. I believe that the holistic learning experience with him will be following me throughout my life.

I would like to thank my doctoral committee members Dr. Goutham Kumar Samanta and Prof. Angom Dilip Kumar Singh for their valuable guidance and constructive discussions. Their insightful guidance and encouragement during the past four years have really helped me growing academically. I am grateful for all the difficult questions they have asked during the seminars. Both of them have taught me during the course work and I enjoyed their classes as well as teaching. I am also grateful to Dr. Samanta for giving me opportunities in being a part of the extra-curricular science outreach activities that he organized in and around PRL. I really enjoyed accompanying him as a teaching assistant during the PTTS training program organized in 2016 in Mysore.

I express my sincere gratitude to all the faculty members who had taught me during the course work including Prof. R. Rengarajan, Prof. J. Banerji, Prof. D. K. Angom, Dr. N. Mahajan, Dr. B. K. Sahoo, Prof. R. Sekar, Dr. D. Chakrabarty, Dr. L. K. Sahu, Prof. P. Venkatakrishnan, Prof. N. Srivastava, Prof. S. K. Mathew, Dr. R. Bhattacharyya, Dr. B. Sivaraman and Dr. M. K. Srivastava. I would also like to thank Dr. S. Vadawale from astronomy division with whom I had done my project during the first semster of my coursework. I would like to express my gratitude to my past teachers Sanal Kumar, Hareendran Manikkoth,

and Veerankutty for inspiring me to carry along my interests in literature and humanities all the way. I would like to thank my teacher Pradeep Kumar who guided me towards choosing studies in basic science and motivating me to follow it. I am indebted to my phyics teachers in Government college, madappally, Prof. K. Suresh Babu, Dr. G. Harikrishnan and Dr. Ramakrishnan P. for guiding me through right channels to pursue studies in physics and for always being there extending a helping hand. Their lectures during my B.Sc. had amazed me and it was then I decided that I want to pursue studying physics. I am indebted to Suresh sir and Hari sir for teaching me to enjoy quantum mechanics and Ramakrishnan sir for making me realize how important is insight and intuition in learning optics. It gets difficult to name everyone, but I am deeply indebted to all those great teachers who have taught and inspired during different stages of life.

I thank the director of PRL, dean, academic committee chairperson, academic committee members, and registrar for their help and support. I am thankful to all the administrative and other staff in PRL for making my stay in PRL comfortable. I am thankful to all the staff members of our division, library, computer center, administration, dispensary, canteen, workshop and maintenance section of PRL for their assistance and support. Special thanks to Munna bhai for constantly keeping my room clean despite my efforts otherwise. I also take this moment to express my gratitude to the academic and administrative staff members of IIT Gandhinagar for helping with the registration procedures. Special thanks to Praggya for the nice words she always carry with and her help on queries related to administrative stuff. Special thanks to her sweet son Ronak for being our friend and our chats.

I would like to thank my group members Anindya, Ayan, Varun, Satyajeet, Sarika, Anju, Subith, Anirban, Ravi, Srinivas, Sandeep, Vardaan, Tanya and Satyaranjan for all the discussions. I thank my collaborators Biveen, Srinivas, and Prof. Balaji for the discussions and the times we worked together. I thank visitors in our group Pranav, Raghu, Aaditya and Nikhil. Special thanks to my seniors Chithrabhanu, Ali, Gangi, Jabir, Shashi, Ashok, Pravin, Vijay and Avesh for their guidance at various times during the course of my research and constructive discussions.

I would like to thank Chithra, Swapna, Jimbalu, Lekshmy, Bivin, Amala, Bhavya, Apurv, Anju, Jabir, Ali, Manu, Aravind, Subith, and Deva for making me feel at home and for all the delicious Kerala food. I am indebted to Chithra for his continuous support as a brother, friend and colleague. Special thanks to Vishnu for always being there and choosing to not

fight with me despite all the motivation. I guess - as we once phrased it - we were always at this perfect place for each other - not too close, not too far. Many thanks to Niharika for being Niharika and Pradeep for the fun time as a buddy. Thanks to my friends-cum-batch mates, Aman, Kiran, Soumik, Anil, Bharti and Bhavesh. I am also grateful to all the fellow researchers from PRL for being cool and friendly. Especially, I would like to mention Ashish, Akanksha, Archita, Aarthy, Kaustav, Subir, Navpreet, Rupa, Shraddha, Ikshu, Anirban, Shrema, Surya, Abhishek, Rukmani, Venkatesh, Shefali, Kuldeep, Priyank, Vishal, Sudipta, Pravin and Hrushikesh. Kindly forgive if I have left out anyone's name and please know that I am thankful to all of you.

The company of Sudhanshu, Aman and Garima brought in a metamorphosis and I cannot imagine the two years I had spent in Bombay without them. Thank you Sudhanshu for being there with me singing 'hakuna-matata' in each of your actions. I learnt not to care too much from you. Thanks Aman for all the funny moments Also thank you for carrying the burden of being the cute guy. Thank you Garima for all the laughs and spreading a bit of yourself everywhere. Thanks Adarsh for keeping the 'mallu' inside me alive in Bombay. I always miss our long walks in the middle of the night, never ending conversations, destination-less expeditions and all the crazy stuff we did together in Mumbai.

I thank my parents for their support throughout my life and especially during the course of my research. I am thankful for my sister and her husband, Laluettan for supporting me always. I am thankful for my cousins, Shyamini, Sajuettan and Nishettan for always being there for me. The smile and phone calls from my nephew Nandu, has always lightened my day. Thanks and kisses to him. Acknowledging Ila would be the most difficult task. She has been there through my tough times as a partner, my best friend and my love. It was her support and love that kept me going. Finally, I thank all my family members and friends for the love and support they have always given to me.

Nijil Lal

Abstract

Information theory based on quantum systems has shown to be amazingly advantageous over that based on classical systems in devising efficient and secure communication protocols. This is a manifestation of two unique properties of quantum systems such as the existence of an indivisible quanta of energy and entanglement. The advances in quantum information processing have led to the quest for suitable candidates to carry quantum bits of information. Single photons are proven to be a suitable qubit candidate as they are fast and do not interact with each other. However, generating stable sources of ideal single photons in an efficient and cost-effective manner is a challenging task. A unique non-linear phenomena called spontaneous parametric down-conversion (SPDC) has been widely explored as an alternate source of single photons over the past few decades. SPDC is a second order, non-linear optical effect where the dipole polarization depends on the electric field in a quadratic manner and photons incident on the non-linear crystal gets converted into two photons with lower frequencies. Heralding the detection of one of the photons by the detection of the other gives rise to single photon behaviour. Such heralded single photons generated in spontaneous parametric down-conversion provide cost-efficient, stable sources of single photons which can be manipulated easily using linear optics for applications in quantum information processing. Orbital angular momentum (OAM) of light is widely being studied to be used in communication as unlike other degrees of freedom of light, OAM provides an infinite dimensional basis. Orbital angular momentum of single photons is also being explored extensively aiming towards increased information transfer as well as robust entanglement protocols. The twin photons generated in paraxial SPDC are correlated in orbital angular momentum following OAM conservation. Thus OAM entanglement can be easily realized in SPDC. The projective measurements corresponding to OAM

are generally carried out through phase-flattening technique using a spatial light modulator (SLM). However, the measurements based on phase-flattening have shortcomings in terms of efficiency and dependence on pump beam characteristics. Alternate interferometric methods for projective measurement and sorting of OAM modes form an active area of research. In this thesis, we study and characterize twisted single photon sources generated from parametric down-conversion based on their statistical correlations. We build the probability distribution of numbers using photon detectors and an oscilloscope which is a ubiquitous instrument present in any undergraduate laboratory. We verify the Poissonian and super-Poissonian statistics of different sources. For the heralded single photon sources generated in parametric down-conversion, we verify the sub-Poissonian behaviour. Further, we study the second order correlation of these single photons in a heralded Hanbury Brown-Twiss experiment. We observe near-zero values for second order correlation coefficient at zero delay, $g^{(2)}(0)$. The correlation parameter is calculated using direct measurement of three-fold coincidences as well by only accounting for the probability of accidental triple coincidences. We show that the latter method gives the same value for the correlation parameter with reduced uncertainty. We investigate the variation of the statistical correlation with the OAM order of the twisted single photons. We observe that the non-classical behaviour of the heralded twisted single photons reduces for higher orders of OAM. We study the OAM distribution of the twin photons generated in the down-conversion process as well. The study reveals that using perfect optical vortices as pump we can obtain narrower OAM spectrum. We also study the effect of pump mode on OAM entanglement. Finally, we demonstrate that the OAM sorting process of indistinguishable photons generated from collinear parametric down-conversion can be utilized to reveal the polarization entanglement. We use even-odd basis of OAM to label and distinguish the photons from a pair. This increases the efficiency of available entangled photon pairs as we

do not eliminate any pairs while selecting the photons in the two-dimensional Hilbert space of even and odd OAMs.

Keywords: Single Photon, Twisted Photons, Photon Statistics, Orbital Angular Momentum, Spontaneous Parametric Down-Conversion, Entanglement.

Abbreviations

SPS	Single Photon Source
HSPS	Heralded Single Photon Source
SPDC	Spontaneous Parametric Down-Conversion
OAM	Orbital Angular Momentum
SLM	Spatial Light Modulator
SPP	Spiral Phase Plate
HBT	Hanbury Brown - Twiss
PWE	Paraxial Wave Equation
LG	Laguerre-Gaussian
HG	Hermite-Gaussian
BG	Bessel-Gaussian
POV	Perfect Optical Vortex
DP	Dove Prism
HWP	Half Wave Plate
QWP	Quarter Wave Plate
SPCM	Single Photon Counting Module
FC	Fiber Coupler
BS	Beam Splitter
PBS	Polarizing Beam Splitter

Contents

List of Figures

List of Tables

Chapter 1

Introduction

What is *Light*? More than a phenomenon that makes basic vision possible, human curiosity has always wanted to understand the underlying physics of this natural entity that lets us see anything and everything including rainbows, mirages and even distant stellar objects. Euclid was the first to summarize the optical phenomena observed naturally based on geometry. With the postulation of rectilinear propagation of light, this could mathematically explain the 'how' of basic optical phenomena, but the 'what' of light was still largely unknown. Corpuscular theory considered light as a stream of discrete particles which follow rectilinear propagation and carries energy. Thomas Young established the wave behaviour of light through the seminal work that explained the interference patterns formed when light is passed through a double slit. Following this, James C. Maxwell paved way towards the foundation of classical electrodynamics with the fundamental equations that predicted the existence of electromagnetic waves.

With Planck's treatment of light-matter interaction as oscillating harmonic oscillators to successfully explain the spectral distribution of a black body, Einstein drew

analogy to the statistical behaviour of a perfect gas of free particles. The suggestion that light might be a discrete quantity in nature carrying an energy, $h\nu$, started gathering attention once again. With experimental verification of the photo-electric effect and Compton scattering, the indivisible quanta of light energy, photons, were successfully introduced.

1.1 Quantized Radiation Field

Planck [1] had introduced the quantization of light energy to explain black body radiation spectra. Around the same time, decades after the corpuscular theory, Einstein [2] reintroduced the concept of particular form of light considering it as a stream of packets of energy in order to explain the photoelectric effect and thereby leading to the concept of photons. However, it was later shown that a semi-classical theory, which assumes light to be a wave and atoms with discrete energy levels, is sufficient to explain the photo-electric effect and most of the phenomena involving atom-field interactions. However, there were some effects still unexplained from a wave-like treatment of the electromagnetic field such as spontaneous emission, the Casimir effect, the Lamb shift etc. P.A.M. Dirac, through his seminal work [3], combined both the wave-like and particle-like aspects of light to present the picture of a quantized radiation field, which can explain both interference phenomena and atomic excitation that absorbs one photon energy from the radiation field. Modes of the radiation field, which are considered as those of a quantum harmonic oscillator, and the fluctuations associated with the zero point energy, called vacuum fluctuations, could explain quantum phenomena like spontaneous emission [4, 5].

The classical description of the electromagnetic field follows Maxwell's description that relates the electric and magnetic field vectors, **E** and **H** respectively, through

the set of Maxwell's relations,

$$\nabla \times \mathbf{H} = \frac{\partial \mathbf{D}}{\partial t} \tag{1.1a}$$

$$\nabla \times \mathbf{E} = -\frac{\partial \mathbf{B}}{\partial t} \tag{1.1b}$$

$$\nabla \cdot \mathbf{B} = 0 \tag{1.1c}$$

$$\nabla \cdot \mathbf{D} = 0. \tag{1.1d}$$

Here, **D** and **B** are the displacement field and magnetic field for the medium of propagation, given as,

$$\mathbf{B} = \mu_0 \mathbf{H} \tag{1.2a}$$

$$\mathbf{D} = \varepsilon_0 \mathbf{E} \tag{1.2b}$$

where ε_0 and μ_0 are the free space permittivity and permeability respectively. It follows

Figure 1.1: Single mode radiation field, considered as equivalent to a quantum harmonic oscillator, within a one-dimensional cavity oriented along z-axis.

that $\mathbf{E}(\mathbf{r},\mathbf{t})$ satisfies the wave equation as,

$$\nabla^2 \mathbf{E} - \frac{1}{c^2}\frac{\partial^2 \mathbf{E}}{\partial t^2} = 0. \tag{1.3}$$

For the radiation field, $\mathbf{E}(\mathbf{r},t) = \mathbf{e}_x E_x(z,t)$, linearly polarized along x-axis, which is

confined in a one dimensional cavity of length L and oriented along z-axis,

$$E_x(z,t) = \sum_j \left(\frac{2\omega_j^2}{V\varepsilon_0}\right)^{1/2} q_j(t)\sin(k_j z) \tag{1.4}$$

where $k_j = j\pi/L = \omega_j/c$ ($j = 1,2,3,...$), q_j is the canonical position (a time-dependent quantity having the dimensions of length), and V is the net volume of the cavity. In a similar manner, one can also express the magnetic field in the cavity, $\mathbf{H}(\mathbf{r},t) = \mathbf{e}_y H_y(z,t)$, as,

$$H_y(z,t) = (\mu_0\varepsilon_0)\sum_j \left(\frac{2\omega_j^2}{V\varepsilon_0 k_j}\right)^{1/2} \dot{q}_j(t)\cos(k_j z). \tag{1.5}$$

Here, $\dot{q}_j = p_j$ is the canonical momentum (for a unit mass). The operator equivalents, $\hat{q}$ and $\hat{p}$ corresponding to q and p respectively, must satisfy the commutation relations,

$$\left[\hat{q}_j, \hat{p}_{j'}\right] = i\hbar\delta_{jj'} \tag{1.6a}$$

$$\left[\hat{q}_j, \hat{q}_{j'}\right] = \left[\hat{p}_j, \hat{p}_{j'}\right] = 0. \tag{1.6b}$$

A canonical transformation of $\hat{q}$ and $\hat{p}$ yields the annihilation ($\hat{a}$) and creation ($\hat{a}^\dagger$) operators,

$$\hat{a} = (2\hbar\omega)^{-1/2}(\omega\hat{q} + i\hat{p}) \tag{1.7a}$$

$$\hat{a}^\dagger = (2\hbar\omega)^{-1/2}(\omega\hat{q} - i\hat{p}). \tag{1.7b}$$

Following the classical representation of the electromagnetic field and correspondence rule, the quantized electric and magnetic fields can be written in terms of the non-

Hermitian operators $\hat{a}$ and $\hat{a}^\dagger$ as,

$$\mathbf{E}(\mathbf{r},t) = \sum_{\mathbf{k}} \hat{\varepsilon}_{\mathbf{k}} \mathcal{A}_{\mathbf{k}} \hat{a}_{\mathbf{k}} e^{-i\omega_k t + i\mathbf{k}\cdot\mathbf{r}} + \text{H.c.} \qquad = \hat{\mathbf{E}}^{(+)}(\mathbf{r},t) + \hat{\mathbf{E}}^{(-)}(\mathbf{r},t) \quad (1.8a)$$

$$\mathbf{H}(\mathbf{r},t) = \frac{1}{\mu_0} \sum_{\mathbf{k}} \frac{\mathbf{k} \times \hat{\varepsilon}_{\mathbf{k}}}{\omega_k} \mathcal{A}_{\mathbf{k}} \hat{a}_{\mathbf{k}} e^{-i\omega_k t + i\mathbf{k}\cdot\mathbf{r}} + \text{ H.c.} \quad = \hat{\mathbf{H}}^{(+)}(\mathbf{r},t) + \hat{\mathbf{H}}^{(-)}(\mathbf{r},t) \quad (1.8b)$$

where the summation is over the discrete values of the wave vector, $\mathbf{k}$. Here, $\mathcal{A} = (\hbar\omega/\varepsilon_0 V)^{1/2}$ and H.c. stands for Hermitian conjugate.

1.2 Single Photon Sources

With the developments in quantum information processing, the quest for optimized candidates to be used as systems for the quantum advantages in storing, transmitting and processing information has motivated and boosted studies in various fields of research. A variety of systems can be used for quantum information processing such as solid state devices [6, 7], atoms [8, 9], nuclear spin systems, superconducting circuits [10], and amalgamation of such systems [11–13].

Photons, as otherwise called ‘flying qubits’, have certain advantages over other systems in quantum information processing [14–17]. Photons travel “fast” and they almost lack any interaction with the external environment of propagation (which thereby increases the decoherence time). Along with this, the inherent existence of an indivisible quantum of energy and the consequent impossibility of photon number splitting attacks on the associated information makes single photon sources (SPSs) one of the prominent choices in quantum information processing and quantum communication. Information can be encoded in different degrees of freedom of light such as path (choice of output ports), polarization (horizontal/vertical), orbital angular momentum (orthonormal OAM states), number (presence or absence of a number of photons),

time (early or late arrival) etc.

An ideal single photon source should consist of a single emitter that delivers one photon at a time on-demand. Examples of ideal SPSs can be realized as crystal color centers [18, 19], quantum dots [20, 21], trapped ions [22, 23], atoms [24, 25] and single molecules [26].

Being non-classical states of light, single photon sources exhibit properties such as sub-Poissonian statistics and anti-bunching. These properties can be observed in the violations of different types of classical bounds defined by certain inequality relations.

1.2.1 Number Statistics of Photons

For a photon source, the number statistics describes how the photon numbers are distributed in time units (bins). The observed statistical distribution of photon numbers can be classified as Poissonian, super-Poissonian and sub-Poissonian [27, 28].

A classical laser beam of light delivers a coherent supply of photons. This coherent, monochromatic laser source can be seen as a classical wave with constant amplitude such that there is no intensity fluctuation. This ensures that the arrival of a photon at a detector within a fixed time interval, Δt, less than the coherence time is completely random. For such a source, the intensity fluctuations (σ^2) are equal to the average intensity (μ) and hence it is said to have Poissonian number statistics ($\sigma^2 = \mu$). Following the quantization of the field in terms of creation and annihilation operators, it is convenient to express the electric field in terms of number states, $|n\rangle$. Hence, the average photon number can be expressed as $\mu = \langle n \rangle = \langle n | n | n \rangle$, and the photon number variance can be expressed as, $\sigma^2 = (\Delta n)^2 = \langle n^2 \rangle - \langle n \rangle^2$. The closest quantum counter

part to a coherent classical field is the coherent state,

$$|\alpha\rangle = e^{-|\alpha|^2/2} \sum_n \frac{\alpha^n}{\sqrt{n!}} |n\rangle \tag{1.9}$$

which is the eigenstate of the annihilation operator $\hat{\boldsymbol{a}}$ and $|n\rangle$ is the number state (or Fock state) containing n photons. The probability of finding n photons in a mode is given by,

$$P(n) = \frac{\langle n \rangle^n}{n!} e^{-\langle n \rangle} \tag{1.10}$$

which follows Poissonian statistical distribution (solid red line in Figure 1.2). Other

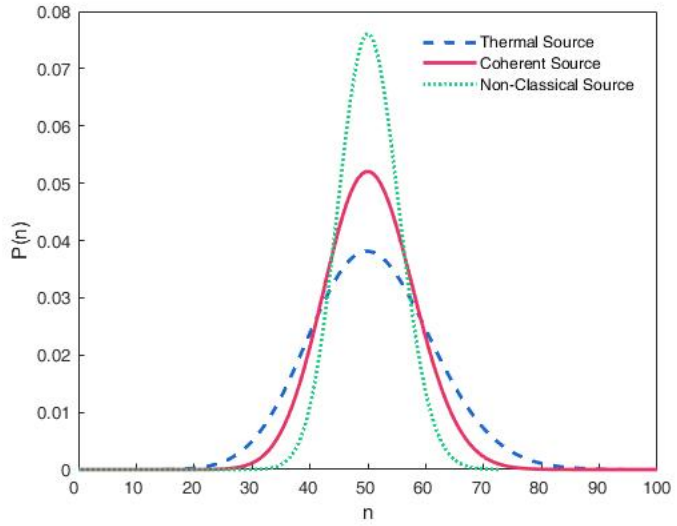

Figure 1.2: Types of photon sources based on the statistical distribution of photon number. The (red) bold line corresponds to Poissonian distribution, (blue) dashes correspond to super-Poissonian and (green) dots correspond to sub-Poissonian probability distribution.

conventional sources like house lamps and chaotic laser follow super-Poissonian statistics (blue dashed line in Figure 1.2). Photons from a classical thermal source will be an incoherent superposition of independent fields, given by the density matrix,

$$\rho = \sum_n P(n) |n\rangle \langle n| \tag{1.11}$$

where $P(n) = \frac{\langle n \rangle^n}{\langle n \rangle^{(n+1)}}$. Sub-Poissonian light (green dotted line in Figure 1.2) where $\sigma^2 < \mu$ cannot be explained through a classical or semi-classical theory. Sources having such distributions have intriguing possibilities in communication where the noise has a lower bound defined by the quantum shot-noise limit due to zero-point fluctuations when classical coherent light is used. The non-classical correlations in such systems are advantageous in achieving below shot-noise accuracy in quantum imaging and sensing [29, 30].

1.2.2 Anti-bunching and Second Order Correlation, $g^{(2)}(\tau)$

The statistics of single-photon states show a unique anti-correlation effect that has no classical analogue. A single photon incident on a beam splitter will not produce any coincidence counts between the two detectors kept in the reflected and transmitted output ports of the beam splitter. This absence of coincidence events between the two detectors or the absence of two photons being present at the same time is called photon anti-bunching.

A mode of the electromagnetic field in a cavity with volume L^3 at position $\vec{r}$ can be written as,

$$\vec{E}(\vec{r},t) = \vec{E}^{(-)}(\vec{r},t) + \vec{E}^{(+)}(\vec{r},t) \tag{1.12}$$

as given in Equation 1.8a. The first-order correlation function (corresponds to field correlation) can be given as,

$$g^{(1)}(\tau) = \frac{\left\langle E^{(-)}(t+\tau)E^{(+)}(t)\right\rangle}{\left\langle E^{(-)}(t)E^{(+)}(t)\right\rangle} \tag{1.13}$$

and the second-order correlation function (intensity correlation) as,

$$g^{(2)}(\tau) = \frac{\langle I(t+\tau)I(t)\rangle}{\langle I(t)\rangle^2} \tag{1.14}$$

whose quantum-mechanical form in terms of operators gives,

$$g^{(2)}(\tau) = \frac{\left\langle E^{(-)}(t)E^{(-)}(t+\tau)E^{(+)}(t+\tau)E^{(+)}(t)\right\rangle}{\left\langle E^{(-)}(t)E^{(+)}(t)\right\rangle\left\langle E^{(-)}(t+\tau)E^{(+)}(t+\tau)\right\rangle}. \tag{1.15}$$

The second order correlation for single photons can be observed through a Hanburry-Brown-Twiss like setup. A single photon reaching the beam splitter in Figure 1.3 has to make a choice between the reflected and transmitted paths being indivisible. Intensity correlation between the output ports of a beam splitter should show anticorrelation for a non-classical source. For zero delay between the two arms, $g^{(2)}(0) = 0$. For a

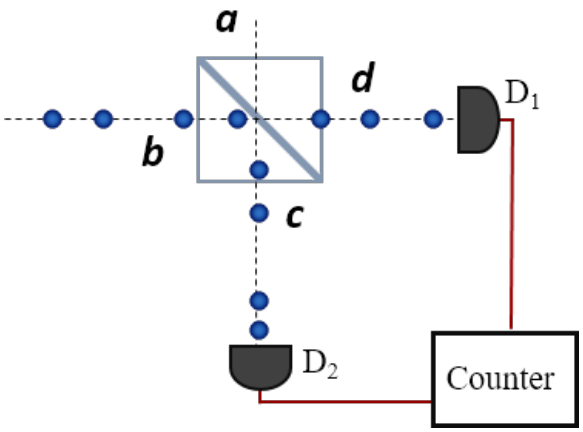

Figure 1.3: A 50:50 beam splitter serving as the HBT setup to measure the second order correlation for a single photon source. The anti-correlation between the output ports of the beam splitter reveals anti-bunching in the single photon source.

thermal source, $g^{(2)}(0) = 2$ and for a coherent source $g^{(2)}(\tau) = 1$ for all τ within the coherence limit.

1.2.3 Heralded Single Photon Sources

Single photon sources were first realized in a system of Hg atoms [31]. Out of the pairs of photons that were generated from atoms undergoing a cascaded de-excitation, one of the photons was used to condition the detection of the other. Such 'heralding' of the companion photon makes the joint state a one-photon state. Later it was shown that a similar method of conditional detection of the correlated pairs of photons generated in spontaneous parametric down-conversion (SPDC) allows them to be used as a heralded single photon source (HSPS) [32, 33].

In spontaneous parametric down-conversion, two lower energy photons (signal and idler) are generated when a higher energy pump photon is incident on a $\chi^{(2)}$ non-linear crystal. It is called 'spontaneous' because the process is not induced by an external input signal, 'parametric' refers to the phase relationship between the input and output fields since the process depends on the input field, and 'down conversion' refers to the lowered frequencies of the output fields. The generation of twin photons and their

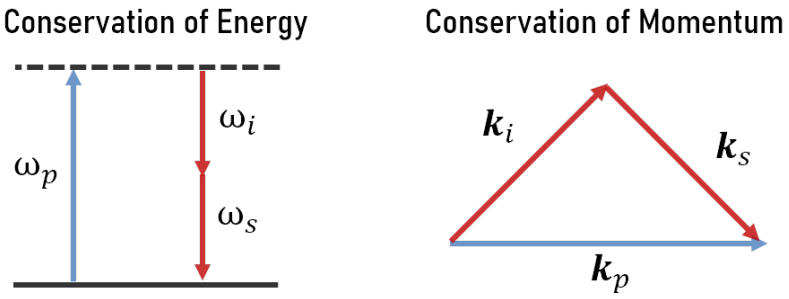

Figure 1.4: Phase matching conditions arising from energy and momentum conservation in spontaneous parametric down-conversion.

direction of propagation are governed by the phase-matching conditions [34] given in Figure 1.4. There are generally two methods used to achieve phase-matching - angle tuning and temperature tuning. Angle tuning is done in birefringent crystals where the

phase-matching constraints are adjusted by tilting the crystal about the normal to the optic axis. Phase-matching in periodically poled crystals is achieved by controlling the temperature of the crystal. The basic illustration of the generation of correlated

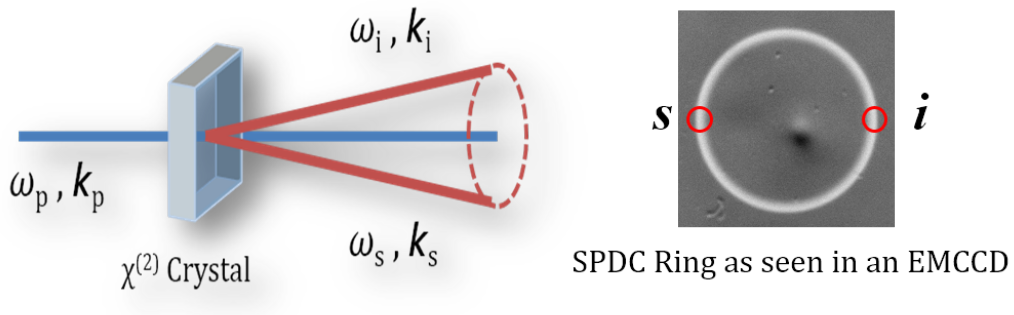

Figure 1.5: Correlated pairs of photons generated in a paramteric down-conversion process.

photon pairs by SPDC is shown in Figure 1.5. A pump laser is incident on a second-order non-linear crystal that generates photon pairs. Spatial distribution of a degenerate parametric down-converted photons is in an annular ring geometry for non-collinear phase-matching where the photon pairs are distributed at every diametrically opposite points of the ring. The diametrically opposite portions of the annular distribution is selected to generate the two mode state which upon heralding gives a single-photon state.

1.3 Structured Beams and Orbital Angular Momentum of Light

Lasers are widely used in optics because of their high monochromaticity and directionality (temporal and spatial coherence, in other words). In normal laser light the wave fronts are considered to be planar with a paraxial approximation - that their wave-

front normals are making a small angle with the axis of propagation. Such waves, or as they are otherwise called beams, must satisfy the paraxial Helmholtz equation. The power is concentrated within a cylinder of very small radius centred at the beam axis. The beams mentioned in the previous section are solutions of Paraxial Wave Equation (PWE). A paraxial wave is a plane wave, e^{-ikz}, modulated by a complex envelope, $A(\mathbf{r})$ which varies slowly with position. Hence, for the complex amplitude,

$$U(\mathbf{r}) = A(\mathbf{r})e^{-ikz} \ ; \qquad k = \frac{2\pi}{\lambda} \tag{1.16}$$

to be a paraxial wave, $A(\mathbf{r})$ should satisfy the paraxial Helmholtz Equation.

$$\nabla_T^2 A - 2ik\frac{\partial A}{\partial z} = 0 \tag{1.17}$$

where $\nabla_T^2 = \dfrac{\partial^2}{\partial x^2} + \dfrac{\partial^2}{\partial y^2}$ is the transverse part of the Laplacian. This form of wave equation is obtained under the slow varying approximations for the complex envelope $A(\mathbf{r})$, $\dfrac{\partial A}{\partial z} \ll kA$ and $\dfrac{\partial^2 A}{\partial z^2} \ll k^2 A$

The most interesting and useful solution of the PWE is the Gaussian beam. One simple solution to the PWE is given by the paraboloidal wave, whose envelope is given by,

$$A(\mathbf{r}) = \frac{A_0}{z}e^{-ik\frac{\rho^2}{2z}} \ ; \qquad \rho^2 = x^2 + y^2.$$

A slightly modified form of this solution gives the expression for Gaussian beam, the fundamental mode of any laser cavity.

$$A(\mathbf{r}) = \frac{A_0}{q(z)}e^{-ik\frac{\rho^2}{2q(z)}} \ ; \qquad q(z) = z + iz_0.$$

This is again a solution for the PWE. The parameter z_0 is called the Rayleigh range.

Redefining q(z) in terms of two new functions R(z) and W(z), $\frac{1}{q(z)} = \frac{1}{R(z)} - i\frac{\lambda}{\pi W^2(z)}$, an expression for the complex amplitude of the Gaussian beam is obtained.

$$U(\mathbf{r}) = A_0 \frac{W_0}{W(z)} e^{-\frac{\rho^2}{W^2(z)}} e^{-ikz - ik\frac{\rho^2}{2R(z)} + i\psi(z)} \tag{1.18}$$

where A_0 is the constant amplitude and,

$$W(z) = W_0 \left[1 + \left(\frac{z}{z_0}\right)^2\right]^{\frac{1}{2}} \tag{1.19a}$$

$$R(z) = z\left[1 + \left(\frac{z}{z_0}\right)^2\right] \tag{1.19b}$$

$$\psi(z) = \tan^{-1}\left(\frac{z}{z_0}\right) \tag{1.19c}$$

$$W_0 = \left(\frac{\lambda z}{z_0}\right)^{\frac{1}{2}}. \tag{1.19d}$$

Hence, the optical intensity of the Gaussian beam is given as a function of both axial and radial distances,

$$I(\rho, z) = I_0 \left[\frac{W_0}{W(z)}\right]^2 e^{-\frac{2\rho^2}{W^2(z)}}. \tag{1.20}$$

where $I_0 = A_0^2$.

There exists other solutions for the paraxial Helmholtz equation, consisting of paraboloid wavefronts like the Gaussian, having different intensity distributions. These paraboloid solutions are of particular interest in laser optics, as they can form the modes of a resonator. One important set of such solutions are called Hermite-Gaussian modes. Consider, a modulated Gaussian beam, whose complex envelope is given by,

$$A(\mathbf{r}) = A(x,y,z) = A_G \;\; \mathcal{X}\left[\sqrt{2}\frac{x}{W(z)}\right] \;\; \mathcal{Y}\left[\sqrt{2}\frac{x}{W(z)}\right] \;\; e^{jZ(z)} \tag{1.21}$$

where

$$A_G = A_0 \left[\frac{W_0}{W(z)}\right] e^{-\frac{\rho^2}{W^2(z)}} e^{-ik\frac{x^2+y^2}{2R(z)}+i\psi(z)}. \tag{1.22}$$

Solving for $\mathcal{X}$,$\mathcal{Y}$ and $\mathcal{Z}$ that satisfy the PWE, we obtain an expression for the complex envelope of the Hermite-Gaussian beam,

$$HG_{m,n}(x,y,z) = A_{m,n} \left[\frac{W_0}{W(z)}\right] G_m\left[\sqrt{2}\frac{x}{W(z)}\right] G_n\left[\sqrt{2}\frac{y}{W(z)}\right] \times e^{-ikz-ik\frac{x^2+y^2}{2R(z)}+i(m+n+1)\psi} \tag{1.23}$$

where

$$G_m(u) = H_m(u)e^{-\frac{u^2}{2}}. \tag{1.24}$$

where $H_m(u)$ Hermite polynomial with the non-negative integer index m. Intensity distribution of the Hermite-Gaussian beam of order (m,n) is,

$$I_{m,n} = |A_{m,n}|^2 \left[\frac{W_0}{W(z)}\right]^2 G_m^2\left[\sqrt{2}\frac{x}{W(z)}\right] G_n^2\left[\sqrt{2}\frac{y}{W(z)}\right]. \tag{1.25}$$

The Laguerre-Gaussian (LG) modes, another set of solutions for the PWE, are the eigen modes of a resonator cavity with cylindrical symmetry. The complex amplitude for the corresponding LG beam of order (p,l), is given by,

$$LG_{p,l}(\rho,\phi,z) = A_{p,l}\, e^{-\frac{\rho^2}{W^2(z)}} L_p^l\left[\frac{2\rho^2}{W^2(z)}\right] e^{-ikz-ik\frac{x^2+y^2}{2R(z)}} e^{il\phi} e^{i(2p+l+1)\psi}. \tag{1.26}$$

where p is the radial index, l is the azimuthal index and L_p^l represents the generalized Laguerre polynomial. The azimuthal phase term, $e^{il\phi}$ causes the screw dislocation of order l in the wavefront. This creates the phase singularity. Light beams with phase singularities are often observed in nature on scattering of light beam from rough

surfaces. These phase singularities in optical field are called optical vortices.

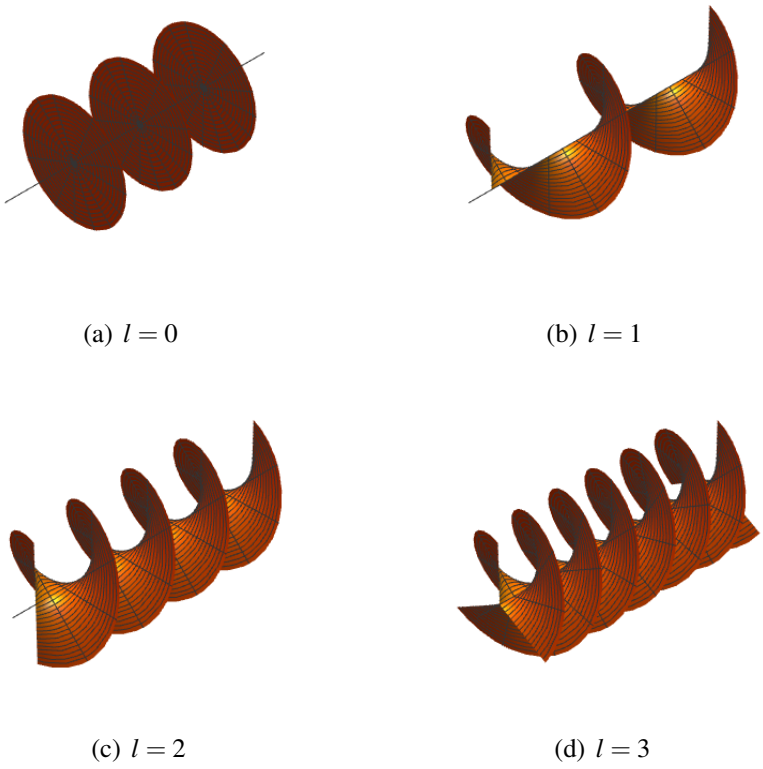

(a) $l = 0$ (b) $l = 1$

(c) $l = 2$ (d) $l = 3$

Figure 1.6: Helical phase fronts corresponding to different OAM orders, l.

Light was well understood as a stream of photons with energy $\hbar\omega$ and momentum $\hbar k$ per photon. Also, polarization was understood as the spin angular momentum of $\hbar$ aligned parallel or anti parallel to the propagation direction. It was only by 1992 [35] that physicists could experimentally establish that beams with helical phase fronts can carry orbital angular momentum. However the phase singularities in beams were known and being studied since 1974, when Nye and Berry [36] had demonstrated the existence of phase singularities in wave fronts, which before were believed to be surfaces of constant phase. They called it dislocations in the wave trains in analogy to those in crystal lattice defects. From then on, the optical vortex and their properties have been studied extensively. At the singularity the phase becomes undetermined and

the wave amplitude vanishes resulting in dark regions within the beam. The transverse

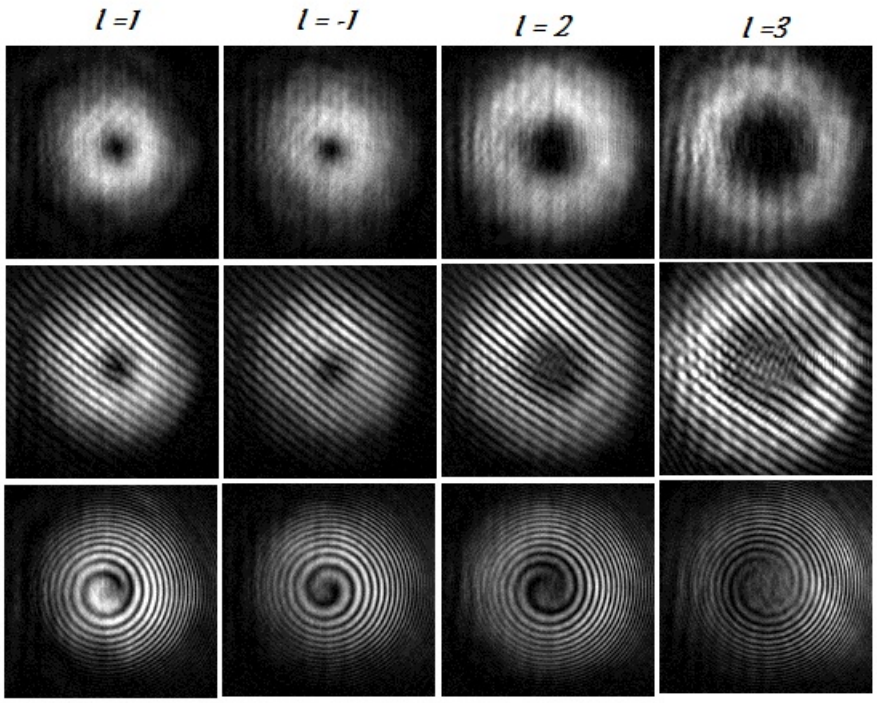

Figure 1.7: (Top row) Intensity output of optical vortices having charges $l = 1$, $l = -1$, $l = 2$, and $l = 3$, (middle row) off-axis interference of each vortex with a plane wave. The orientation of the fork-pattern corresponds to the sign of the topological charge, and (bottom row) spiral rings obtained in the interference of a vortex with a spherical wave. The helicity corresponds to the sign of the charge.

projection of an optical vortex will look like a ring of light, with the center being a dark spot of phase singularity (top row of Fig. 1.7). The phase singularities are topological objects and carry a topological charge attributed to the amount of helicity of the wave front around the phase singularity. The radius of the dark core increases with the absolute value of charge. The optical vortex contains orbital angular momentum of ($l\hbar$) per photon, where l is called the topological charge or the order of OAM of the vortex. Helical phase fronts corresponding to different OAM order are given in Figure

1.6. Topological charge of the vortex is given by

$$\text{Charge}(l) = \frac{1}{2\pi} \oint \nabla\phi \mathbf{.dh}. \tag{1.27}$$

where ϕ is the azimuthal phase and dh is the length element along the azimuthal direction. The interference of a wave possessing such screw dislocations with a normal reference wave having spherical wave fronts will produce spiral fringe patterns. The number of fringes originating from the center equals the modulus of the topological charge and the direction of rotation of the spirals refers to the sign of the charge (Figure 1.7). The charge of a vortex beam can also be determined by a simple method using a tilted lens [37].

1.3.1 Generation and Measurement of Orbital Angular Momentum

One of the simplest ways to generate beams carrying OAM is to let a Gaussian beam pass through an optical retarder which introduces an azimuthally varying phase. This is achieved through spiral phase plates (SPP). The azimuthal phase introduced by the SPP to the beam is given as

$$\delta = \frac{(n-1)h}{\lambda}\phi \tag{1.28}$$

where n is the refractive index of the material, h is the difference between maximum and minimum of the thickness, and λ is the wavelength of light.

Another technique to generate OAM is using spatial light modulators. Computer generated holograms (CGH) as given in Figure 1.8 are displayed on liquid crystal spatial light modulator (SLM). The simulated vortex and its phase profile are given in Figure 1.8b and 1.8c respectively. In SLMs, a phase delay is added to the incoming

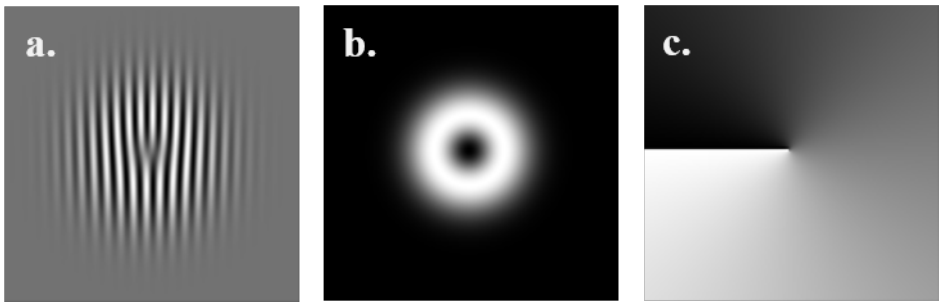

Figure 1.8: Vortices carrying different OAMs can be generated using computer generated holograms. The fork interferogram (a) generates a vortex (b) whose phase profile is given by (c).

light depending upon the voltage imparted across the liquid crystal array which thereby manipulates the transverse phase profile of the output beam. SLMs are advantageous over SPPs as they can dynamically vary the displayed hologram and manipulate the OAM of the incident beam. The measurement of OAM is mainly carried out through phase flattening the incident OAM with a negative charged hologram/SPP and by collecting the resultant Gaussian field using single mode fibers. The intensity collected in the single mode fiber is proportional to the corresponding OAM content in the incident beam.

1.3.2 Sorting of Orbital Angular Momentum States

Most of the quantum protocols require us to postselect the OAM states of a subspace. This leaves a large amount of photons in the output unused and reduces the efficiency of the protocol. An efficient method to address this challenge is to sort the SPDC output into a new basis of even and odd modes of OAM and thereby making use of all the available photons [38, 39]. A Sagnac interferometer involving a Dove prism (DP) can serve this purpose. The Dove prism introduces a charge dependent phase $e^{il(2\alpha)}$ where α is the angle of rotation of the DP with the interferometer plane. A rotation of Dove prism by an angle, $\alpha = \frac{\pi}{4}$ introduces a relative phase of $\Delta\psi = l\pi$ between

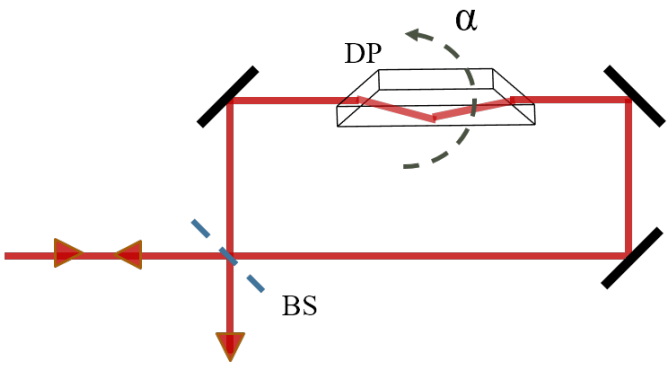

Figure 1.9: An illustration of the action of Dove prism (DP) within an interferometer based even-odd OAM sorter. The DP introduces an OAM dependent phase, $2l\alpha$, where α is the relative angle of rotation of the Dove prism. For a common path interferometer as in figure, this phase becomes $4l\alpha$.

the two counter-propagating beams in the interferometer and odd and even modes are separately obtained at the different ports of the interferometer.

1.4 Quantum Entanglement

Entanglement [40, 41] is one kind of quantum correlations and is key to many quantum information protocols. A pure bipartite ('two-particle') state, $|\Psi_{AB}\rangle \in \mathcal{H}_A \otimes \mathcal{H}_B$, is said to be entangled if and only if it can not be written as the product of two subsystems $|\phi_A\rangle$ ($\in \mathcal{H}_A$) and $|\psi_B\rangle$($\in \mathcal{H}_B$) as,

$$|\Psi_{AB}\rangle = |\phi_A\rangle\,|\psi_B\rangle\,. \tag{1.29}$$

The simplest example is the set of four Bell-states,

$$\left|\psi^{\pm}\right\rangle = \frac{1}{\sqrt{2}}(|0\rangle|1\rangle \pm |1\rangle|0\rangle) \tag{1.30a}$$

$$\left|\phi^{\pm}\right\rangle = \frac{1}{\sqrt{2}}(|0\rangle|0\rangle \pm |1\rangle|1\rangle) \tag{1.30b}$$

which form a set of bases.

The existence of entanglement lies closely to the idea of quantum non-locality and realism. *Realism* requires that for physical properties that can be assigned with certainty to a system, an element of physical reality exists corresponding to such a property. The *Locality* principle requires, that the result of any measurement performed on one system cannot influence the physical elements of reality at the second system.

If we take the subsystems A and B related as $|\psi^-\rangle$ from Equation 1.30a such that they are not causally connected (space-like separated), it can be seen that a measurement on subsystem A will cause subsystem B to be in a corresponding state. For example, a measurement of A in $\hat{\sigma}_z$ that yields $\sigma_z = +1$ (corresponds to $|0\rangle$) will make B to fall into a state $|1\rangle$. This seemed to be in violation of the locality principle and hence causality. In their seminal EPR paper [42], Einstein, A. Podolsky, B. and Rosen, N. wondered whether the existing quantum theory was complete as it prevents such a correlation and should there be other theories based on the *hidden variables* that control such *spooky actions* at space-like separated points. This led to further discussions on the philosophy as well as the understanding of quantum mechanics including the famous Einstein-Bohr series of debates [43]. Inequalities based on Bell's theorem [44, 45] put an upper limit for classical correlations in terms of measurement probabilities and distinguish between local hidden variable theories and predictions of quantum mechanics. A series of experiments [46–49] discarded any local hidden variables and the violation of Bell-CHSH inequality is attributed to the stronger correlations resulting from quantum mechanics. The Bell-CHSH inequality for a two dimensional system is given by,

$$S = \left|E(\theta,\chi) - E\left(\theta,\chi'\right) + E\left(\theta',\chi\right) + E\left(\theta',\chi'\right)\right| \leq 2 \tag{1.31}$$

where the correlation coefficient $E(\theta,\chi)$ is calculated from the coincidence amplitude $C(\theta,\chi)$ according to

$$E(\theta,\chi)=\frac{C(\theta,\chi)+C\left(\theta+\frac{\pi}{2},\chi+\frac{\pi}{2}\right)-C\left(\theta+\frac{\pi}{2},\chi\right)-C\left(\theta,\chi+\frac{\pi}{2}\right)}{C(\theta,\chi)+C\left(\theta+\frac{\pi}{2},\chi+\frac{\pi}{2}\right)+C\left(\theta+\frac{\pi}{2},\chi\right)+C\left(\theta,\chi+\frac{\pi}{2}\right)} \tag{1.32}$$

where $C(\theta,\chi)$ refers to the probability of a state for being in $|\theta\rangle\,|\chi\rangle$.

1.4.1 Polarization Entanglement

Polarization is the conventional choice for quantum information using photons as the property is very well understood for a long time and could be manipulated using simple linear optics devices. The joint output polarization state of SPDC shows strong polarization correlations. When both both signal and idler photons are oriented along

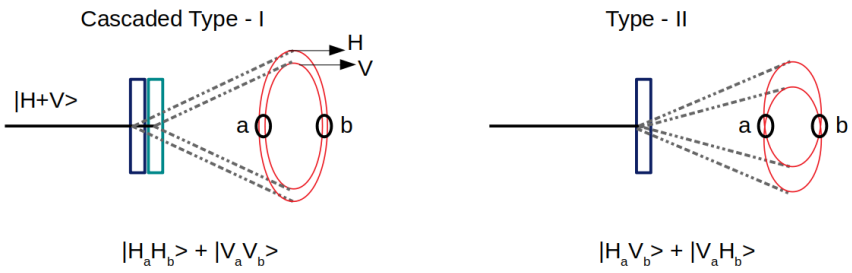

Figure 1.10: Method for generating polarization entanglement using (left) cascaded type-I SPDC and (right) type-II SPDC processes.

the ordinary axis in their polarization it is called Type-I down-conversion. In type-II down-conversion, one among the photon pairs is extraordinarily polarized while the other is ordinary. Cascaded type-I down-conversion [50], where two type-I crystals are placed together with their optic axis orthogonal to each other, gives $|HH\rangle+|VV\rangle$ while the intersecting regions in a type-II process [51] give $|HV\rangle+|VH\rangle$. Thus one

can obtain the entangled states, which are maximally entangled, given as,

$$|\psi^{\pm}\rangle = \frac{1}{\sqrt{2}}(|H\rangle_s|V\rangle_i \pm |V\rangle_s|H\rangle_i) \tag{1.33a}$$

$$|\phi^{\pm}\rangle = \frac{1}{\sqrt{2}}(|H\rangle_s|H\rangle_i \pm |V\rangle_s|V\rangle_i) \tag{1.33b}$$

which form the Bell basis for measurement. Here, subscripts s and i refers to the signal and idler photons from the spontaneous parametric down conversion.

1.4.2 OAM Entanglement

Orbital angular momentum (OAM) of light has been explored to have great applications in quantum information processing since OAM can serve as an additional degree of freedom with an infinite dimensional basis. OAM entanglement can be easily realized in the parametric down conversion process [52]. The output signal and idler photons from the parametric down-conversion can be individually considered to be in an incoherent mixture of different spatial modes. However, the conservation of orbital angular momentum ensures that their spatial modes are strongly correlated with each other. Hence, we obtain pairs of photons entangled in their OAM modes in the output of SPDC.

The output OAM state of the SPDC for an incident pump photon having OAM, l, is the entangled state,

$$|\Psi\rangle = \sum_{m=0}^{\infty} C_m(|m\rangle_s|l-m\rangle_i + |l-m\rangle_s|m\rangle_i) \tag{1.34}$$

where C_m corresponds to the probability of the two photon output to be in a specific $(m, l-m)$ mode and is estimated from the mode overlap integral for parametric down

conversion.

1.4.3 Hybrid Entanglement

A system of two photons can be simultaneously and independently entangled in both polarization and OAM. This is an example of hyper-entanglement. Another type of entanglement is hybrid entanglement where two independent degrees of freedom of the same particle are entangled. For example, the state of a photon entangled maximally in polarization and OAM can be expressed as,

$$\left|\psi^{+}\right\rangle = \frac{1}{\sqrt{2}}\left(|H,l\rangle + |V,-l\rangle\right) \tag{1.35}$$

Non-separability can be defined in the case of classical beams as well where the different degrees of freedom of the single beam are considered as the subsystems [53]. While this "classical entanglement" does not possess non-locality, it is of particular interest in classical communication as well as to study and simulate quantum systems [54–59].

1.4.4 Duality of Entanglement

In order to meaningfully describe a bipartite entangled state of two identical particles, at least two variables are required. One variable A is used to label the particles while they are entangled in another variable B ($[A,B]=0$). From second quantization, the generalized expression for two identical particles in a bipartite entangled state can be written as,

$$|\Psi\rangle_{12} = \left(\alpha\ \hat{c}^{\dagger}_{A_1,B_1}\hat{c}^{\dagger}_{A_2,B_2} + \beta\ \hat{c}^{\dagger}_{A_1,B_2}\hat{c}^{\dagger}_{A_2,B_1}\right)|0\rangle \tag{1.36}$$

where A_i and B_i are the distinct eigen values of the observables A and B, $|0\rangle$ is the vacuum state and $\hat{c}^{\dagger}_{i,j}$ creates a particle in the joint state $|i,j\rangle$. This state can be rewritten as,

$$|\Psi\rangle_{12} = \alpha\,|B_1\rangle_{A_1}\,|B_2\rangle_{A_2} + \beta\,|B_2\rangle_{A_1}\,|B_1\rangle_{A_2} \tag{1.37}$$

and alternatively as,

$$|\Psi\rangle_{12} = \alpha\,|A_1\rangle_{B_1}\,|A_2\rangle_{B_2} + \beta\,|A_2\rangle_{B_1}\,|A_1\rangle_{B_2}\,. \tag{1.38}$$

Hence two identical particles can be shown to be entangled in one variable or the other depending upon which variable is being used to distinguish the photons. Thus just the distinguishability reveals the entanglement. This property is called *dualism* in entanglement [60].

1.5 Objective of the Thesis

Twisted single photons, or photons carrying orbital angular momentum are gaining interest in quantum information applications. Photons are one of the most successful candidates for quantum information processing while OAM of photons further 'adds a cherry on the top' by providing an infinite dimensional degree of freedom for enhanced information transfer. Our main objective is to study and characterize twisted single photons generated from SPDC. In order to characterize the single photon nature, we study the statistical correlations of the twisted photons. We study the number statistics as well as second order correlations of HSPS. Studies on intensity correlations of classical vortex beams have shown dependence of statistical properties on the vorticity of the beam. For a single photon carrying OAM, such variations if any would be significant when single photon OAM states are being used for quantum information processing. We wish to study the variation of the photon statistics with different

orders of the OAM. We further study about the OAM distribution of the twisted photons. OAM of the photons could be in different spatial modes. We wish to explore the dependence of OAM correlations and entanglement in twin photons from the SPDC on these spatial modes. We study the behaviour of the distribution for different spatial modes of the pump as well as different modes of projections. We also explore using the OAM degree of freedom of the single photons to separate indistinguishable photons and observe entanglement.

1.6 Overview of the Thesis

We present this thesis in six chapters. Chapter 1 briefly discusses necessary concepts for understanding the work described further in the thesis. This chapter gives a brief introduction on the single photon souorces, heralded single photons generated in parametric down-conversion, photon statistics, orbital angular momentum of photons, and quantum entanglement.

In chapter 2, we study the number distribution of photon sources. We build the probability distribution of numbers using the time series data of detection events. We observe sub-Poissonian distribution of heralded single photons generated in parametric down-conversion.

In chapter 3, we study the second order correlation of the heralded single photons. The correlation coefficient is calculated whose value determines the non-classicality of the source. We observe the variation of the statistical correlations with the OAM of the twisted single photons, both theoretically and experimentally.

In chapter 4, we study the OAM correlations of the twin photons generated in parametric down-conversion. We obtain the OAM spectra for different pump modes

as well as in different projection bases and compare the results.

In chapter 5, we demonstrate that we can use the OAM of twisted photons for efficient sorting of indistinguishable photons. We observe polarization entanglement of the indistinguishable photons from the output of a collinear SPDC after sorting them in the even-odd basis of OAM.

Finally we summarize the study and present the impact of the results in chapter 6.

Chapter 2

Observing Sub-Poissonian Statistics of Heralded Single Photons

The number statistics of a single photon source (SPS) follows sub-Poissonian photon number distribution. However, the pair production from different positions within an SPDC crystal evokes the possibility of occurrences of multiple photons and hence would qualify the source as less quantum than it is expected to be. The occurrence of multiple photon pairs and consequent photon bunching threatens the security in cryptography related applications. Thus, it is important to study and quantify the non-classicality of the single photon sources being used. A general classification puts the sources into three categories, super-Poissonian, Poissonian and sub-Poissonian according to the photon number distribution. Classical sources, like thermal and coherent radiation, show super-Poissonian and Poissonian statistics respectively while certain non-classical sources, such as a single photon source, show sub-Poissonian distribution. Violations of bounds defined for the number statistics of classical sources imply the non-classical behavior of single photon sources [61–64]. Photon antibunching

is another manifestation of the non-classical behavior of the source and can be observed through the measurement of the degree of second-order coherence, $g^{(2)}(\tau)$. Single photon sources show antibunching and hence $g^{(2)}(0)$ falls to zero. Though antibunching and sub-Poissonian statistics are completely non-classical effects and tend to occur together in many systems, they are distinct effects and need not necessarily be associated with one another [65, 66]. Twisted single photons carrying orbital angular momentum (OAM) are gaining interest in quantum information processing as they provide infinite number of orthogonal states to encode information [67, 68]. In this chapter, we verify the sub-Poissonian nature of heralded single photons generated in parametric down-conversion using a simple and ubiquitous setup consisting of photodetectors and an oscilloscope which can be easily found in any undergraduate laboratory. We also study the number statistics of twisted single photons generated in parametric down-conversion.

2.1 Sub-Poissonian Number Statistics and Mandel Q-parameter

One can define an ideal single photon source as a Fock state for which the number statistics gives mean, $\mu = 1$ and variance $\sigma^2 = 0$. Treatment of the electromagnetic field as a quantum harmonic oscillator allows us to define quadrature field operators, $\hat{X}_1$ and $\hat{X}_2$, which can be shown to follow the uncertainty relation [69], $\langle \Delta\hat{X}_1^2 \rangle \langle \Delta\hat{X}_2^2 \rangle \geq 1/16$. The minimum uncertainty state, with $\langle \Delta\hat{X}_1^2 \rangle = \langle \Delta\hat{X}_2^2 \rangle$, is the coherent state,

$$|\alpha\rangle = \exp^{\frac{-|\alpha|^2}{2}} \sum_{n=0}^{\infty} \frac{\alpha^n}{\sqrt{n!}} |n\rangle \tag{2.1}$$

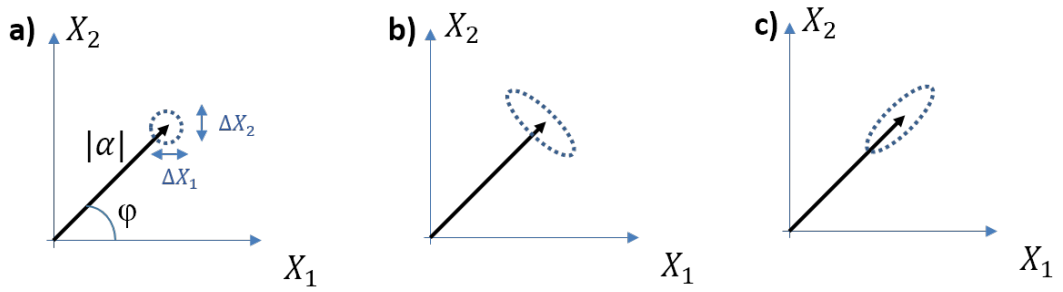

Figure 2.1: a) Phasor diagram corresponding to classical coherent field with amplitude $|\alpha|$ and optical phase , ϕ. The dotted circle corresponds to the region of uncertainty when the uncertainty in both the quadratures are equal. When the uncertainty in one of the quadratures is reduced while compromising the other, we observe different types of squeezing, examples to which are b) amplitude squeezing and c) phase squeezing.

which defines a Poissonian distribution [70] of photon number, n, with $\langle(\Delta\hat{n})^2\rangle = \langle\hat{n}\rangle$. Squeezing these states in terms of number or phase is achieved when the respective variance is less than that corresponding to the coherent state. The phasor diagrams corresponding to a classical field and quadrature squeezed fields are given in Figure 2.1.

The photon number variance can be written as,

$$\langle\Delta\hat{n}^2\rangle = \langle\hat{n}\rangle + \langle\hat{a}^\dagger\hat{a}^\dagger\hat{a}\hat{a} - \langle\hat{a}^\dagger\hat{a}\rangle^2\rangle \tag{2.2}$$

where $\hat{a}$ and $\hat{a}^\dagger$ are the annihilation and creation operators. Based on the variance, the Mandel Q-parameter [71] is defined by,

$$Q \equiv \frac{\langle\hat{a}^\dagger\hat{a}^\dagger\hat{a}\hat{a} - \langle\hat{a}^\dagger\hat{a}\rangle^2\rangle}{\langle\hat{a}^\dagger\hat{a}\rangle} = \frac{\langle(\Delta\hat{n})^2\rangle - \langle\hat{n}\rangle}{\langle\hat{n}\rangle}. \tag{2.3}$$

It classifies light sources on the basis of photon number fluctuations. $Q \geq 0$ for coherent and all other classical sources of light while sub-Poissonian light is identified with $Q < 0$ [71, 72].

The detected photo-electron statistics and the statistics of the incident photons can be different depending upon various factors such as coherence time of the incident light, detector dead-time and efficiency of detection. Appropriate size of the binning window has to be selected to make sure that it is less than the coherence time and pump intensity has to be kept low such that the probability of more than one incidences within the dead time is negligibly small. This is discussed in detail in the next section. Taking efficiency of detection into account, the mean and standard deviation for the detected-photon distribution can be written as [73],

$$\langle m \rangle = \eta \langle n \rangle \tag{2.4a}$$

$$\sigma^2(m) = \eta^2 \sigma^2(n) + \eta(1-\eta)\langle n \rangle \tag{2.4b}$$

where m is the detected photo-counts, n is the actual photo-counts, η is the detector quantum efficiency and σ^2 is the variance. Therefore, correction for the efficiency of detection can be taken care by writing the Q-parameter for the incident photons, Q_n, in terms of that of the detected photons, Q_m, as

$$Q_n = Q_m/\eta. \tag{2.5}$$

2.2 Building Statistics using an Oscilloscope

In order to build the statistics, the detection events at the photo diodes are counted within a defined time interval (binning window) and the distribution of the number of such occurrences is obtained. This is done by converting the analog output from the oscilloscope into a series of 1's and 0's which corresponds to the presence or absence of a detection respectively. We built a MATLAB code which identifies an event pulse

in the oscilloscope output time series and labels its onset as 1 and the rest as 0. This generates a binary time series of events in terms of the occurrences or non-occurrences of photon detection (Figure 2.2). A probability distribution of events is built from this generated time series.

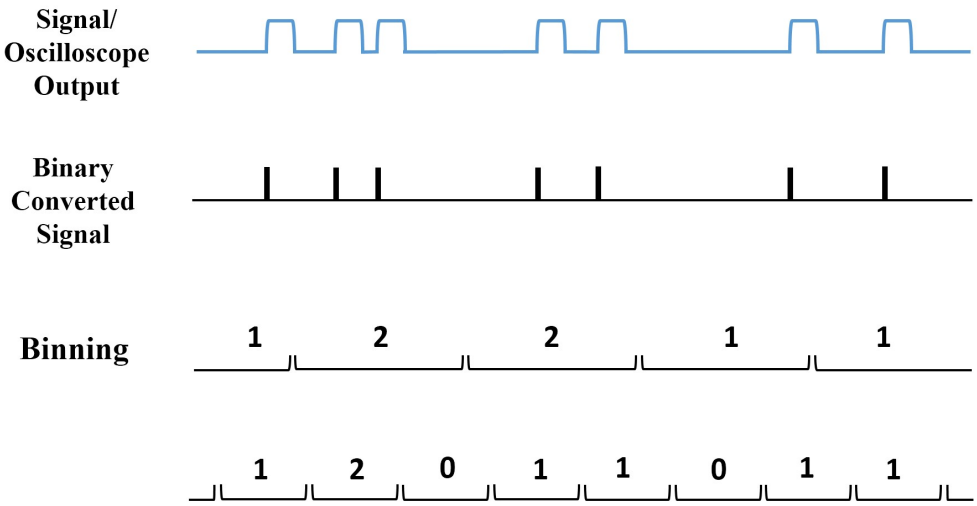

Figure 2.2: Converting the signal to a binary time series. The average photon number depends on the size of the binning window.

The time series of binaries generated for both the signal and idler are then sliced into smaller binning windows in such a way that statistically one detection falls in a bin. The number distribution is developed for these individual arms. A new time series corresponding to the coincidences of photon pairs is developed from the time series corresponding to signal and idler, in a way that a count is observed in one arm (within the coincidence window, τ_c = 10 ns) given a detection in the other arm. The number distribution of this new time series corresponds to the statistics of the heralded single photon source from SPDC. Another important factor to be taken care is the coherence time of the input pump field. If the binning window is considerably larger than the coherence time, the statistics of the photo-electrons will result in a Poissonian distribution independent of the inherent photon statistics [74]. Since we are taking

two photon coincidence here, the coherence of the pump will determine the coherence of paired down-converted photons. The pump coherence time is 80 ns, which in turn results in a coherence time ∼80 ns for the bi-photon output of the SPDC. The binning window (20 ns) defined for building the coincidence series during post-processing is much within this two photon coherence time. The MATLAB code to build the statistics from the recorded time series is shared in GitHub repository for open access [75] and given in Appendix A.

2.3 Number Statistics of Twisted Single Photons

Twisted single photons of different orders are obtained in SPDC by pumping with optical vortices of different orders and projecting the idler photon in a single mode fiber and hence selecting only those with OAM, l =0. Due to OAM conservation in SPDC, this will result in only those signal photons which have the same OAM as the pump contributing to the coincidence counts [52]. Hence, a photon number distribution obtained for the coincidence events will correspond to the number statistics of single photons carrying OAM.

2.3.1 Experiment

The experimental setup used for building the statistics of the heralded single photon source (HSPS) is given in Figure 2.3 [76]. A 405 nm diode laser (Toptica Topmode) is used as a pump to generate photon pairs from a Type-I BiBO crystal (Castech, 5 mm thickness). The polarization of the pump is oriented along the crystal axis using a half-wave plate. The output pairs are spectrally filtered using interference filters of pass-band 810 ± 5 nm to rule out the non-degenerate pairs. Two diametrically opposite regions are selected from the cone of correlated pairs of photons generated in the Type-

I SPDC. These individual arms (signal and idler) are then collimated and coupled to a single mode fibre (SMF, *idler*) and a multi mode fiber (MMF, *signal*) through a fibre coupler.

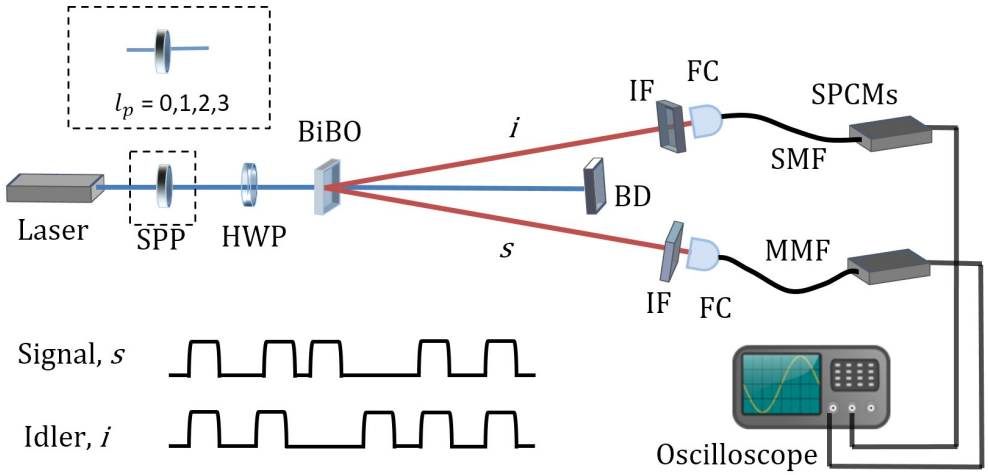

Figure 2.3: Experimental setup to determine the photon number statistics of the heralded PDC source. HWP - half wave plate, BiBO - non linear crystal, BD - beam dump, IF - interference filters, FC - fiber couplers, SPCMs - single photon counting modules. Different OAM orders can be imparted to the heralded single photon by placing SPPs of different orders in pump and projecting idler photon in a single mode fiber.

The individual signal and idler photons are detected using single photon detectors. We have used two single photon counting modules (SPCM, Excelitas SPCM-AQRH-16-FC) placed in both signal and idler arms for the detection of the photon pairs. Photomultiplier tubes (PMTs), which will be more common in laboratories than an SPCM, can also be used for the detection. The coincidences are maximized by optimizing the coupling to the fiber. The SPCM (or PMT) generates a TTL pulse in response to each photon incidence. However, the total number of photon incidences that can be recorded by a detector is limited by the detector dead time. If more than two photon incidences occur at the detector within the dead-time, the detector will not be able to register the second detection and the number statistics will not give the correct distri-

bution [77, 78]. Therefore it is important to verify that the probability of such multiple detection within the dead-time is negligible. The individual count rates are $\sim 10^4/s$ for the single mode fibre and $\sim 10^5/s$ for the multi mode fibre. The detector dead time is 27 ns (t_d) for the SPCMs used in the setup. If R is the total count rate in the detector associated with MMF (chosen since it is greater than the count rate corresponding to SMF) and t_d is the dead time corresponding to the detector, then $R << 1/t_d$ ensures that the probability that more than two photons arriving within the dead time interval is very small. Our count rates are such that this probability is negligible and dead time effects on the total counts can be ignored. In addition to this, since the detectors being used are not photon number-resolving, the output pulses can correspond to the incidence of one or more photons. The pump power is kept in the low power regime (1 mW for our experiment) in order to avoid such incidents due to the possible multiple photon generations [79].

The output waveform from each arm of the SPDC is recorded using a digital oscilloscope (Infiniium 90000A series) for an exposure time of 20.5 ms. Ten iterations of such time series have been recorded to calculate the Q-parameter. Each iteration records a time series of 20.5 Mpts and a resolution of 1 ns, for the oscilloscope used in the experiment. Oscilloscopes with lower specifications (in terms of bandwidth and sampling rate) can also be used at the cost of the length of the time series to be captured and time resolution.

2.3.2 Results

Initially, to see the photon number distribution for a classical coherent source, we select a coherent laser source (Thorlabs 2 mW HeNe, 632.8 nm). The intensity is attenuated such that the detected photo-counts are below the saturation level of the detectors.

The time series of events recorded using an oscilloscope was converted into a binary series of photon incidence events. A counting histogram that gives the probability of detection of n events within the corresponding time bin is generated for this time series that shows Poissonian distribution (Figure 2.4). For a time bin width such that an average number of less than one photon falls within the bin ($\mu = 0.1$), the variance (σ^2) is determined to be 0.103. The Q-parameter is calculated to be 0.045 ± 0.03 (for net efficiency, $\eta = 0.66$ in Equation 2.5) which is close to a Poissonian distribution of photon numbers.

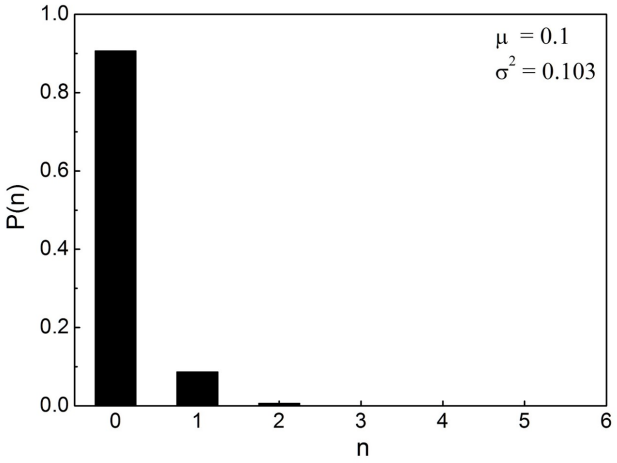

Figure 2.4: Photon number distribution for a coherent source. Mean photon number is approximately equal to the variance.

For the heralded single photon source, the number statistics is built from the binary series of coincidences generated by post-processing the recorded events of individual signal and idler photons (Figure 2.5). For $\mu = 0.1$, the variance (σ^2) for this source is calculated to be 0.0901. The Mandel Q-parameter comes out to be -0.099. The negative value of Q is indication of the sub-Poissonian behavior of the source. The detectors that are used in the experiments have a quantum efficiency of 0.6 at the spectral region in which the experiment has been undertaken. Along with this, taking the cou-

pling efficiency of the fibre and other losses into account, net efficiency of detection is determined to be $\eta = 0.3$. Incorporating this value, the Q-parameter for the heralded single photon source is determined as -0.33. A set of repeated measurements reveals the average value, $Q = -0.331 \pm 0.004$ for a heralded SPS generated using a Gaussian pump profile. $Q = -1$ implies an ideal single photon source where photons come out in order with a variance that equals to zero. Intuitively, Q is expected to be less negative (i.e., reduced non-classicality) for the case of heralded SPS, as the pair generation is occurring from different positions inside the crystal which would result in multiple photon pairs and a non-zero variance. In addition to this, various losses randomize the detection of a HSPS and hence result in a reduced non-classicality in measurement. While the intention of this work is not to formulate a rigorous theoretical model for the number statistics of heralded photons, we matched the experimentally observed data with the statistics of a simulated coincidence series. A coincidence series is generated from two correlated time series with entries consisting only 0 and 1 which correspond to the individual idler and signal series. The correlated time series can be generated by

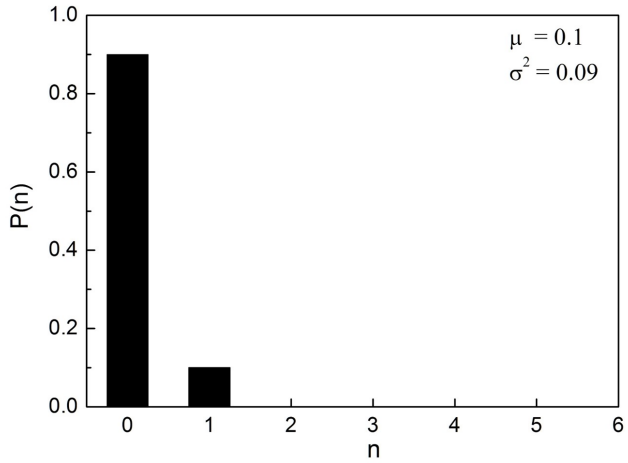

Figure 2.5: Photon number distribution for a heralded single photon source.

randomly distributing 1's in a time series (such that the sum of 1's is matched with the

experimentally observed single counts) and duplicating it. The random distribution of 1's replicate the spontaneous nature of the pair generation process. However, the actual scenario would differ from this as losses in the system would individually randomize these series further. After incorporating a loss of 0.7 in both the channels (by randomly erasing 70% of 1's independently in each time series), we build the coincidence series the same way we did during post-processing of the experimental data as given in Figure 2.2. For parameters such as efficiency, binning window, coincidence window, total counts and time series length used in the experiment, the Q-parameter turns out to be -0.3. Hence, the experimentally observed value of Q for HSPS is in reasonable agreement with the predictions from a "lossy" model for spontaneously generated correlated pairs of photons.

In the same way, photon number histograms are generated for the individual arms of the down-converted pairs of photons (Figure 2.6). For an average photon number $\mu = 0.1$, the variances were 0.126 and 0.128 respectively for the signal and idler arms which are significantly apart from that corresponds to a Poissonian distribution. With $\eta = 0.3$, the Q-parameter is calculated to be 0.87 and 0.93 for the idler and signal arms respectively with statistical errors of the order of 10^{-3}. This super-Poissonian behaviour is expected since the individual signal as well as idler photons from the down-conversion process are in a mixed state [74, 80, 81]. For the special case of these arms being in thermal state, the single arm statistics would have been expected to be such that $Q = 1$. A study by looking at SPDC as a multimode squeezing process may shed more light to the observations in this case.

Q-parameter for the heralded single photons having different OAM, obtained by pumping with an optical vortex and projecting the idler arm to $l = 0$, are given in Table 2.1. Time series of photon detection events of length 20.5 ms are recorded

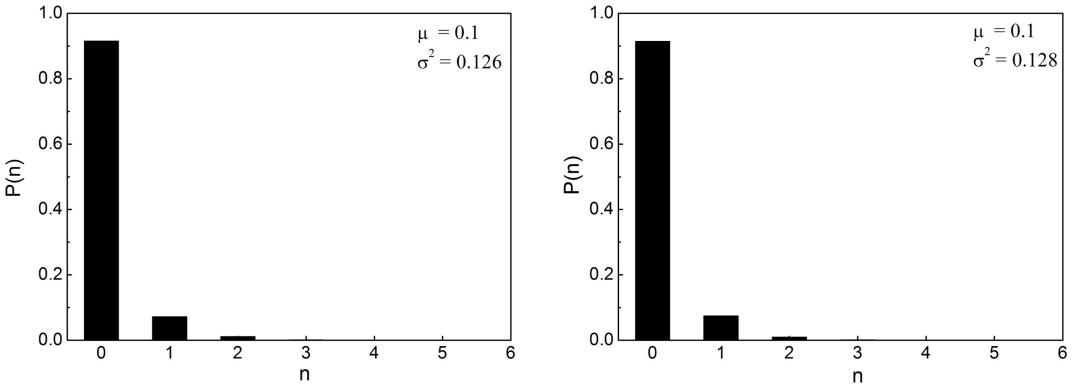

Figure 2.6: Number distribution for photons in the individual (left) idler and (right) signal arms of the down converted pairs.

using the oscilloscope. Ten such iterations are recorded to determine the Q-parameter within statistical error. It is found to violate the classical bounds of number statistics (i.e., $Q \geq 0$) by ~ 10 standard deviations for photons carrying different OAM. The Q-parameter is observed to be a constant with a very small but consistent decrease with increasing order of twisted photon OAM. This can be attributed to the reduction in the number of coincidence events with higher order pump as the singles counts in the idler arm (with $l = 0$) decreases with pump order. The effects on probability amplitude of the two photon coincidences and spectral bandwidth when pumped with different Laguerre-Gaussian modes is already discussed in literature [82, 83].

The background counts due to ambient stray light (< 100 cps) has been measured and subtracted from the detected counts. After-pulsing probability for the detectors that are used is about 0.5% and is negligible. Ringing is taken care of by appropriately terminating the output pulse into a 50Ω load at the oscilloscope. Triggering from noise signals is also taken care of during post-processing. This is done by keeping a threshold of 1.0 V while doing the conversion of the time series to binary series since the output TTL levels after BNC couplers are > 1.5 V.

Twisted photon OAM, l	Q-parameter
0	-0.331 ± 0.002
1	-0.336 ± 0.003
2	-0.343 ± 0.005
3	-0.353 ± 0.008

Table 2.1: Mandel Q-parameter obtained for the photon number distributions of twisted single photons having different orders generated in parametric down conversion.

2.4 Conclusions

Conventional quantum optics experiments to determine the non-classical statistical behavior of single photon sources involve time-to-digital converters along with associated post-processing. Here, we introduce a simple technique to build the number statistics of heralded single photon source using a digital oscilloscope. The signal and idler in the SPDC output are detected and registered in the oscilloscope. From the recorded data, a time series corresponding to the coincident detection and the corresponding number distribution are obtained. In this way, one can observe the sub-Poissonian behavior of the photon number statistics of the source using a set of detectors and an oscilloscope available in almost all the optics laboratories. We also show that in this way we can determine the number statistics of heralded single photons carrying OAM and thus can characterize them for further applications involving OAM of single photons. The number distribution of the heralded single photons is observed to be not affected by their orbital angular momentum. However, it requires that one investigate other statistical parameters as well such as second-order correlation to further understand the non-classical behaviour of twisted photons.

Chapter 3

Second-order Correlations of Twisted Photons

Spontaneous parametric down conversion (SPDC) process in a $\chi^{(2)}$ nonlinear crystal [84, 85] is one of the most successful and widely accepted technique to produce a single photon source. Since the two down converted photons are generated at the same time, detection of one photon heralds the presence of the other [32, 86]. Therefore, single photon sources obtained by using this technique are generally called heralded single photon sources. They show a peculiar quantum phenomenon called "antibunching". Antibunching is in contrast to the classical bunching of photons observed in thermal fields and characterized by the absence of more than one photon at an instant of time. For a heralded SPS, antibunching can be observed using a heralded Hanbury Brown-Twiss (HBT) type experiment [87, 88].

Optical vortices or Laguerre Gaussian (LG) beams with zero radial index are gaining popularity in implementing various quantum information protocols [67, 68] as they

provide an extra degree of freedom in the form of orbital angular momentum (OAM) [35, 89] that can be measured using standard experimental techniques [52, 90, 91]. Optical vortices of different orders or azimuthal indices form different spatial modes of light with their characteristic properties [92–96]. The intensity correlations of classical beams, while scattered from a rotating ground-glass plate [92, 97], are found to have dependence on the order of the vortex. Such studies evoke interest in the correlation properties of single photons carrying OAM generated in spontaneous processes such as parametric down conversion.

In this chapter, we use different order of vortices as a pump to the nonlinear crystal starting with the fundamental Gaussian mode and study the second order correlations of down converted photons. The observed second order correlation parameter (for zero delay) can be used to characterize the twisted single photons generated from spontaneous parametric down conversion before being used in applications involving the orbital angular momentum of single photons.

3.1 Antibunching in Heralded Single Photon Sources

The measurement of second order correlation ($g^{(2)}(\tau)$) has been important in quantum optics, especially in observing antibunching which is a purely quantum mechanical behaviour. The normalized second order correlation function [98], for a fixed position, is given as

$$g^{(2)}(\tau) = \frac{\langle \hat{E}^{(-)}(t)\hat{E}^{(-)}(t+\tau)\hat{E}^{(+)}(t+\tau)\hat{E}^{(+)}(\tau)\rangle}{\langle \hat{E}^{(-)}(t)\hat{E}^{(+)}(t)\rangle \langle \hat{E}^{(-)}(t+\tau)\hat{E}^{(+)}(t+\tau)\rangle} \tag{3.1}$$

and is usually measured in a Hanbury Brown-Twiss (HBT) experiment [88, 99], which gives the correlation between two photons separated by a time delay, τ. For an ideal single photon source from which individual photons are emitted one after another as

given in Figure 3.1a, a photon either gets transmitted (along arm ***1***) at the beam splitter or gets reflected (along arm ***2***). There are no simultaneous incidences at the detectors D_1 & D_2 when there is no delay between the paths ***1*** and ***2*** ($\tau = 0$).

For heralded single photon sources generated by spontaneous parametric down conversion (SPDC), the photon correlation in the HBT experiment has to be done in the signal (***s***) with the conditioned detection of idler (***i***) (Figure 3.1b). For the ideal case of a single photon source when the delay between i, s_1 and s_2 are zero, the three fold detection probability between these arms would be zero. This probability, P_{i,s_1,s_2} when normalized with respect to the corresponding two-fold coincidences gives the second order correlation (for zero delay)

$$g^{(2)}(0) = \frac{P_{i,s_1,s_2}}{P_{i,s_1} P_{i,s_2}} \tag{3.2}$$

where P_{i,s_1} and P_{i,s_2} are the two-fold coincidence probabilities between $i - s_1$ and $i - s_2$ pairs. The conditioned probability of coincidence detection can be expressed as $P_{i,j} =$

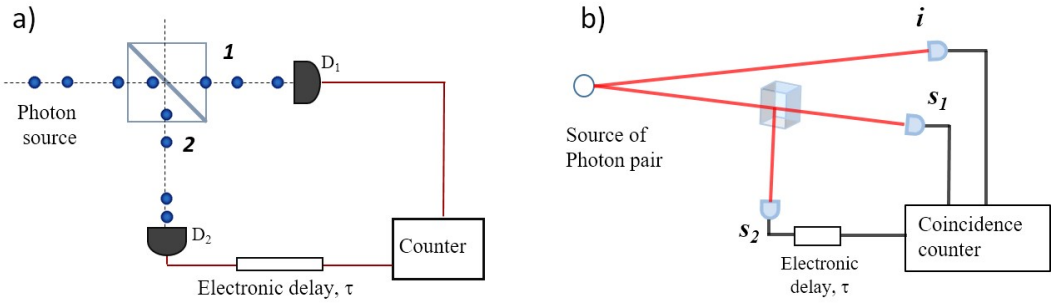

Figure 3.1: A simplified illustration of HBT experiment for a) an ideal single photon source where photons reaching the beam splitter through the input port will choose any of the paths 1 or 2 without resulting in any coincidence detection between the detectors, D_1 & D_2 and b) a heralded single photon source.

$R_{i,j}/R_i$ where $R_{i,j}$ corresponds to the coincidence rates in the respective arms and R_i is the count rate of the heralding arm. Substituting for different probabilities in Equation

3.2, $g^{(2)}(0)$ in terms of experimentally measured rates takes the form [87, 88]

$$g^{(2)}(0) = \frac{R_{i,s_1,s_2}R_i}{R_{i,s_1}R_{i,s_2}}. \tag{3.3}$$

This involves the calculation of $g^{(2)}(0)$ from the direct measurement of the three fold coincidences between the heralding idler mode and two signal modes. The second

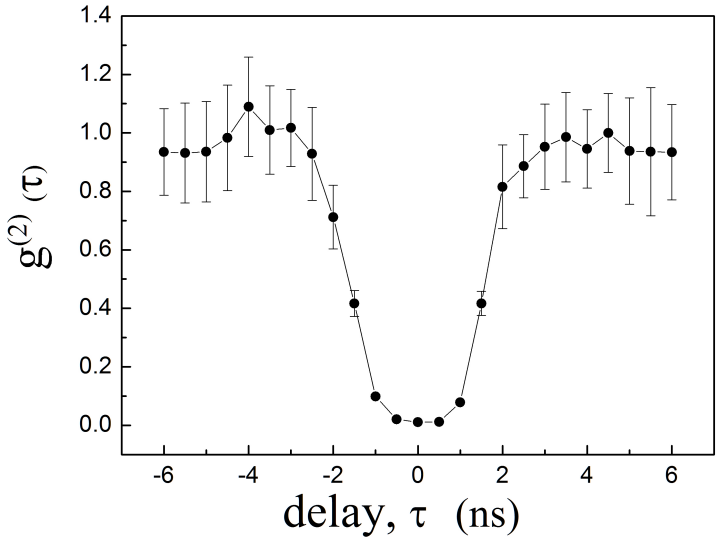

Figure 3.2: The variation of second order correlation function with delay, τ for a fundamental Gaussian mode as pump (l_p=0). The error bar corresponds to the standard deviation obtained from the measured count rate uncertainties. The error is smaller than the size of the symbol used in the plot for regions near zero time delay. Coincidence window, $\Delta t = 810ps$.

order coherence function, $g^{(2)}(\tau)$, is calculated from Equation 3.3 as a function of the time delay between photons reaching the beam splitter for a Gaussian pump. A delay generator introduces electronic delay in steps of 0.5 ns between the two output ports of the beam splitter (s_1 & s_2) in the signal arm. Coincidence measurements recorded for pair of detectors $SPCM_1$ & $SPCM_2$ kept in these two arms are heralded by the detection of a photon in the idler arm, i. Antibunching (for $\tau = 0$) is observed by varying the

temporal delay between arms s_1 and s_2 (Fig. 3.2).

3.1.1 Effect of Pump Power on Correlations

While the expected value of $g^{(2)}(0)$ for a true single photon source is zero, the non-zero values in a heralded detection can be attributed to accidental coincidences between the three detectors which can arise from simultaneous generation of multiple photon pairs, dark counts, background fluorescence etc. We have studied $g^{(2)}(0)$ by increasing the pump power and observed an increase with power (Figure 3.3). The steady increment

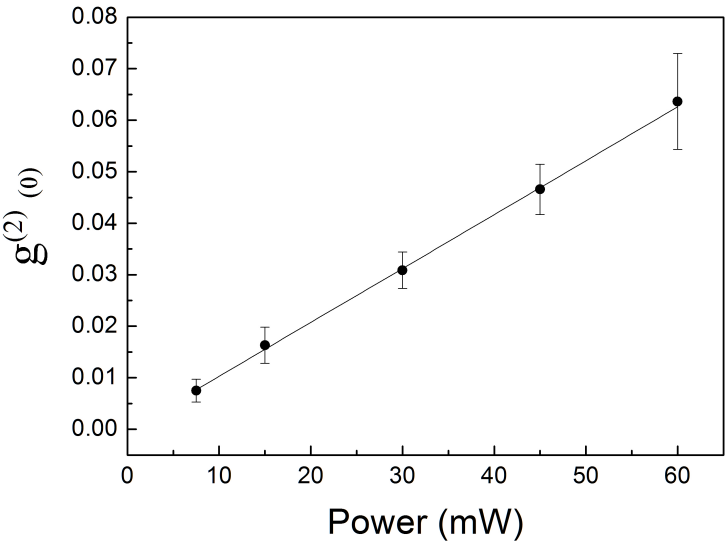

Figure 3.3: The variation of $g^{(2)}(0)$ with increasing pump power. A linear fit (line) to the experimental points (symbols) extrapolates to the origin, suggesting that multi-pairs from the down-converted output are the dominant contributors to a non-zero $g^{(2)}(0)$. Pump is a fundamental Gaussian mode. Error bar corresponds to standard deviation obtained from count rate uncertainties.

in $g^{(2)}(0)$ with pump power is due to the fact that the rate of pair production and hence the probability of simultaneous creation of multiple photon pairs are proportional to the pump power [79]. This results in more than two photons reaching together at the beam splitter leading to coincidences between the two signal arms. A higher $g^{(2)}(0)$ shows a

reduced non-classical behaviour. Hence, it is crucial for quantum optical experiments using heralded single photon sources to be done in the lower pump power regime.

3.1.2 Accidental Coincidences and Non-zero $g^{(2)}(0)$

The non zero values for three-fold coincidence rate R_{i,s_1,s_2} could be attributed to accidental coincidences due to the finite width of our coincidence window. Assuming the probability of completely uncorrelated photons reaching all three detectors simultaneously as zero (for practical purposes), we can attribute the accidental coincidences to the occurrence of a random detection along with a coincidence detection. Rewriting the three-fold coincidence in terms of two-fold coincidence and a probabilistic detection at the third detector, i.e., $P_{i,s_1,s_2} = P_{i,s_1}R_{s_2}\Delta t + P_{i,s_2}R_{s_1}\Delta t$ where Δt is the coincidence window, a modified expression for $g^{(2)}(0)$ is obtained as [100]

$$g^{(2)}(0) = R_i\Delta t(R_{s_1}/R_{i,s_1} + R_{s_2}/R_{i,s_2}). \tag{3.4}$$

3.2 Second Order Correlation of Twisted Single Photons

The orbital angular momentum is conserved in parametric down conversion [52] such that the sum of the orbital angular momenta of the down converted photons equals the pump OAM. While the output beams of the parametric down conversion are incoherent sum of multiple spatial modes, the signal-idler photon pairs will have OAM l_s and l_i respectively, restricted by the OAM conservation $l_i + l_s = l_p$, where l_p is the pump OAM. By coupling the idler into a single mode fiber, we restrict the idler spatial mode to be Gaussian, (i.e. $l_i = 0$), and thereby selecting the signal OAM to be the same

as that of the pump. Hence, the heralded correlation measurements done in the signal arm give the statistics of twisted photons whose OAM is defined by that of the pump. The pump OAM is varied using SPPs of different orders to study the statistics of generated twisted single photons. The heralded second order correlation is measured for each order of pump OAM.

3.2.1 Theoretical Predictions

In the interaction picture, the Hamiltonian for SPDC process is given by,

$$H_I = \chi^{(2)} \int_V d^3 r E_p^+ (r,t) \hat{E}_s^- (r,t) \hat{E}_i^- (r,t) \tag{3.5}$$

where $\chi^{(2)}$ is the second order non-linear coefficient, E_j is the electric field corresponding to the j-th mode. Subscripts s and i refers to the signal and the idler modes in SPDC respectively. The two photon wave function is given by,

$$|\Psi\rangle \propto \int_V d^3 r \psi_p (r) \psi_s (r) \psi_i (r) |\psi_s, \psi_i\rangle \tag{3.6}$$

derivation of which is given in greater detail in *Section* 4.1. Here ψ_s and ψ_i corresponds to the signal and idler mode functions respectively.

In order to study the effect of OAM on the second order correlation function of SPDC photons, we need a more generic expression which clearly establishes the connection between the two. As is well known, OAM forms a complete basis and any state can be expanded in terms of it. The down converted two-photon state can be written as

$$|\psi\rangle = \sum_{l_s, l_i} C_{l_s, l_i} |l_s\rangle |l_i\rangle \tag{3.7}$$

where $l_s, l_i \in \{-\infty, \infty\}$. The normalized $|C_{l_s,l_i}|^2$ is the probability of the signal and idler photons having OAM l_s and l_i respectively. The OAM of signal and idler modes are constrained by the conservation relation $l_s + l_i = l_p$ where l_p is the OAM of pump photon. To see how the OAM affects the second order correlation function, we consider the case where the idler photon is in the OAM state such that $l_i = 0$ and $l_s = l_p - l_i = l_p$. The corresponding coefficient $C_{l_p,0}$ can be calculated from the mode overlap integral as follows

$$C_{l_p,0} = \int \mathrm{d}\mathbf{r} \Phi_p\left(l_p, \mathbf{r}\right) \Phi_s^*\left(l_p, \mathbf{r}\right) \Phi_i^*\left(0, \mathbf{r}\right) \tag{3.8}$$

where $\Phi_k\left(l_k, \mathbf{r}\right)$ is the spatial mode function of the k-th mode. In case the pump, signal and idler are all written in terms of LG modes, Equation 3.8 is evaluated to have the following closed form [83]

$$C_{l_p,0} = \frac{1}{3}\sqrt{\frac{8}{\pi}}\left(\frac{2}{3}\right)^{|l_p|}. \tag{3.9}$$

The coincidence probability, or probability of the idler and signal photons being in $l = 0$ and l_p OAM states respectively, is then calculated simply by taking the square of Equation 3.9. These are the probabilities P_{i,s_1} and P_{i,s_2}. Equation 3.2 can be re-framed in terms of these probabilities as follows

$$g^{(2)}(0) = \frac{P_{i,s_2} R_{s_1} \Delta t + P_{i,s_1} R_{s_2} \Delta t}{P_{i,s_1} P_{i,s_2}} \tag{3.10}$$

where we have assumed that all triple coincidence events happen only due to accidentals resulting from finite coincidence window, following the prescription of [100]. This can be further simplified to

$$g^{(2)}(0) = \left(\frac{R_{s_1}}{P_{i,s_1}} + \frac{R_{s_2}}{P_{i,s_2}}\right)\Delta t. \tag{3.11}$$

In an ideal situation, the rate of singles R_{s_1} and R_{s_2} should be equal to each other. Also, from Equation 3.9, it is easily seen that the coincidence probabilities P_{i,s_1} and P_{i,s_2} only depend on the OAM and therefore should be equal to each other. With these considerations, we can arrive at the following simplified form of the second order correlation function

$$g^{(2)}(0) = 2\left(\frac{R_s}{P_{i,s}}\right)\Delta t. \tag{3.12}$$

Since the quantity R_s is essentially a constant, the second order correlation function varies as the inverse of the coincidence probability.

3.2.2 Experiment and Results

In experiment we generate heralded signal photons from the SPDC process (Fig. 3.4) to study their statistical correlations. A diode laser (Toptica Topmode) of wavelength 405 nm is used as pump. Optical vortices of different orders, generated using spiral phase plates (SPP) (Holo/Or), are incident on a $\chi^{(2)}$ non-linear crystal (β-Barium Borate or BBO, 5x5x2 mm), which generates a cone of correlated pairs of down-converted photons at phase-matching conditions. Degenerate signal-idler pairs are selected using interference filters. The pump polarization is adjusted along crystal optic axis using a half wave plate ensuring maximum down-conversion. The idler photons are coupled to a single-mode fiber due to which only photons with OAM, $l_i = 0$ are selected in the idler arm. This ensures that the corresponding signal photons are carrying same OAM as the pump photon following the OAM conservation. The signal is equally split using a 50:50 beam splitter and each portion is coupled to a multi mode fiber. The idler and signals from the two ports of the beam splitter are then guided to single photon counting modules (Excelitas SPCM-AQRH-16-FC, dark counts $\sim$ 25 cps). The interference filters (IF) of pass band 810 $\pm$5 nm cut the undesired light at

detection. Optimizing fiber coupling using fiber collimators, maximum coincidences are achieved between signal and idler arms. The coincident photons are counted using a time to digital converter (ID800 TDC, IDQuantique). The coincidence window (Δt) for heralding is kept as 810 ps. The detector position, length of fibers and BNC connectors from SPCM to TDC are optimally matched such that the relative delay between all three detectors are zero. This is ensured by obtaining maximum two fold coincidences between i - s_1 and i - s_2.

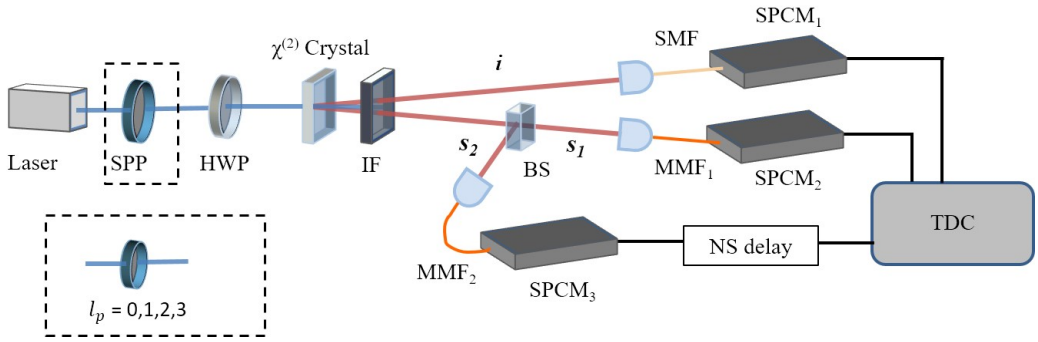

Figure 3.4: HBT-like setup to determine the second order correlation for a heralded single photon source. The delay generator (NS delay) introduces electronic delay in steps of 0.5 ns between the two output ports of the beam splitter (BS) in the signal arm.

The second order correlation function for $\tau = 0$, $g^{(2)}(0)$, measured in low power regime (pump power = 7 mW) for different OAM values of single photons is given in Table 3.1. For a single photon with $l = 0$, we have obtained $g^{(2)}(0) = 0.0082 \pm 0.0043$ from Equation 3.3. As the probability of detection of three-fold coincidences is very low, the statistical error in such measurements can be relatively high. Hence, we have also calculated $g^{(2)}(0)$ using Equation 3.4, where the direct measurements of three-fold coincidences are not used (bottom row, Table 3.1). Here, $g^{(2)}(0)$ is calculated with the assumption that three-fold coincidences result from the simultaneous occurrence of a two-fold coincidence (between the heralding photon and one of the signal photons) and an accidental coincidence in the third detector. In both cases, an increment in

$g^{(2)}(0)$ has been observed with the increasing orders of the OAM. We have calculated

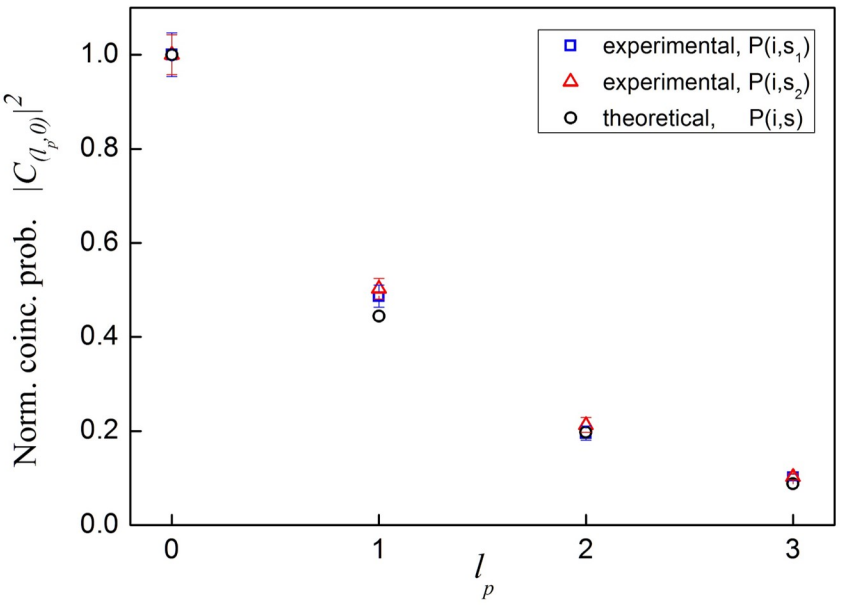

Figure 3.5: Variation of normalized probability $|C_{l_p,0}|^2$ (circle) and experimentally measured normalized probabilities $R_{i,s_1}/R_i$ (square) and $R_{i,s_2}/R_i$ (triangle), with l_p. Since idler is selected as Gaussian mode ($R_i = 1.75 \times 10^3/(s.mW)$), the twisted single photon OAM, $l = l_p$.

the two-fold detection probability, $P_{i,s_j} = R_{i,s_j}/R_i$ from experimentally observed rates and studied the variation for photons carrying different OAM. This is calculated for both P_{i,s_1} and P_{i,s_2} and when normalized they are shown to be matching exactly with theoretically calculated values for normalized two-fold detection probability, $|C_{l_p,0}|^2$, for the down-converted pair of photons to have OAM, $(l_p, 0)$ (Figure 3.5).

Second order correlation parameter, $g^{(2)}(0)$, has been calculated for the heralded single photons corresponding to different orders of the twisted single photon. The top row in Table 3.1 lists $g^{(2)}(0)$ obtained through the direct measurement of triple coincidences between the three detectors using Equation 3.3 for different orders of OAM. It can be seen that the error is larger compared to the bottom row since very few triple co-

incidences are registered even for longer exposure times. This error corresponds to the statistical standard deviation determined using the error propagation formula in Equation 3.3. The bottom row gives the same, but the non-zero value of $g^{(2)}(0)$ is modelled to be due to potential accidental coincidences which arise when a random detection is recorded along with a true two-fold coincidence between the other two detectors (Equation 3.4). This indirect method provides a better alternative, as the two-fold coincidences are easier to measure and optimize compared to three-fold coincidences. Here, we obtain slightly lower value for $g^{(2)}(0)$ with reduced standard deviation compared to the direct measurement from three-fold coincidences. It is also observed that $g^{(2)}(0)$ is increasing with increasing order of OAM of twisted photons. It is shown in Figure 3.5 that the two-fold coincidence probability between the idler-signal arms decreases with pump OAM since the OAM content corresponding to $(0, l_p)$ modes in the down-converted output decreases. As a result, the relative probability of accidental coincidences with respect to true two-fold coincidences increases and it is visible as an increment in $g^{(2)}(0)$ with OAM.

Twisted photon OAM, $l = l_p$	0	1	2	3
a) $g^{(2)}(0)$: direct	0.0082 $\pm$ 0.0043	0.015 $\pm$ 0.011	0.030 $\pm$ 0.057	0.045 $\pm$ 0.17
b) $g^{(2)}(0)$: indirect	0.0047 $\pm$ 0.00013	0.0094 $\pm$ 0.00028	0.021 $\pm$ 0.00094	0.042 $\pm$ 0.0016

Table 3.1: Second order correlation, $g^{(2)}(0)$, for a single photon source calculated **a)** directly from the measured three fold coincidences using Equation 3.3 and **b)** indirectly from the two-fold coincidences by considering the three-fold detection as probabilistic accidental coincidences with the heralding arm using Equation 3.4.

The experimentally calculated values for second order correlation (Table 3.1) obtained from the indirect method given in Equation 3.4 are plotted in Figure 3.6. The error bars correspond to the standard deviation obtained from uncertainties in count(and

coincidence) rates. The theoretical plot for the OAM dependent $g^{(2)}(0)$ as calculated from the coincidence probability (Equation 3.12) is also given. The coincidence win-

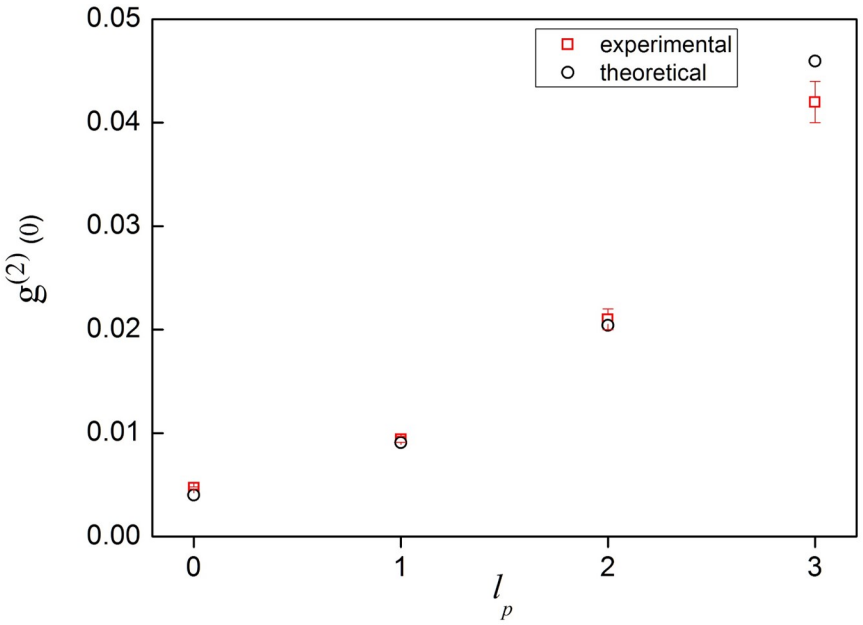

Figure 3.6: The variation of second order correlation function with OAM of the heralded single photon, $l = l_p$. Experimental (squares) and theoretical (circles) values are in good agreement.

dow is taken to be 810 ps. The experimental values are in good agreement with the theoretical predictions. Orbital angular momentum of photons has emerged over years as a strong candidate for information encoding in quantum information protocols using heralded single photons. Variations in the statistics of twisted single photons will become relevant while dealing with OAM of photons generated in parametric down-conversion. The results are of greater importance since an intuitive guess do not associate a quantity like second order correlation ($g^{(2)}(0)$) to be dependent on the OAM of the photon.

3.3 Conclusions

We have calculated the second order coherence function with zero delay, $g^{(2)}(0)$ for different OAM values of heralded single photons. It was calculated from the direct measurement of the simultaneous detection between the three detectors in a heralded HBT experiment as well as through a model that accounts for the accidental three-fold coincidences. In both cases, $g^{(2)}(0)$ is found to be increasing with the increasing order of the OAM for the twisted photons. We project the SPDC output in a specific state, $(0,l)$, in order to obtain twisted photon carrying an OAM value, l. The probability of generation of correlated photons in a specific state $(0,l)$ is dependent on l which we have also shown from the calculation of the overlap integral. The conditioned second-order correlation for HSPS is inversely proportional to this probability and hence $g^{(2)}(0)$ increases with OAM order as this probability decreases with OAM. An ideal single photon source need not show this kind of variation as we attribute this observation to the probability values arising from the overlap integral for the specific OAM selection that we are doing. In experiments related to quantum information using OAM of photons, pumping an SPDC crystal using vortex beams of different order and post-selecting the idler photon to a single mode fibre ($l_i = 0$) is a general technique to produce single photons carrying OAM. The results can be of significance while using such OAM states of single photons for quantum information applications.

Chapter 4

Engineering the OAM Spectrum in Parametric Down-Conversion

The method of spontaneous parametric down conversion or SPDC in short has been a long standing method for the generation of entangled photons [101]. In this method, a pump photon at a higher frequency is absorbed in a nonlinear crystal and two photons at lower frequencies are emitted. The emitted photons obey the energy and momentum conservation laws which leads to the following conditions

$$\hbar\omega_p = \hbar\omega_s + \hbar\omega_i \tag{4.1a}$$

$$\hbar\vec{k}_p = \hbar\vec{k}_s + \hbar\vec{k}_i \tag{4.1b}$$

where the subscripts p, s and i denote *pump*, *signal* and *idler*, respectively. Under degenerate phase matching condition, the emitted photons have identical angular frequencies $(\omega_s = \omega_i = \omega_p/2)$. In this situation, photons sampled from diametrically opposite points on the emission cone (assuming noncollinear phase matching) exhibit

maximum correlations in various degrees of freedom (DOF). These correlations arise from conservation principles of respective DOFs and have been verified to give rise to entanglement between the two photons [32, 102–105]. The presence of these correlations have led to the study of higher dimensional entanglement [106] as well as the generation and study of hyperentangled [107, 108] and hybrid-entangled states [109]. If the pair of photons are entangled in such a DOF that has an infinite dimensional Hilbert space, it may lead to higher dimensional entanglement. One such DOF is the orbital angular momentum (OAM) [110]. The OAM degree of freedom has been subjected to intense scrutiny over the years [111]. Light beam with OAM is most commonly defined by the Laguerre-Gauss (LG) modes [35] which are exact solutions of the paraxial wave equation in cylindrical coordinates and form a complete basis. Such modes are characterised by a well-defined azimuthal phase structure and spatially varying amplitude.

The conservation of OAM in the process of SPDC was experimentally demonstrated by Mair et al [52]. They also confirmed that besides conservation, the signal and idler photons are entangled in OAM. This gave rise to an entire array of literature that studied the use of OAM as a basis in various quantum information protocols. It was realised that d-dimensional quantum states or *qudits* can be implemented using the OAM basis [112, 113]. Amidst all these developments, the study of OAM spectrum of signal and idler photons assumed a lot of importance specifically from the point of generation of higher dimensional entangled states. But majority of the work have addressed the spectrum of down converted photons for either a Gaussian pump mode [114] or the LG pump modes [82, 115, 116]. Recently, it has been shown that any arbitrary spatial mode of the pump can be directly transferred to the signal and idler photons [117, 118]. Therefore, it becomes interesting to study how different spatial modes affect the OAM spectrum. In the work presented here, we aim to dwell on this

issue.

In this chapter, we study and compare the OAM spectrum of the SPDC photons for different spatial modes of the pump. First we take LG modes of varying order as the pump field and look into the spectrum when both the output photons are projected onto LG modes. Later, we replace the LG mode in the pump with perfect optical vortex (POV) [119] that is characterised by an annular ring shaped transverse profile, the radius and width of which remains fixed for all OAM values and look at the OAM distribution in signal and idler modes when projected to the LG modes. How the projection of the signal and idler modes to POV modes affects the spectrum, when a POV pump is used, is also discussed. In the last part of chapter, we discuss the effect of the OAM spectrum for different modes on the higher dimensional entanglement of biphotons.

4.1 Theoretical Background

The SPDC process is generally represented in the interaction picture using the Hamiltonian

$$H_I = \chi^{(2)} \int_V d^3 r E_p^+(r,t)\, \hat{E}_s^-(r,t)\, \hat{E}_i^-(r,t) \tag{4.2}$$

where $\chi^{(2)}$ is the susceptibility of the crystal, E_j is the electric field associated with the j-th mode. Signal and idler represented by subscript s and i are two output modes of the SPDC process. In a semi-classical approach, the pump field is considered strong compared to the signal and idler fields and treated classically. We write it as

$$E_p^+(r,t) = \psi_p(r) \exp\left(i\left(k_p z - \omega_p t\right)\right) \tag{4.3}$$

where $\psi_p(r)$ is the mode function governing the transverse field distribution of the pump. The signal and idler fields are treated quantum mechanically and written as

$$\hat{E}_j^-(r,t) = a_j^\dagger \psi_j(r) \exp\left(i\omega_j t\right) \tag{4.4}$$

where $j \in \{s,i\}$. $a_j^\dagger$ is the bosonic creation operator for the j-th mode. It creates a photon in the j-th mode with transverse mode function ψ_j and energy $\hbar\omega_j$. The two photon wavefunction is then written as

$$|\psi(t)\rangle = -i\exp\left(\int dt' H\left(t'\right)\right)|00\rangle \tag{4.5}$$

which under first order expansion yields the form

$$|\psi(t)\rangle = \int dt' H\left(t'\right)|00\rangle \tag{4.6}$$

The time integral can be solved by invoking the phase matching conditions of Eq. (4.1a). It results in a factor that modulates the wavefunction in time. Since it does not affect the spatial distribution of the signal and idler modes, we scale this factor to unity without any loss of generality. Eq. (4.6) can then be written as

$$\begin{aligned} |\psi(t)\rangle &= A\int_V d^3r E_p^+(r,t)\,\hat{E}_s^-(r,t)\,\hat{E}_i^-(r,t)\,|00\rangle \\ &= A\int_V d^3r \psi_p(r)\,\psi_s(r)\,\psi_i(r)\,a_s^\dagger a_i^\dagger |00\rangle \\ &= A\int_V d^3r \psi_p(r)\,\psi_s(r)\,\psi_i(r)\,|\psi_s,\psi_i\rangle \end{aligned} \tag{4.7}$$

where $|\psi_s,\psi_i\rangle$ is the two photon quantum state of the signal and idler photons associated with the mode functions $\psi_s(r)$ and $\psi_i(r)$ respectively and A is some constant in arbitrary units. The spectrum for any given pump can thus be calculated from Eq.

(4.7) by suitably modifying the mode functions to suit the purpose and calculating the overlap integral.

4.2 Orbital Angular Momentum Spectrum of Heralded Single Photons

Single photons carrying orbital angular momentum are most commonly represented using Laguerre-Gauss mode functions. These mode functions are exact solutions of the paraxial wave equation in cylindrical coordinates (ρ, ϕ, z). In the most general case, they can be represented as

$$\begin{aligned} \psi_{lp}(r,\phi,z) &= \sqrt{\frac{2p!}{\pi(|l|+p)!}}\sqrt{\frac{1}{w(z)}}\left(\frac{\sqrt{2}r}{w(z)}\right)^{|l|} e^{-il\phi} \\ &\times L_p^{|l|}\left(\frac{2r^2}{w^2(z)}\right)\exp\left(-\frac{r^2}{w^2(z)}\right) \end{aligned} \tag{4.8}$$

where l is the azimuthal index describing the helical structure of the photon, p is the number of radial nodes, $w(z) = w_0\sqrt{1+z^2/z_R^2}$ is the Gaussian beam width at distance z, z_R is the Rayleigh range and $L_p^{|l|}(x)$ is the associated Laguerre polynomial which is given by

$$L_p^{|l|}(x) = \sum_{m=0}^{p} \frac{(|l|+p)!}{(p-m)!(|l|+m)!m!}x^m \tag{4.9}$$

Optical fields described by Eq. (4.8) are also known as optical vortex fields due to the helical phase structure. The azimuthal index is then also referred to as the charge of the optical vortex. Now, looking at the $z = 0$ plane and scaling the beam waist w_0 to unity in arbitrary units, Eq. (4.8) can be simplified to

$$\psi_{lp}(r,\phi) = \sqrt{\frac{2p!}{\pi(|l|+p)!}}\left(\sqrt{2}r\right)^{|l|} L_p^{|l|}\left(2r^2\right)\exp(-r^2)\exp(-il\phi) \tag{4.10}$$

The above equation describes a photon with a Laguerre-Gaussian transverse mode function. Now, the two photon output state of SPDC can be written in the OAM basis as follows

$$|\psi\rangle = \sum_{l_s,l_i,p_s,p_i} C_{l_s,l_i}^{p_s,p_i} |l_s,p_s\rangle |l_i,p_i\rangle \tag{4.11}$$

where $|l_j,p_j\rangle$ denotes a single photon in the j-th mode characterised by the transverse distribution an LG mode with azimuthal index l_j and radial index p_j. The azimuthal index runs from $-\infty$ to ∞ while the radial index runs from 0 to ∞. The states with different OAM thus span an infinite-dimensional Hilbert space.

We are interested to find out how the azimuthal order l_p of the incident pump is distributed between the signal and idler photons. In order to do so, we need to calculate the expansion coefficients $C_{l_s,l_i}^{p_s,p_i}$. Comparing with Eq. (4.7), it is easily seen that

$$C_{l_s,l_i}^{p_s,p_i} = \int_V d^3r\ \psi_p(r)\,\psi_s(r)\,\psi_i(r) \tag{4.12}$$

where the mode functions are to be suitably replaced by LG mode functions as in Eq. (4.10) with proper indices. Taking the radial index of the pump, signal and idler to be identically 0, we can write Eq. (4.12) as

$$\begin{aligned} C_{l_s,l_i} &= \sqrt{\frac{2^3}{\pi^3 |l_p|!|l_s|!|l_i|!}}\, 2^{\frac{|l_p|+|l_s|+|l_i|}{2}} \\ &\times \int r dr d\phi\ r^{|l_p|+|l_s|+|l_i|} e^{-3r^2} e^{i\Delta l\phi} \end{aligned} \tag{4.13}$$

where $\Delta l = l_p - l_s - l_i$. Since OAM is conserved in a down conversion process, l_s and l_i should always add up to l_p in both magnitude as well as helicity. Using this criterion, the ϕ integral is evaluated to 2π. The rest of the integral is evaluated using standard

integration technique to the following

$$C_{l_s,l_i} = P\left(\frac{2}{3}\right)^{L}\sqrt{\frac{1}{|l_p|!|l_s|!|l_i|!}}L! \tag{4.14}$$

where $L = (|l_p| + |l_s| + |l_i|)/2$. P is a constant independent of the azimuthal indices of any of the modes and is equal to $(1/3)\sqrt{8/\pi}$.

The probability that the signal and idler photons are created in the two-photon mode specified as (l_s,l_i), is given by,

$$P_{l_s,l_i} = |C_{l_s,l_i}|^2. \tag{4.15}$$

This probability is plotted against the modes corresponding to the signal photons for

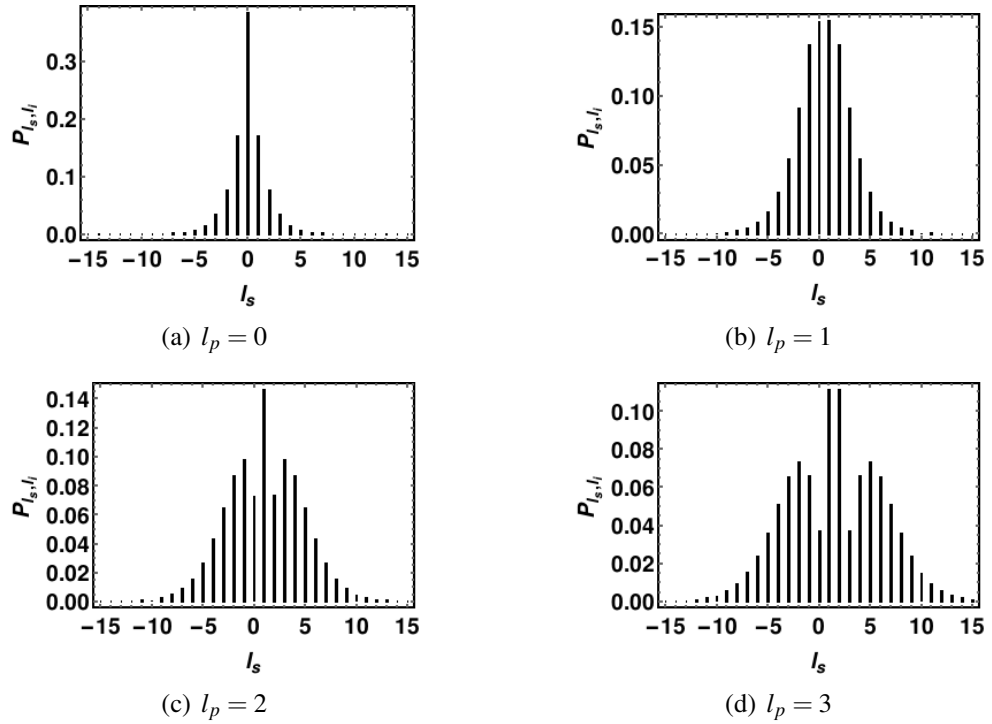

(a) $l_p = 0$ (b) $l_p = 1$

(c) $l_p = 2$ (d) $l_p = 3$

Figure 4.1: OAM spectrum of the signal and idler photons for different pump OAM such as a) fundamental Gaussian mode and b,c,d) LG modes with $l_p = 1,2,3$ respectively.

different OAM values of the pump, keeping the idler photon being selected for $l_i = 0$. In Fig. (4.1), we study the OAM spectrum of the LG modes. For a pure Gaussian mode ($l_p = 0, r_p = 0$), it is observed that the signal and idler modes always carry equal and opposite azimuthal charge. But the probability of both the photons being in a Gaussian mode is maximum. So, the combined two photon state does not carry any net azimuthal charge. This arises solely from OAM conservation. In this case the output state of the down conversion process can be simply written as

$$|\psi\rangle = \sum_{l=-\infty}^{\infty} C_l |l\rangle_s |-l\rangle_i \tag{4.16}$$

This means, individually, each mode is in a mixed state of the OAM basis. In case of the pump field being an optical vortex of charge 1, it is seen that the maximum probability shifts. The superposition state $|1,0\rangle + |0,1\rangle$ is the most probable state. An interesting pattern in the OAM spectrum is observed for all higher orders of the pump mode. For even orders, the superposition state $|\frac{l}{2}\rangle + |\frac{l}{2}\rangle$ has the maximum probability where l is the azimuthal index of the pump field. For odd orders, it is $|\frac{l+1}{2}, \frac{l-1}{2}\rangle + |\frac{l-1}{2}, \frac{l+1}{2}\rangle$ that has the maximum probability. Also, there is a secondary maxima for all higher orders of the pump field. This anomaly can be explained by further investigating Eq. (4.14). The factorial in the denominator is a decreasing function where as the factorial in the numerator is an increasing function. The secondary maxima occurs at those points where both the functions have similar weightage. This anomaly can be removed by using perfect optical vortex (POV) modes in place of LG modes [120, 121].

4.2.1 Spectral Decomposition for a Perfect Optical Vortex Pump

In literature, an ideal perfect optical vortex (POV) mode is written as

$$\psi(r,\phi) = \frac{i^{l-1}}{k_r}\delta(r-r_0)\exp(il\phi) \tag{4.17}$$

where l is the azimuthal index as before, r_0 is the radius of the vortex in the transverse plane and k_r is the radial wave vector. But realizing such a distribution is an experimental impossibility. In practice, a modified form of Eq. (4.17) can be generated by Fourier transforming an optical vortex in the Bessel-Gauss mode as shown in [119]. A Bessel-Gauss vortex mode has the distribution

$$\psi_l^{BG}(\rho,\theta) = J_l(k_r\rho)\exp(il\theta)\exp\left(\frac{-\rho^2}{w^2}\right) \tag{4.18}$$

where J_l is the Bessel function of the first kind of order l and w is the beam waist of the Gaussian envelope. This is Fourier transformed using a simple lens governed by the equation

$$\begin{aligned}\psi(r,\phi) &= \frac{k}{i2\pi f}\int_0^\infty\int_0^{2\pi}\psi(\rho,\theta) \\ &\times \exp\left(\frac{-ik}{f}\rho r\cos(\theta-\phi)\right)dV\end{aligned} \tag{4.19}$$

where f is the focal length of the lens used, $k = 2\pi/\lambda$ is the magnitude of the total wave vector and $dV = \rho d\rho d\phi$. Eq. (4.18) and Eq. (4.19) can be used to derive an usable form of the POV mode as follows

$$\psi_l^{POV}(r,\phi) = i^{l-1}\frac{w}{w_0}\exp(il\phi)\exp\left(-\frac{r^2+r_0^2}{w_0^2}\right)I_l\left(\frac{2r_0r}{w_0^2}\right) \tag{4.20}$$

where, I_l is the l-th order modified Bessel function of first kind and has the form, $I_l(Z) = e^{\frac{-im\pi}{2}} J_l(Ze^{\frac{i\pi}{2}})$.

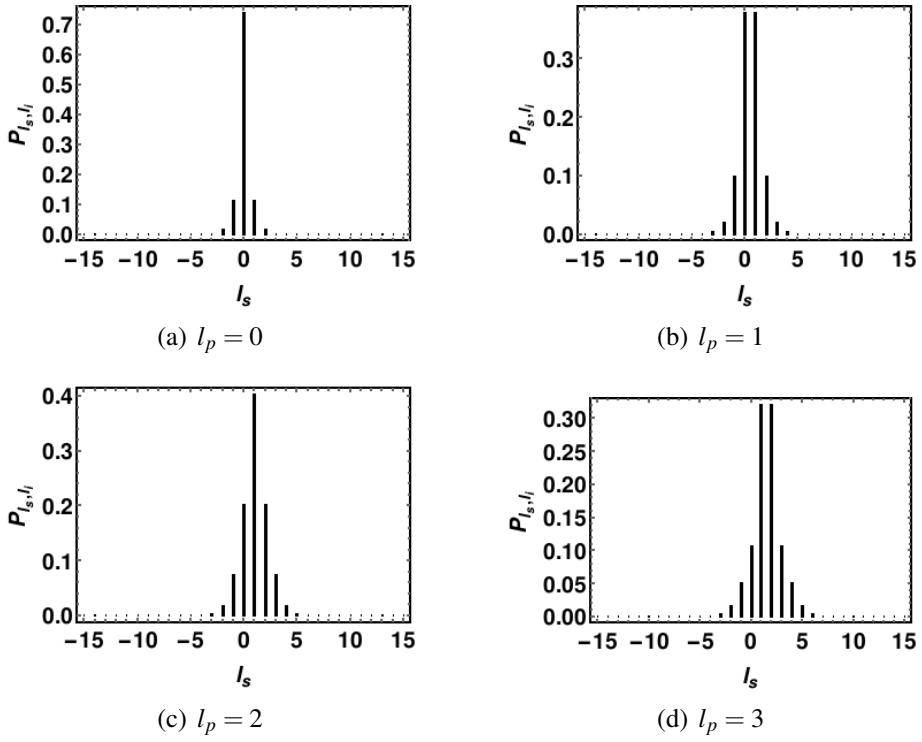

(a) $l_p = 0$ (b) $l_p = 1$

(c) $l_p = 2$ (d) $l_p = 3$

Figure 4.2: OAM spectrum of the signal and idler photons for different pump OAM. Here the pump is in a POV mode ($l = l_p$) and the signal and idler are projected to LG modes.

This is the same equation as Eq. (7) in [119]. Here, $r_0 = k_r f/k$ is the radius of the vortex ring of width w_0. An advantage of POV modes over other conventional vortex modes like LG and Bessel-Gaussian is that the diameter of the vortex ring is independent of the order of the vortex. The transverse distribution increases in size with increasing order of the vortex in case of LG and BG modes. But in case of POV modes, it remains invariant. This leads to better coupling efficiency with single mode fibers after phase flattening by using a computer generated hologram or a spatial light modulator.

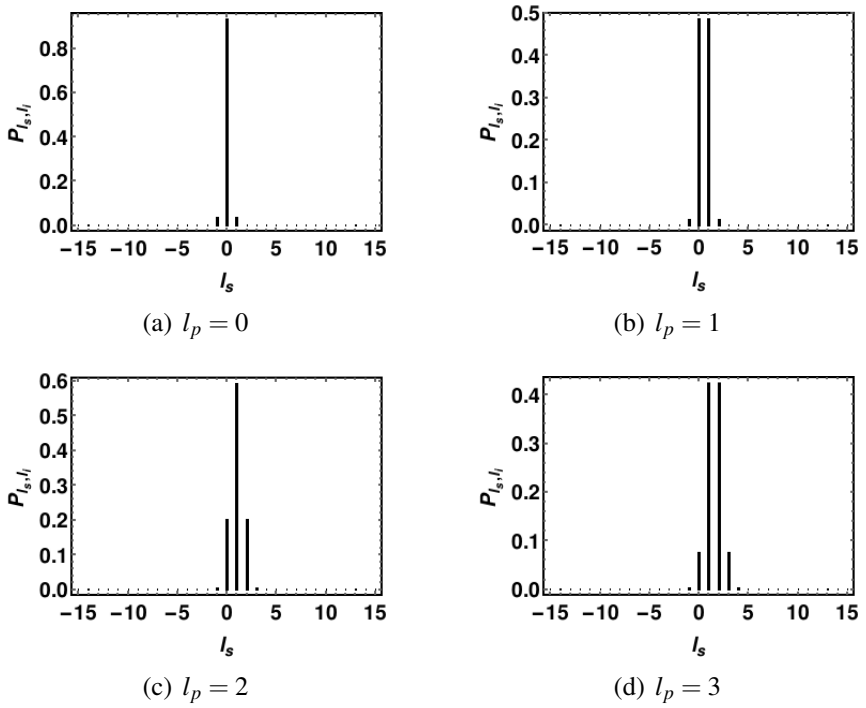

(a) $l_p = 0$ (b) $l_p = 1$

(c) $l_p = 2$ (d) $l_p = 3$

Figure 4.3: OAM spectrum of the signal and idler photons for different pump OAM. Here the pump is in a POV mode and the signal and idler are projected to POV modes.

Let us now consider the case where we use an optical vortex in a POV mode as the pump and project the signal and idler modes to LG modes given by Eq. (4.10). We want to study how the projection of a POV mode to LG modes affects the OAM spectrum. In this case the overlap integral Eq. (4.12) takes the form

$$C^{POV}_{l_s,l_i} = \int_V d^3r \; \psi^{POV}(r)\, \psi_{l_s}(r)\, \psi_{l_i}(r) \tag{4.21}$$

where the indices are self-explanatory and have similar meaning as before. Using Eq. (4.20) and Eq. (4.10) with correct indices in the above equation gives rise to the expansion coefficients $C^{POV}_{l_s,l_i}$. Proceeding as before we see from Fig. 4.2 that it gives rise to a much narrower OAM spectrum. As expected, the most probable states are still the same as before with an added advantage that the decomposition does not give rise to the previously observed secondary maxima. The spectrum can be further

narrowed by projecting the output modes to POV modes as can be seen from Fig. 4.3. In this case the presence of higher order OAM modes is further reduced. This shows that projecting onto POV modes is the most efficient method to generate entangled photons in specific OAM modes with maximum probability as compared to the other two cases. It would be interesting to study how higher dimensional entanglement between the signal and idler photons are affected by the different OAM spectra which we do in the next section.

4.3 Experimental Results

The experimental scheme for studying the OAM spectrum corresponding to different spatial modes is given in Figure 4.4. A 405 nm pump laser is incident on spa-

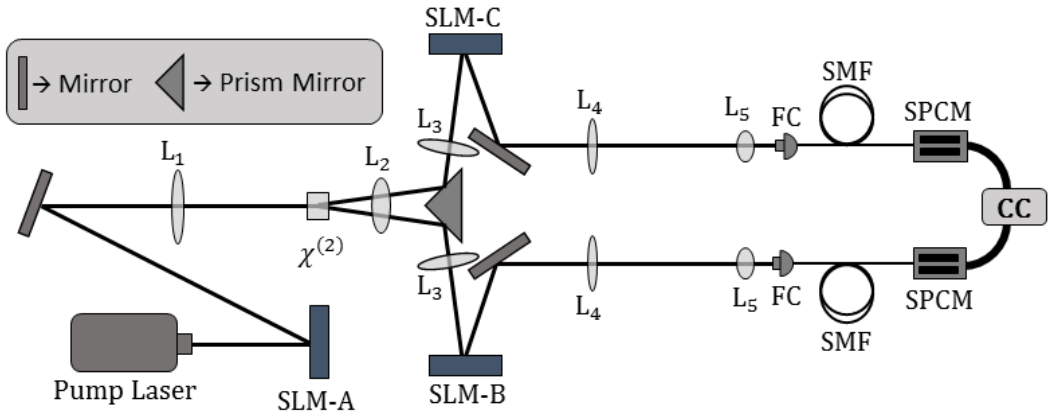

Figure 4.4: Experimental schematic. The pump is prepared in any desired spatial mode by using the spatial light modulator (SLM-A). L1 is Fourier transforming lens that is used along with SLM-A to prepare the pump in POV modes. χ^2 is a nonlinear crystal where the downconversion takes place. A prism mirror is used to deflect the signal and idler along different paths. SLM-B and SLM-C is used to project the signal and idler photons to different spatial modes which are then detected at the SPCM (single photon counting module). FC is fibre coupler, SMF is single mode fibre, CC is coincidence counter and L2-L5 are imaging lens.

tial light modulator (SLM-A) where any desired mode is generated through computer generated holograms. The structured pump beam is then incident on a $\chi^{(2)}$ non-linear

crystal. The down-converted signal and idler photons are separately imaged from the crystal plane to individual SLMs (SLM-B and SLM-C) using lens pairs. A prism mirror is used to separate the idler and signal photons falling at diametrically opposite regions. The SLM plane is again imaged using lens combinations to the fiber tip con-

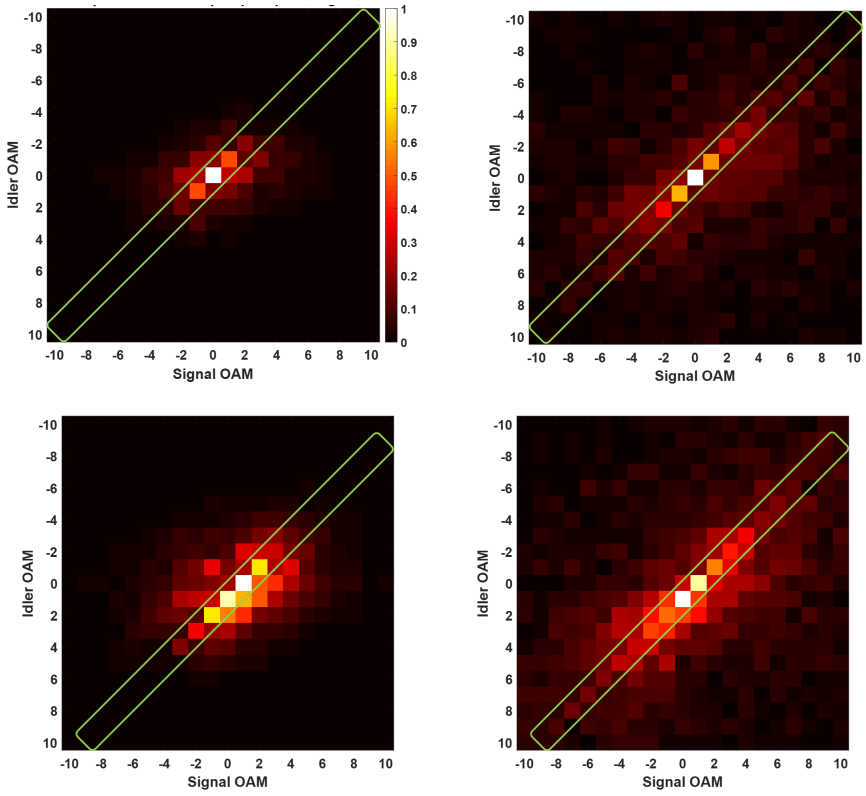

Figure 4.5: Coincidence profiles corresponding to projections in LG and BG basis for a POV pump. (Top row, left) projections in LG, $l_p = 0$, (top row, right) projections in BG, $l_p = 0$, (bottom row, left) projections in LG, $l_p = 1$, and (bottom row, right) projections in BG, $l_p = 1$.

nected to fiber couplers (FC) which then couple the phase-flattened Gaussian photons to the single mode fibers. A time-to-digital correlator gives the coincidence counts corresponding to each choice of mode projections. We used a perfect optical vortex (POV) as pump and OAM projections are carried out in the down-converted output in LG and BG basis. The coincidence profiles corresponding to projections in different OAM orders in each basis is calculated for a Gaussian as well as vortex pump (Figure 4.5).

The top row corresponds to a Gaussian pump while the bottom row corresponds to a vortex pump having $l_p = 1$. The left panel shows coincidence profile corresponding to projections in the Laguerre-Gaussian (LG) basis whereas the right panel corresponds to projections in the Bessel-Gaussian (BG) basis. As it can be clearly seen from the fig-

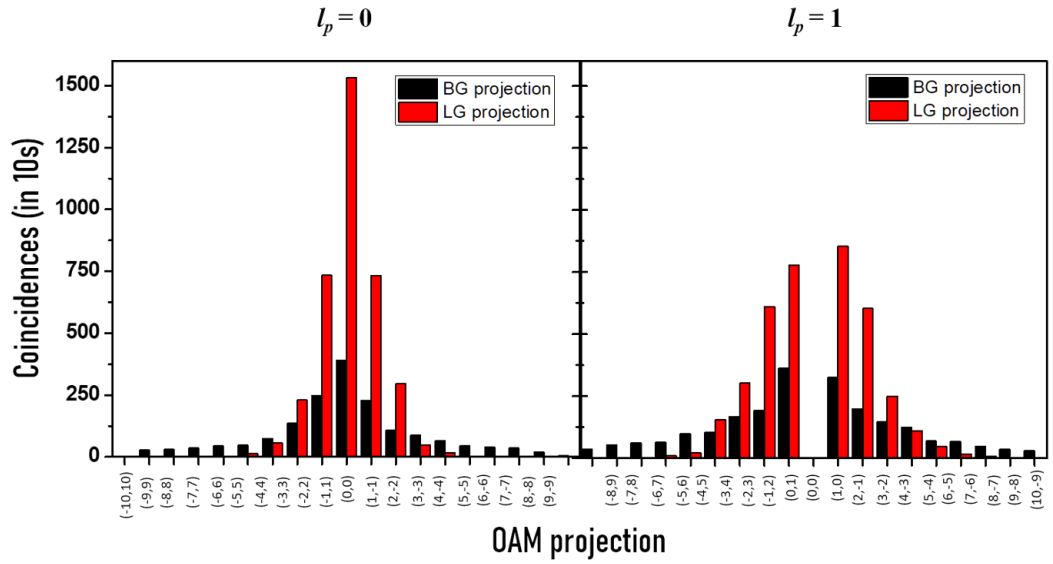

Figure 4.6: OAM correlations corresponding to the combinations along the diagonals marked within the green rectangles in Figure 4.5 corresponding to (left) Gaussian pump and (right) vortex pump with $l_p = 1$. On the right hand side the central position is vacant as (0,0) correlations will be absent for a vortex pump with $l_p = 1$.

ure, the OAM distribution in LG basis provides a narrower spectrum compared to that in BG basis. The projections corresponding to the correlated pairs, predicted by OAM conservation, is highlighted in a green rectangle. The OAM spectrum corresponding to these values are given separately for a better understanding in Figure 4.6. It can be clearly seen that the OAM correlations in the LG basis give a narrower spectrum compared to the BG basis.

4.4 Entanglement in the OAM basis

In this section we study the entanglement between the signal and idler modes in the OAM basis. Rewriting Eq. (4.11) in a basis independent form, we obtain

$$|\psi\rangle = \sum_{l_s=-\infty}^{\infty} C_{l_s}^{l_p} |l_s\rangle |l_p - l_s\rangle \tag{4.22}$$

where only OAM conservation $l_p = l_s + l_i$ is assumed. Since this is a pure state, the entanglement between the signal and idler modes can be faithfully quantified using the von Neumann entropy [122, 123]. For a bipartite state $|\psi_{AB}\rangle$, it is defined as

$$S_B = -\sum_k \lambda_k \log_d \lambda_k \tag{4.23}$$

where λ_k's are the eigenvalues of the reduced density matrix $\rho_B = Tr_A\ (\rho_{AB})$. Here Tr_A stands for partial trace operation that acts only on the A part and $\rho_{AB} = |\psi_{AB}\rangle\langle\psi_{AB}|$ is the density matrix of the combined system. Here the logarithm is taken on base d where d stands for the dimensionality of the system. For example, $d = 2$ for a two dimensional system. Therefore, an advantage of using the von Neumann entropy as a quantifier of entanglement is that it can be used even for higher dimensional entanglement. From Eq. (4.22) it is easy to see that

$$\rho_{s,i} = \sum_{l_s, l_s'} C_{l_s}^{l_p} C_{l_s}^{l_p *} |l_s, l_p - ls\rangle\langle l_s', l_p - l_s'| \tag{4.24}$$

from which it immediately follows that

$$\rho_i = \sum_{l_s} |C_{l_s}^{l_p}|^2\ |l_p - ls\rangle\langle l_p - l_s| \tag{4.25}$$

where ρ_i is the reduced density matrix for the idler mode. Equation 4.25 resembles the Schmidt decomposition for a biphoton state in the OAM basis. It is the diagonal representation of the reduced density matrix of any quantum state. The expansion coefficients are the non-zero elements of this diagonal matrix. It has the interesting property that the Schmidt rank or the number of the coefficients in the decomposition can be directly used as an indicator of entanglement [124]. The reduced state is entangled iff the Schmidt rank is more than *1*, else it is separable. The coefficients $|C_{l_s}^{l_p}|^2$ can then be used in place of λ_k in Eq. (4.23) to calculate the entropy. These coefficients are the same as calculated from the overlap integral in the previous section.

l_p	LG $\rightarrow$ (LG,LG)	POV $\rightarrow$ (LG,LG)	POV $\rightarrow$ (POV,POV)
0	1.8537	0.8850	0.3662
1	2.4014	1.3921	0.8165
2	2.7030	1.6016	1.0025
3	2.9133	1.6998	1.1361
4	3.0683	1.7469	1.2397

Table 4.1: von Neumann entropy (in arbitrary units) of the idler mode calculated after tracing out the signal mode. l_p is the OAM of the pump field.

In Table I, we study the higher dimensional entanglement of the down converted photons for each of the decomposition considered earlier while studying the OAM spectrum. Please note that the results presented are in non-normalized arbitrary units. It is observed that maximum entanglement is seen to be present in case of LG $\rightarrow$ (LG, LG) for all values of the pump OAM as compared to the other two cases. The entanglement between the signal and idler photons is least when all the three modes, pump, signal and idler, are in POV modes. This is due to the decreasing probability of the occurrence of higher order OAM states in the OAM basis expansion for each decomposition. Comparing Fig. 4.1, Fig. 4.2 and Fig. 4.3, the probability of higher order OAM states is much higher when using a LG mode as the pump as well as

projecting both signal and idler photons to LG modes. The probability decreases when the pump is replaced by a POV mode for the same projection scenario and is least when both the output photons are projected to POV modes.

4.5 Conclusions

We have studied the OAM spectrum of down converted photons for different pump modes. We considered LG and POV pump modes of various orders and looked at the resulting OAM spectrum of the SPDC photons for multiple projection scenarios. Specifically, we looked at those cases when both signal and idler photons are projected onto LG modes or POV modes. In order to compare the different projection scenarios on an equal footing, we considered only those LG modes for which the radial index is 0 since POV modes do not have any radial index. We found that projection of the output photons onto LG modes for a LG pump gave rise to a wide spectrum. It was noticed that higher order LG pump gives rise to secondary maxima. Replacing the pump with a POV mode removed this anomaly as well as narrowed down the spectrum. The narrowest spectrum was obtained when down converted photons were projected onto POV modes. In this case the probability of occurrence of higher order OAM states in the spectrum was reduced to a minimum and the spectrum was seen to be sharply peaked at those values of OAM for which the difference in OAM carried by signal and idler photon, $|l_s - l_i|$ is either 0 or 1. This narrowing can be attributed to the improved orthogonality between modes when we introduce POV instead of LG. The orthogonality condition in the mode overlap is better satisfied when proper mode matching takes place. In POV, the mode size is invariant of the OAM order and the orthogonality condition is satisfied very well. This amounts to greater correlation between the complimentary modes and reduced correlation with the other modes resulting in a narrow distribution. The narrowing of the spectrum, however, comes with a trade-off. It leads

to lower overall high-dimensional entanglement between signal and idler photons. So, to generate greater high-dimensional entanglement, a wider spectrum is required. This is found in the case of LG $\rightarrow$ (LG, LG). But if a narrower spectrum is required (higher probability of the downconverted photons being in a specific OAM state), the best case scenario is the use of POV mode as pump as well as projection of signal and idler photons to POV modes.

Chapter 5

Investigating Duality of Entanglement using Twisted Photons

Complementarity is a unique manifestation of quantum mechanics, like entanglement. Introduced as a concept by Niels Bohr [125] and developed through further rigorous scientific discussions, complementarity broadly states that objects possess mutually exclusive properties such that the full knowledge of one property precludes full knowledge of the conjugate one. The wave-particle duality, Heisenberg's uncertainty principle etc. could be understood as consequences of the complementarity principle. *Welcher weg* (which-path) experiments demonstrate the complementarity between distinguishability and interference visibility implying that quantum interference will take place only if the measurement does not distinguish between the interfering pathways [126–128]. In other words, indistinguishability leads to quantum interference. In addition, the distinguishability of photons reduces the entanglement as well. Many studies have aimed towards reducing the distinguishability in entangled systems [129–131].

5.1 Indistinguishability of Photons and Duality of Entanglement

Indistinguishablity of photons evoke interest in quantum information protocols. It is a necessary criteria in quantum teleportation [132]. Indistinguishability requires perfect overlap in spatio-temporal positions, energy, and polarization which can be demonstrated through two-photon interference experiments. Recent studies involving integrated semiconductor chips aim towards providing sources that generate indistinguishable photons [133, 134]. Two-photon interference of identical photons gives an output of indistinguishable photons. But, it is not possible to observe the entanglement between such indistinguishable photons unless we sort and separate them under some label, be it position, polarization, OAM etc. In this chapter, we demonstrate the entanglement separation using the orbital angular momentum of the twisted photons.

As it is discussed in Chapter 1, entanglement can be of different types. For the simple case of a bipartite entanglement, the entangled particles could belong to a single vector space spanned by the tensor product of the Hilbert space corresponding to two particles. For a photon showing hybrid entanglement, they could as well belong to the vector space spanned by the tensor product of Hilbert spaces defined for different degrees of freedom. The most discussed examples involve the entanglement in the same degree of freedom (polarization/OAM/time etc.) of two spatially separated photons. In the case of hybrid-entanglement, entanglement is between two different degrees of freedom of a single photon (or beam in the case of classical non-separability). In the former case, the spatial position (or momentum) is used to label the subsystems while the independent degrees of freedom (such as polarization-path or polarization-OAM etc.) differentiates the subsystems in the latter. The entanglement between identical

particles can be observed by using their degrees of freedom to label the particles. For a general case of degenerate, non-collinear Type-II SPDC output, we can write the identical photons in terms of their different degrees of freedom as,

$$|\Psi\rangle = \frac{1}{\sqrt{2}}\left(|H,\mathbf{k}_i\rangle\,|V,\mathbf{k}_s\rangle + |V,\mathbf{k}_i\rangle\,|H,\mathbf{k}_s\rangle\right), \tag{5.1}$$

where the state is written in terms of polarization and linear momentum. This can also be written as the general expression for a polarization entanglement as,

$$|\Psi\rangle = \frac{1}{\sqrt{2}}\left(|H\rangle_{k_i}\,|V\rangle_{k_s} + |V\rangle_{k_i}\,|H\rangle_{k_s}\right), \tag{5.2}$$

using their linear momentum as a label to differentiate the subsystems. The principle of duality of entanglement as discussed in Chapter 1 allows us to express the same state as,

$$|\Psi\rangle = \frac{1}{\sqrt{2}}\left(|k_i\rangle_H\,|k_s\rangle_V + |k_s\rangle_H\,|k_i\rangle_V\right). \tag{5.3}$$

This complimentarity between the two independent degrees of freedom of the indistinguishable particles is called duality in entanglement [60, 135].

For collinear output, the position labelling given in Equation 5.2 becomes unavailable since $k_i = k_s = k_p$. Hence it becomes impossible to observe the entanglement. We propose that the OAM of the twisted photons defined in their even-odd basis can be used to separate the otherwise completely indistinguishable photons in the collinear output. If we use a pump carrying an odd OAM, following the conservation of OAM, the generated OAM state of SPDC photons will be generated in pairs of even and odd OAM states. For example, if we use pump OAM, $l_p = 1$, in a collinear Type-II SPDC process where the idler-signal pairs are generated in orthogonal polarization states, the

output OAM state can be written as,

$$\begin{aligned}|\Psi\rangle_{SPDC} &= \sum_{m=-\infty}^{+\infty} c_m |m\rangle_H |1-m\rangle_V \\ &= c_{0,1}|0\rangle_H|1\rangle_V + c_{1,0}|1\rangle_H|0\rangle_V + c_{2,-1}|2\rangle_H|-1\rangle_V + c_{-1,2}|-1\rangle_H|2\rangle_V + ... \\ &= \frac{1}{\sqrt{2}}(|even\rangle_H|odd\rangle_V + |odd\rangle_H|even\rangle_V).\end{aligned} \tag{5.4}$$

Here, the idler and signal photons are not distinguishable, but when we use the polarization state to label the individual photons generated in a pair, we see the entanglement in even-odd basis of the OAM. In the same way, the state in Equation 5.4 can be written by labelling them as even and odd OAM states,

$$|\Psi\rangle_{SPDC} = \frac{1}{\sqrt{2}}(|H\rangle_{even}|V\rangle_{odd} + |V\rangle_{even}|H\rangle_{odd}). \tag{5.5}$$

Hence, depending upon whether the polarization or OAM has been used for the labelling, we can observe the entanglement in the other degree of freedom. It can be seen that the distinguishability of the associated particles reveal the entanglement. Sorting the photons based on the polarization can be achieved using a simple polarizing beam splitter which separates H and V, revealing the entanglement in even-odd OAM states. To observe the polarization entanglement, we use an even-odd OAM sorter which would function exactly as the name suggests.

5.2 Even-Odd basis for Orbital Angular Momentum of Light

The orbital angular momentum of light presented a new degree of freedom for quantum information processing using photons. Optical communication and quantum

information transfer using OAM states of light has gathered interest more than ever in the past decade [52, 136–140]. The Hilbert space associated with the OAM states generated in SPDC could be arbitrarily large in principle and hence find applications in higher-dimensional quantum information processing [67, 141]. However, it is a fundamental requirement to sort and separately measure the OAM states from the incoherent mixture coming out in signal as well as idler arms. The conventional and commonly used method for sorting and measuring the OAM component of photons is by phase-flattening the spiral phase corresponding to a desired OAM state, and coupling the resulting fundamental Gaussian mode to a single mode fiber. The phase-flattening could be done using a spatial light modulator carrying the corresponding computer generated holograms or Spiral phase plates. However, such projective measurements based on phase-flattening have shortcomings in terms of efficiency and dependence on pump characteristics [142].

In most protocols involving the entanglement of orbital angular momentum of photons, the infinite dimensional OAM spectrum in the output of parametric down-conversion is restricted to a two-dimensional basis by the post-selection of the twin-photons. This method omits a huge portion of the generated photons and thereby reduces the efficiency of entangled pair generation and the associated quantum information protocol itself. An alternate basis involves grouping all the generated pairs into two sections based on whether the photon OAM is even or odd [38]. The twin-photon OAM state in the output of the parametric down-conversion can be written in terms of

the even-odd basis as,

$$\begin{aligned}|\Psi\rangle_{12} &= \sum_{m=-\infty}^{+\infty} c_m |m\rangle_1 |1-m\rangle_2 \\ &= \sum_{k=-\infty}^{+\infty} c_{2k} \left(|2k\rangle_1 |1-2k\rangle_2\right) + \sum_{k=-\infty}^{+\infty} c_{2k+1} \left(|2k+1\rangle_1 |-2k\rangle_2\right) \\ &= \frac{1}{\sqrt{2}}(|e\rangle\,|o\rangle + |o\rangle\,|e\rangle)\end{aligned} \tag{5.6}$$

Using this two-dimensional even-odd basis for the twin-photon OAM states, the efficiency of entanglement protocols could be increased. To formulate the state represented in the even/odd basis, we define the projective operators that are,

$$\begin{aligned}P_0 &= \sum_k (|2k\rangle\langle 2k| + |2k+1\rangle\langle 2k+1|) \\ P_1 &= \sum_k (|2k\rangle\langle 2k| - |2k+1\rangle\langle 2k+1|) \\ P_2 &= \sum_k (|2k\rangle\langle 2k+1| + |2k+1\rangle\langle 2k|) \\ P_3 &= \sum_k i(|2k\rangle\langle 2k+1| - |2k+1\rangle\langle 2k|)\end{aligned} \tag{5.7}$$

The corresponding Stokes parameters can be obtained as,

$$\begin{aligned}s_0 &= \langle\psi\,|P_0|\,\psi\rangle \equiv \sum_k \left(c_{2k}c_{2k}^* + c_{2k+1}c_{2k+1}^*\right) \\ s_1 &= \langle\psi\,|P_1|\,\psi\rangle = \sum_k \left(c_{2k}c_{2k}^* - c_{2k+1}c_{2k+1}^\dagger\right) \\ s_2 &= \langle\psi\,|P_2|\,\psi\rangle \equiv \sum_k \left(c_{2k}^*c_{2k+1} + c_{2k}c_{2k+1}^*\right) \\ s_3 &= \langle\psi\,|P_3|\,\psi\rangle \equiv i\sum_k \left(c_{2k}^*c_{2k+1} - c_{2k}c_{2k+1}^*\right).\end{aligned} \tag{5.8}$$

Measurements in the linear basis, which can be simply obtained at the even and odd output ports of an even-odd sorting setup would give us s_0 and s_1. The remaining two

Stokes parameters can be obtained through the measurements in a diagonal basis that can be experimentally achieved using a spiral phase plate (which acts as a NOT gate in even-odd basis) and setting up an interferometer in the sorter output. The validation of this basis as well as the associated projective measurements and Bell's inequality are discussed in detail in [143].

5.2.1 Sorting of OAM in Even-odd Basis

Figure 5.1 illustrates a basic set up for an even-odd OAM sorter. A dove prism flips the OAM from $+l$ to $-l$ during the internal reflection. When two Dove prisms are kept in the two arms of an interferometer, it introduces an OAM dependent relative phase $2l\alpha$ where α is the relative rotation of the Dove prisms. In Figure 5.1, the two Dove prisms are oriented perpendicular to one another and hence $\alpha = \pi/2$. This introduces a phase $l\pi$ between the two arms of the interferoemeter. For all odd OAM orders this would

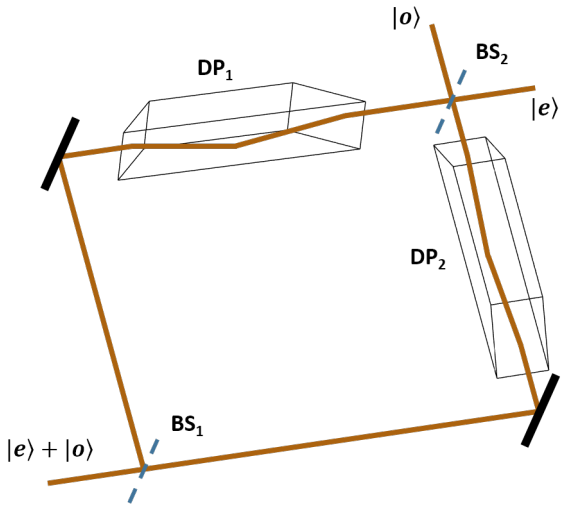

Figure 5.1: Interferometric sorter for even and odd OAM states of light using Dove prism. The Dove prism introduces an OAM dependent phase $2l\alpha$ where α is the relative rotation of the Dove prisms in both the arms of the interferometer. In the figure, $\alpha = \pi/2$.

turn out to be odd multiples of π and even multiples of π for even OAM orders. The relative phase difference between the two interfering fields will differ by π for even and odd orders. As a result, the constructive interference will take place in different output ports for even and odd OAMs.

A common path Sagnac interfereometer provides a more stable sorting apparatus (Figure 5.2). The spatial light modulator changes the input spatial mode such that different orders of vortices are entering the sorting intereferometer. The SLM is sensitive to vertical polarizer, hence the HWP rotates the polarization to horizontal such that it is not lost in reflection at the intermediate polarizing beam splitter. The quarter wave plate kept at 45° rotates this horizontally polarized state to circular polarization. On

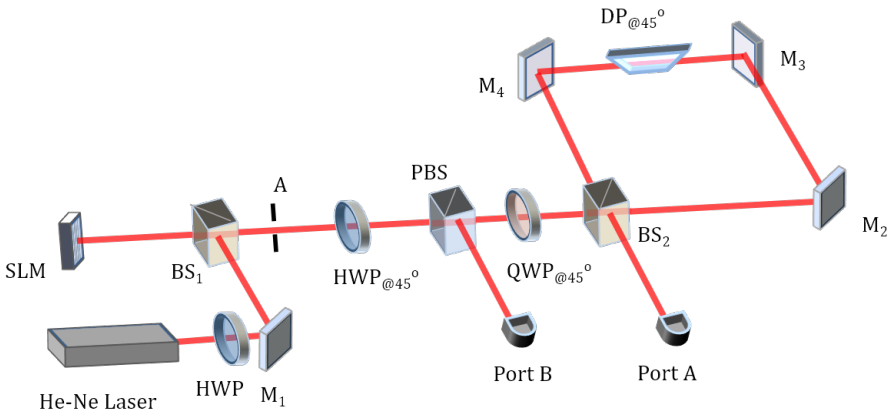

Figure 5.2: The experimental set-up corresponding to an even-odd OAM sorter using a common path interferometer. Different OAM orders are imparted in the source using a spatial light modulator (SLM), which gets separated in the two output ports A (odd port) and B (even port).

the way back, it again transforms the output of the interferometer along the input beam direction to vertically polarized light, which can be separated at the reflective output of the PBS (port B). When the Dove prism is absent in the interferometer, port A becomes the destructive port and we get constructive interference in port B. inside the common path interferometer, both the beams are passing through the Dove prism. Therefore

the relative phase introduced by the Dove prism would be twice here. When the Dove prism is kept at 45°, it introduces an l dependent phase $l\pi/2$ along say clockwise direction and $-l\pi/2$ along counter-clockwise direction. Hence, for odd OAM orders, a relative phase of $(2n+1)\pi$ is introduced between the counter-propagating beams, and $2n\pi$ for even orders where n is an integer.

The output intensity images of the sorter output is given in Figure 5.3. The top row corresponds to port B and the bottom row refers to port A in Figure 5.2. It shows that the even and odd OAM orders are effectively sorted in the two output ports. The common path interferometer provides a stable sorting setup compared to a Mach-Zehnder type configuration.

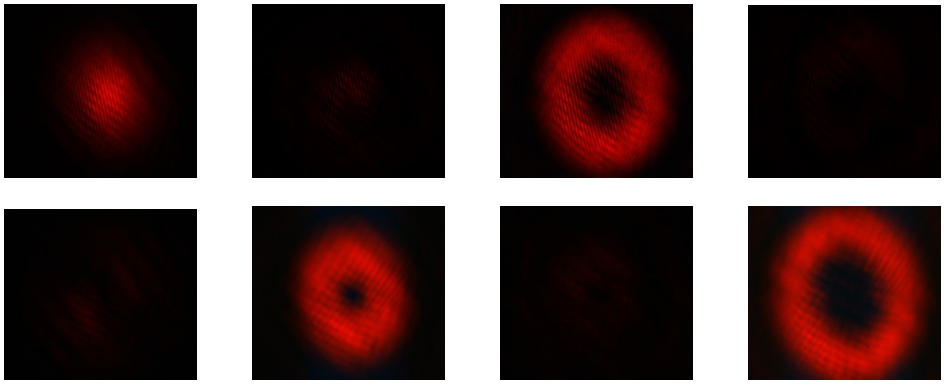

(e) $l_p = 0$ (f) $l_p = 1$ (g) $l_p = 2$ (h) $l_p = 3$

Figure 5.3: Output intensity images from the even port (top row) and odd port (bottom row) of the interferometric OAM sorter. Different charges corresponding to a) $l = 0$, b) $l = 1$, c) $l = 2$ and d) $l = 3$ can be seen to be giving constructive interference in the corresponding ports depending upon whether their OAM is even or odd.

5.3 OAM Sorting and Polarization Entanglement

We take a periodically-poled type-II KTP crystal to observe the duality in entanglement of polarization and OAM of twin photons generated in SPDC. In type-II SPDC, the idler and signal photons will have perpendicular polarizations along ordinary and

extra-ordinary directions such that,

$$o \longrightarrow e + o \tag{5.9}$$

The output state can be written in terms of polarization as,

$$\Psi = \frac{1}{\sqrt{2}} |H\rangle_i |V\rangle_s \pm |V\rangle_i |H\rangle_s \tag{5.10}$$

Firstly we consider the non-collinear generation of photon-pairs where the two pho-

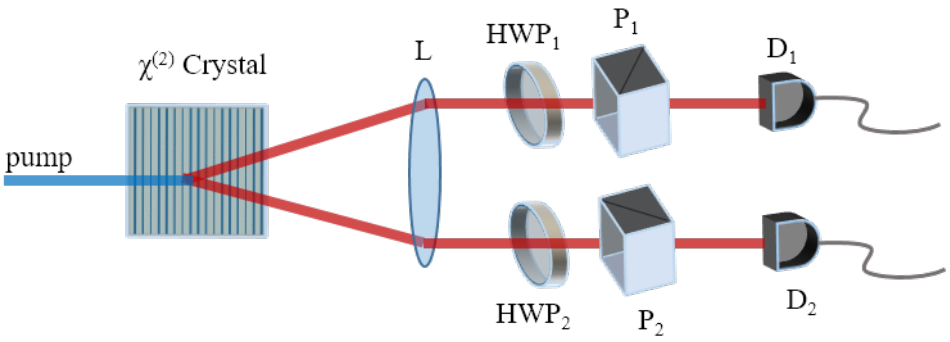

Figure 5.4: Experimental setup to observe the entanglement in a type-II SPDC from a ppKTP crystal ($\chi^{(2)}$). Polarization measurements in the collimated SPDC output is carried out using a combination of half-wave plate (HWP) and a polarizing beam-splitter (P) in each arm.

tons are emitted along directions following the phase-matching condition,

$$\mathbf{k_s} + \mathbf{k_i} \approx \mathbf{k_p}.$$

This phase matching condition says that the down-converted output would form a cone of correlated signal-idler photon pairs (Figure 5.4). The diverging cone of SPDC photons is ensured to be collimated for the total length of the experiment using lens, L, having focal length, f=10 cm (Figure 5.5). The low intensity photon distributions are imaged using an EMCCD (Andor iXon3). The broad angular intensity pattern of the

SPDC output is due to the uncertainty associated with the phase-matching parameter, $\Delta k = k_p - k_s - k_i$. This is the reason why the SPDC cone looks like a ring with a spatial broadening when looked in its transverse plane along the direction of propagation. Signal and idler phtons are then coupled to individual detector systems involving a fiber coupler, single mode fiber, a single photon counting module and a time-to-digital converter which provide the coincidence counts. Polarization projections in different basis is carried out using a combination of half wave plate and a polarizing beam splitter in each of the arms. To observe maximum entanglement, maximum overlap between the

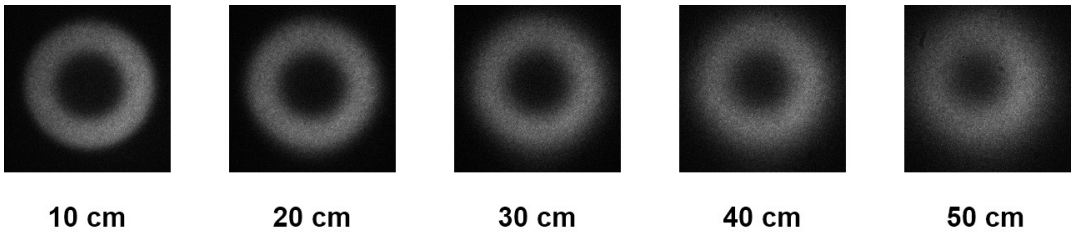

Figure 5.5: A 10 cm lens placed after the SPDC output collimates the diverging cone of photon pairs. The figure shows the collimated SPDC output images obtained using an EMCCD kept at different distances from the crystal plane.

two photons has to be ensured. The crystal position and tilt are adjusted such that the spatial overlap between the H-polarized cone and V-polarized cone of photons are overlapping (Figure 5.6). The correlated photons will be falling along diametrically opposite points following the phase matching conditions. Two regions, marked in red circles, are selected and coupled to the detector system.

The polarization projections are done using the combination of half wave plate and a polarizing beam splitter kept in each arm of the SPDC output (Figure 5.4). HWP_1 in the idler arm is kept at fixed angles of rotation, $\theta_1 = 0°, 45°, 90°$ and $135°$ and the second half wave plate kept in the signal arm is rotated as θ_2 to observe the polarization correlation. The experimentally observed polarization correlations corresponding to the projections in H-V basis as well as D-A basis are given as the visibility curves in

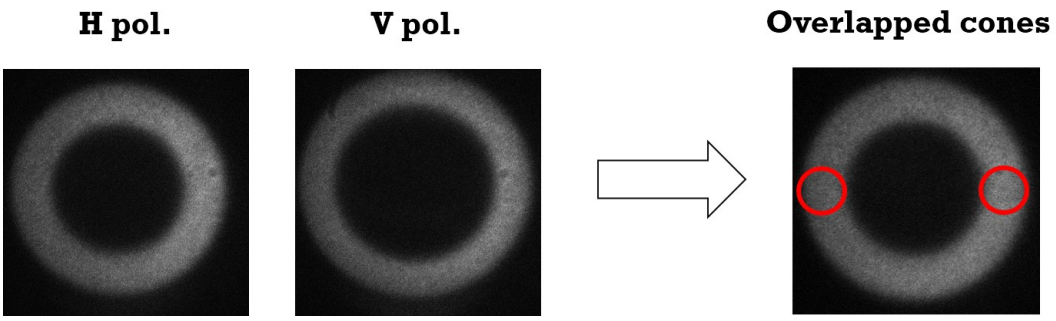

Figure 5.6: The crystal position and tilt are adjusted such that the SPDC output corresponding to both the polarizations are spatially overlapping. Diametrically opposite regions (in red circles) corresponds to the entangled photons.

Figure 5.7.

5.3.1 Indistinguishable Photons in the Collinear SPDC

The non-linear coefficient of an ideal periodically-poled crystal has a square-wave shape with an amplitude $\pm d_{eff}$, where d_{eff} is the effective nonlinearity of the material of the crystal. The conversion efficiency depends on the Fourier transform of the position dependent nonlinear coefficient, $d(x)$, where x is along the length of the crystal. The Fourier transform of $d(x)$ contains odd-m harmonics given as $k_m^{\pm} = \pm 2\pi m/\Lambda_0$, where Λ_0 is the poling period of the crystal. The conversion efficiency becomes maximum corresponding to the wave vector mismatch, $\Delta k = k_m^{\pm}$. The cumulative phase mismatch, acquired over half the crystal length with respect to quasi phase matching order, m, is given by,

$$\phi_m = \frac{L_0}{2}\left[|\Delta k| f(T) - \frac{2\pi m}{\Lambda_0}\right] \tag{5.11}$$

where L_0 is the crystal length, T_0 is the reference temperature and $f(T)$ is the temperature dependent material expansion factor. The wave vector mismatch is given as,

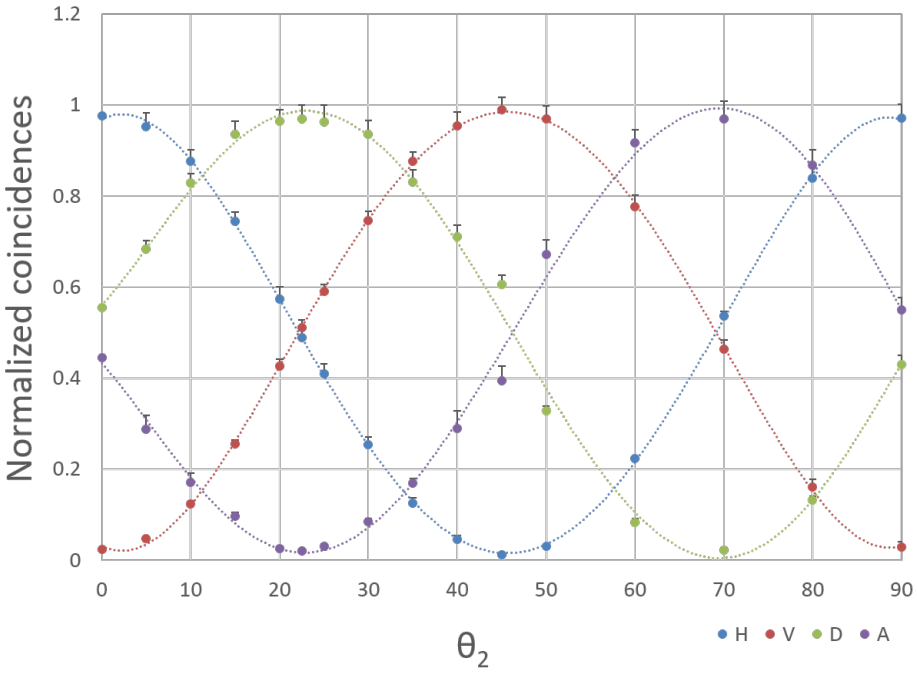

Figure 5.7: Polarization correlations corresponding to projections using the half wave plate in Figure 5.4. The normalized coincidences are plotted along y-axis with the variation of θ_2 for (blue) $\theta_1 = 0°$, (green) $\theta_1 = 45°$, (red) $\theta_1 = 90°$ and (purple) $\theta_1 = 135°$ where θ_1 and θ_2 are angle of rotation of HWP_1 and HWP_2 respectively in Fig. 5.4. Error bars indicate statistical uncertainty of one standard deviation. Visibility is 97.7±0.2% (HV basis) and 92.1±0.3% (DA basis).

$$\begin{aligned}\Delta k_{\text{SPDC}} =& k(2\omega,T) - 2k(\omega,T) \\ &+ k(\omega,T)\left[\theta_y^2 + \left(\frac{n_z}{n_x}\right)^2 \theta_z^2\right] \\ &- \frac{\partial^2 k}{\partial \omega^2}\bigg|_{\omega,T} \left(\frac{\Omega}{2}\right)^2\end{aligned} \tag{5.12}$$

where θ_y and θ_z is the emission angle inside the crystal, and n_z and n_x are the refractive index along z and x directions respectively [144]. Thus, for the periodically poled crystal, the phase matching will be governed by temperature of the crystal and hence the crystal is mounted on a temperature controlling oven. By varying temperature, one can achieve collinear phase matching conditions which can be verified from the

variation of the angular intensity pattern with temperature as given in Figure 5.8. For our crystal, the collinear condition is achieved at 40°C.

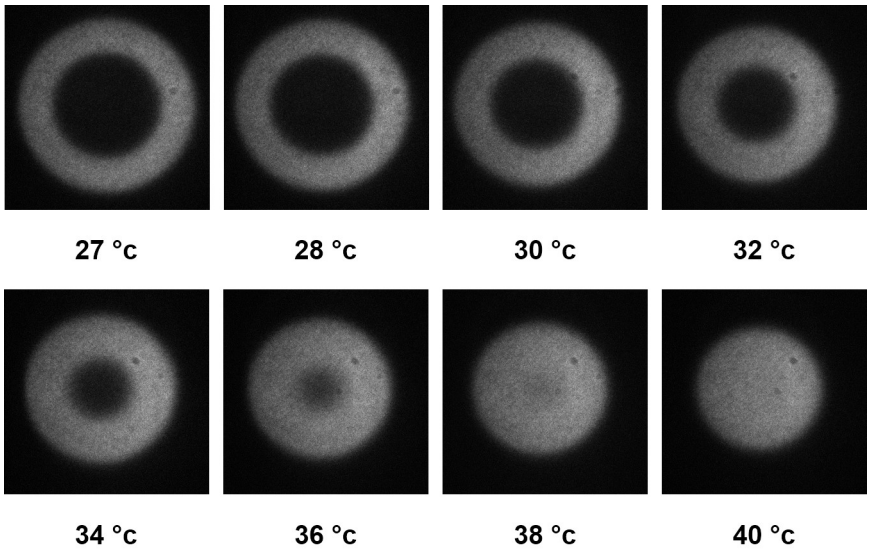

Figure 5.8: Variation of the spatial distribution of the SPDC output from a type-II ppKTP crystal with different temperature values for quasi-phase matching. We observe that collinear output is obtained for a temperature, 40° c.

5.3.2 Observation of Polarization Entanglement through OAM Sorting

Indistinguishable photons are obtained in the collinear SPDC output at a temperature 40° c in the temperature controller. As discussed before, when pumped with a vortex having $l_p = 1$, the output OAM distribution from a type-II SPDC process could be written in the form,

$$|\Psi\rangle = \frac{1}{\sqrt{2}}(|e\rangle_H |o\rangle_V + |o\rangle_H |e\rangle_V) \tag{5.13}$$

as well as,

$$|\Psi\rangle = \frac{1}{\sqrt{2}}(|H\rangle_e |V\rangle_o + |V\rangle_e |H\rangle_o). \tag{5.14}$$

Hence, separating the collinear photons in one degree of freedom allows us to observe entanglement in the other degree of freedom. We propose a setup where we separate the collinear photons using a double Mach-Zehnder OAM sorting interferometer to reveal the entanglement in polarization. A double Mach-Zehnder type interferometer could be understood as a normal Mach-Zehnder interferometer, folded back such that the input and output beam splitters become the same. Such a configuration will have the stability of a common path interferometer, since both the arms see same optical components, and the ease of inserting independent components in the interfering arms as in a Mach-Zehnder interferometer.

The collinear correlated pairs of photons having even and odd OAM orders are sent to a double Mach-Zehnder interferometer containing two Dove prisms which are kept in the individual paths as given in Figure 5.9. The Dove prisms are kept such that

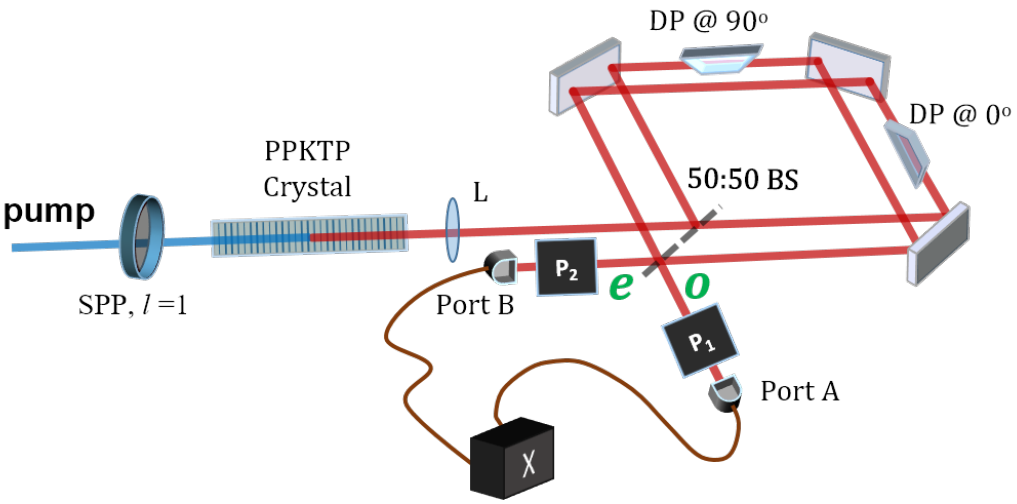

Figure 5.9: Experimental setup to sort the even-odd states of OAM from a collinear SPDC with vortex pump ($l = 1$). The Dove prisms within the double Mach-Zehnder interferometer is kept orthogonal to each other. P_i corresponds to the polarization projectors consisting of a half wave plate and a polarizing beam splitter. Port A is the constructive port for odd OAM and B is the constructive port for even OAM.

their relative orientation is perpendicular to each other. The photon carrying an odd

OAM will constructively interfere to show up in port A whereas photons having even OAM will show up in port B. P_i corresponds to the polarization projection using the combination of a half wave plate and a polarizing beam splitter as shown in Figure 5.4. At first, classical alignment laser (810 *nm*, Thorlabs) is used to verify the sorting of even and odd OAM modes. The collinear output is then sent along the same path. Coincidences are maximized in the detectors kept in ports A and B, and polarization projection measurements are carried out to observe the entanglement visibility.

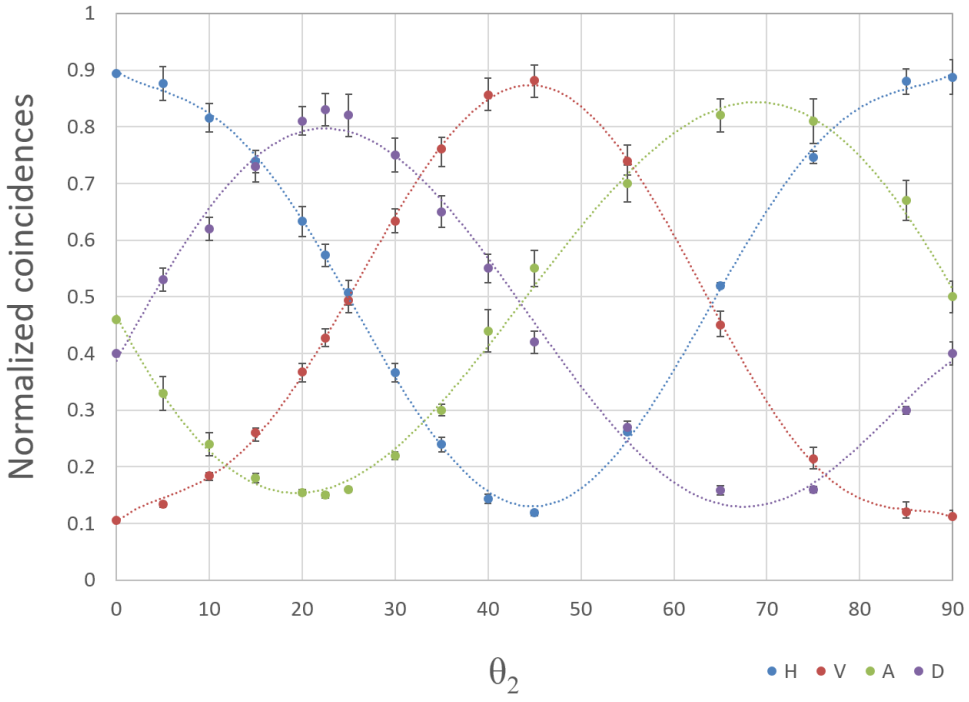

Figure 5.10: Polarization correlations corresponding to projections in the output ports of the even-odd sorted collinear SPDC output. The normalized coincidences are plotted along y-axis with the variation of θ_2 for (blue) $\theta_1 = 0°$, (green) $\theta_1 = 45°$, (red) $\theta_1 = 90°$ and (purple) $\theta_1 = 135°$. Error bars indicate statistical uncertainty of one standard deviation. Visibility is 76.6±0.3% (HV basis) and 71.7±0.3% (DA basis).

Figure 5.10 shows the polarization correlations between the even and odd output ports of the sorter set up in the collinear SPDC. The indistinguishable photons are efficiently sorted under the label of their orbital angular momentum and polarization

visibility is observed in both HV as well as DA basis.

5.3.3 Observation of OAM Entanglement through Polarization Sorting

In a similar way, the entanglement in the even-odd basis of orbital angular momentum can be observed by separating the indistinguishable photons using their polarization label. A polarizing beam splitter separates the H and V polarized photons in the transmitted and reflected ports respectively as given in Figure 5.11. OAM projections are

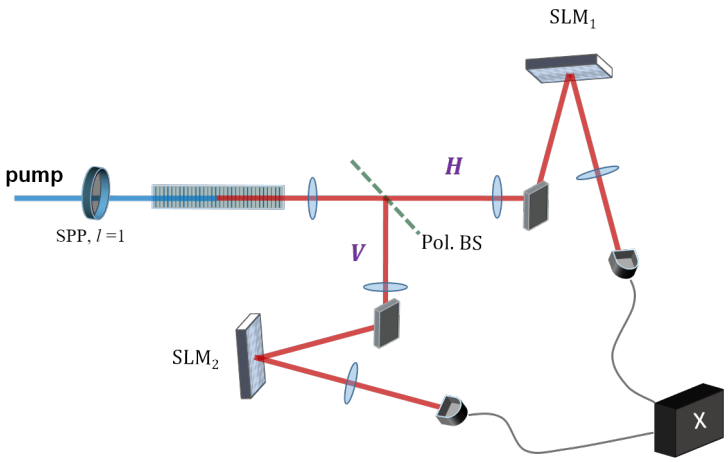

Figure 5.11: Proposed experimental setup to observe entanglement in the even-odd basis of OAM by sorting photons in polarization. Indistinguishable photons in the type-II down-converted pairs are sorted in polarization using a polarizing beam splitter. OAM projections are done using a spatial light modulator (SLM) through phase-flattening and coupling to single mode fibers. Additional lenses are used to image the crystal plane to the SLM, as well as the SLM plane to the coupling fibre tip to enhance effective coupling.

done using a spatial light modulator (SLM) through phase-flattening and coupling to single mode fibers. Additional lenses are used to image the crystal plane to the SLM, as well as the SLM plane to the coupling fibre tip to enhance effective coupling. The two lenses before the SLM image the modes generated in the crystal plane on the SLM, while the lens after the SLM along with the aspheric lens within the fiber coupler per-

form imaging of the modes generated at the SLM surface onto the fiber tip. The lenses need to be selected such that the mode sizes match the numerical aperture of the fiber coupling system. OAM projections in the even-odd basis could be carried out with the help of identical spatial light modulators kept in the two arms. One can consider holograms displaying superpositions of even orders and odd orders as the counterparts of D and A projections.

5.4 Conclusions

We propose the entanglement sorting scheme using twisted photon OAM defined in terms of their even or odd nature. This method increases the efficiency of available entangled photons since we are not eliminating any photon from the generated output as in the case of limiting them to two-dimensional bases such as $(+l, -l)$ or $(0, l)$. All the down-converted photons are sorted using an even-odd sorter in order to observe the polarization entanglement of otherwise indistinguishable collinear photons. In the similar way, one can do polarization sorting using a simple polarizing beam splitter and executing OAM projections on the photon pairs in the even-odd basis.

Chapter 6

Summary

Information processing using photons as quantum systems has gained immense popularity over the past few decades due to the two most unique characteristics of quantum mechanics - the existence of indivisible quanta of energy and entanglement. These properties help to ensure secure and efficient information transfer. Photons are considered as one of the ideal candidates to be used in quantum information processing as they are fast and do not interact with each other. Orbital angular momentum of light has been explored to have great applications in quantum information processing since OAM can serve as an additional degree of freedom with an infinite dimensional basis. This thesis studies photon statistics as well as intensity correlations of the twisted single photons generated in the spontaneous parametric down-conversion process along with the OAM spectrum of twin photons. Finally, it shows that the OAM sorting can be utilized to demonstrate polarization entanglement for indistinguishable photons produced through collinear parametric down process.

In chapter 1, we give a brief introduction to single photon sources and what char-

acterizes a single photon source. We discuss the quantization of the radiation field and the concept of single photons as mode carriers of the quantized radiation field. We further discuss the number statistics and second order correlations for photon sources and how parameters such as the Mandel Q-parameter and second order correlation function define the classification between classical and non-classical sources of light. A brief introduction is given about orbital angular momentum of classical beams as well as heralded single photons generated in parametric down-conversion. We briefly explain quantum entanglement and discuss different types of entangled systems involving the orbital angular momentum of photons. In short, we describe single photons carrying orbital angular momentum and the implications of such twisted photons in quantum information processing.

In chapter 2, we build the number statistics of the heralded single photons generated in parametric down-conversion. The time series corresponding to the signal and idler photons are recorded using the oscilloscope and the coincidence series corresponding to the simultaneous detection of correlated photon pairs is generated. This is done by converting the analog output from the oscilloscope into a binary series. The detection events at the photo diodes as well as coincidence events are counted within a defined time interval (binning window) and the distribution of the number of such occurrences is obtained. For the heralded single photon source, the number statistics is built from the binary series of coincidences generated by post-processing the recorded events of individual signal and idler photons. We obtain the Mandel Q-parameter as -0.331$\pm$0.004. The negative value of Q is indication of the sub-Poissonian behavior of the source. Here we demonstrate the observation of sub-Poissonian statistics for the heralded single photons generated in parametric down-conversion using photodetectors and an oscilloscope, which is a ubiquitous instrument in any undergraduate laboratory.

Chapter 3 explores the second order correlations corresponding to twisted photons carrying different OAM. We have calculated the second order coherence function with zero delay, $g^{(2)}(0)$ for different OAM values of heralded single photons. It was calculated from the direct measurement of the simultaneous detection between the three detectors in a heralded HBT experiment as well as through a model that accounts for the accidental three-fold coincidences. In both cases, $g^{(2)}(0)$ is found to be increasing with the increasing order of the OAM for the twisted photons. This suggests that the non-classicality of the twisted photons generated in parametric down-conversion deteriorates in terms of the second-order correlations, with higher orders of their OAM. The results are shown to be in good agreement with the theoretical predictions.

In chapter 4, we study the OAM spectrum of down converted photons for different pump modes. We consider LG and POV pump modes of various orders and observe the resulting OAM spectrum of the SPDC photons when both signal and idler photons are projected onto LG modes or POV modes. We found that projection of the output photons onto LG modes for a LG pump gave rise to a wider spectrum. A secondary maxima was observed in the OAM spectrum of the down-converted photons when pumped with higher order LG modes. Replacing the pump with a POV mode removed this anomaly as well as narrowed down the spectrum. We obtained the narrowest spectrum when down converted photons were projected onto POV modes. The narrowing of the spectrum, however, comes with a trade off since it is also observed that such narrowing of the spectrum lowers the overall high-dimensional entanglement between signal and idler photons. We have experimentally obtained the OAM spectrum corresponding to POV pump. Greater entanglement was observed when the output modes were projected in Bessel-Gaussian modes than conventional Laguerre-Gaussian mode.

In chapter 5, we investigate the entanglement between identical twin photons trav-

elling along the same direction in the collinear output of SPDC. For indistinguishable photon pairs produced in a collinear parametric down-conversion process, we demonstrate entanglement being revealed in one degree of freedom if we sort the photons in another degree of freedom. We consider polarization and OAM as the two independent degrees of freedom required by the duality principle of entanglement. We use a double Mach-Zehnder with two Dove prisms oriented orthogonal to each other in the two arms as a sorter for even and odd OAM states. For a pump carrying an odd OAM, the twin photons generated in SPDC will carry even-odd pairs of OAM following OAM conservation. In short we demonstrate that using the twisted photon OAM, we can effectively separate the identical photons to observe the entanglement in polarization.

Scope for future work

We have studied and characterized the twisted single photons carrying orbital angular momentum. Despite the fact that they provide an infinite dimensional degree of freedom for communication, the decay of modes through turbulent media is one of the biggest challenges faced in using OAM states of photons for free-space quantum communication [145, 146]. The study of scattering of structured beams reveals about their spatial correlations and coherence properties when passing through turbulent media [147]. Similar studies are of significance for single photons to be used for quantum communication through free space. Studies involving classical non-separable states have shown that the non-separability of polarization and OAM degrees of freedom helps preserving the information encoded in one of the degree of freedom even after scattering [148]. Such hybrid-entangled states of single photons are gaining interest for transmission through turbulent media [149].

We will be extending this study to single photons generated from parametric down-

conversion to investigate the effects of random scattering media on their hybrid-entanglement. The spin-orbit projections will be done in the signal arm using a combination of half wave plates, polarizers and spatial light modulators (SLMs). The scattering media could be generated using a rotating ground glass plate or suspended silica microspheres or polysterine latex beads or random phase screens displayed on a spatial light modulator. Studies involving the turbulence-induced decay of OAM entanglement has shown the entanglement to be more robust in turbulence for higher order OAM states [150]. We will be studying the dependence on the decay of hybrid-entanglement with higher OAM orders as well. They can be generated merely by changing the pump OAM in the experiment described above.

Parametric down-conversion is a very well established method for generating OAM entanglement [52, 111]. Defining the entanglement in an even-odd basis of OAM is shown to be more efficient compared to conventional two-dimensional Hilbert spaces such as those defined by $(+l,-l)$ or $(0,l)$. In the even-odd basis, we will not be eliminating any photons as all the generated pairs are selected in either even or odd values of their OAM. This increases the efficiency of entangled photon pair generation. State tomography and projective measurement are well defined in the even-odd basis [143]. We would like to verify the entanglement of twin photons from SPDC in the even-odd basis of OAM and investigate their possible advantages over conventional OAM entanglement demonstrations.

Appendix A

MATLAB code for building the number statistics of a photon source

We have given below the MATLAB source code written to build the statistics of a photon source from the detection time series as given in Chapter 2.

Note: The source code originally written in MATLAB is displayed using LATEX with the help of the style file mcode.sty [Copyright (c) 2015, Florian Knorn. All rights reserved.].

```
1 %%%%%%%%%%%%%%%%%%%%%%%%%%%%%%%%%%%%%%%%%%%%%%%%%%%%%%%%%%%%%%%%%%%%%%%
2 % Written by Nijil Lal and Biveen Shajilal to build the ...
      statistics of Poissonian, super-Poissonian and ...
      sub-Poissonian light sources.
3 %%%%%%%%%%%%%%%%%%%%%%%%%%%%%%%%%%%%%%%%%%%%%%%%%%%%%%%%%%%%%%%%%%%%%%%
4
5 %% ------------------- Reading Data---------------------- %%
```

```
6
7  % A usual oscilloscope records the waveworm with the ...
       timestamp in the first column and the input channels in ...
       the onward columns.
8
9  data = csvread('/home/user/data.csv');
10 A = data(:,[1 2]);  % channel 1
11 B = data(:,[1 3]);  % channel 2
12
13 %% ----------- Conversion to Binary Signals -------------%%
14
15 % The recorded time series from oscilloscope is converted ...
       into a series of binaries (1-event, 0-no event). To ...
       isolate the events from noise signals and possible after ...
       pulses, a threshold (thresh) is determined which is above ...
       the noise level and any undesired afterpulses. In case of ...
       an event signal that crosses the threshold, 1 is assigned ...
       to the binary series at the onset of the signal - defined ...
       by signal_pos, whpse value is much smaller than the ...
       threshold. Here, they are chosen as 0.4 and 0.1 respectively.
16
17 N = length (data);
18     thresh = 0.4;
19     signal_pos = 0.1;
20
21 A_binary(:,1) = A(:,1);
22 B_binary(:,1) = A(:,1);
23 AB_binary(:,1)= A(:,1);
24 AB_binary(1:N,2)=0;
25
26 for i=1:N
```

```
27      if A(i,2)>thresh
28          j=i;
29           while A(j,2)>signal_pos
30               A_binary(j,2)=0;
31               j=j-1;
32           end
33           A_binary(j,2)=1;
34      else
35          A_binary(i,2)=0;
36      end
37  end
38
39  for i=1:N
40      if B(i,2)>thresh
41          j=i;
42           while B(j,2)>signal_pos
43               B_binary(j,2)=0;
44               j=j-1;
45           end
46           B_binary(j,2)=1;
47      else
48          B_binary(i,2)=0;
49      end
50  end
51
52  % The coincidence time series is built from the binary ...
        series, A and B.
53
54  tc = 1;
55
56  % tc x resolution (of the recorded time series) gives the ...
```

```
    width of the coincidence window.

for i=1:N
    if A_binary(i,2)==1
        for k=i:i+tc
            if B_binary(k,2)==1
                AB_binary(k,2)=1;
            end
        end
    end
end

%% -------- Determining the size of the time bin ------- %%

% Bin size is defined for rach series for a mean photon ...
    number = 1/bin.

nA = sum(A_binary(:,2));
nB = sum(B_binary(:,2));
nAB = sum(AB_binary(:,2));

% Total number of photons corresponding to each series.

binA = round(N/nA); binB = round(N/nB); binAB = round(N/nAB);

% Average photon number per bin is defined by the size of bin.

MaxA = N-binA; MaxB = N-binB; MaxAB = N-binAB;

% Upper limit while slicing the time series into bins.

```

```
%% ------------ Building The Statistics --------------- %%

% Arm A statistics

j=1;
for i=1 : binA : MaxA
A_count=0;
    for k=i:(i+binA)
        if A_binary(k,2)==1
        A_count=A_count+1;
        end
    end
    A_stat(j,1)=A_count;
    j=j+1;
end

% Arm B statistics

j=1;
for i=1 : binB : MaxB
B_count=0;
    for k=i:(i+binB)
        if B_binary(k,2)==1
        B_count=B_count+1;
        end
    end
    B_stat(j,1)=B_count;
    j=j+1;
end

% Heralded single photon statistics
```

```
117
118 j=1;
119 for i=1 : binAB : MaxAB
120 AB_count=0;
121     for k=i:(i+binAB)
122         if AB_binary(k,2)==1
123         AB_count=AB_count+1;
124         end
125     end
126     AB_stat(j,1)=AB_count;
127     j=j+1;
128 end
129
130 %% -------------- Building the Histogram ---------------- %%
131
132 % h is the number of photons,n, in each bin.
133 for h=1:20
134     U(h,1)=sum(A_stat==h-1);
135     V(h,1)=sum(B_stat==h-1);
136     W(h,1)=sum(AB_stat==h-1);
137 end
138 %% %%%%%%%%%%%%%%% ---- End ---- %%%%%%%%% %%
```

Bibliography

[1] M. K. E. L. Planck, *Über eine verbesserung der wienschen spectralgleichung,* Verhandl. Dtsc. Phys. Ges. **2**, 202 (1900).

[2] A. Einstein, *Concerning an heuristic point of view toward the emission and transformation of light,* Am. J. Phys. **33**, 367 (1965).

[3] P. A. M. Dirac, *The quantum theory of the emission and absorption of radiation,* P. R. Soc. Lond. A - Conta. **114**, 243–265 (1927).

[4] M. O. Scully and M. S. Zubairy, *Quantum optics* (AAPT, 1999).

[5] C. Gerry, P. Knight, and P. L. Knight, *Introductory quantum optics* (Cambridge university press, 2005).

[6] I. Aharonovich, D. Englund, and M. Toth, *Solid-state single-photon emitters,* Nat. Photonics **10**, 631 (2016).

[7] H. Bernien, B. Hensen, W. Pfaff, G. Koolstra, M. S. Blok, L. Robledo, T. Taminiau, M. Markham, D. J. Twitchen, L. Childress *et al.*, *Heralded entanglement between solid-state qubits separated by three metres,* Nature **497**, 86 (2013).

[8] J. J. Pla, K. Y. Tan, J. P. Dehollain, W. H. Lim, J. J. Morton, D. N. Jamieson,

A. S. Dzurak, and A. Morello, *A single-atom electron spin qubit in silicon,* Nature **489**, 541 (2012).

[9] D. Schrader, I. Dotsenko, M. Khudaverdyan, Y. Miroshnychenko, A. Rauschenbeutel, and D. Meschede, *Neutral atom quantum register,* Phys. Rev. Lett. **93**, 150501 (2004).

[10] G. Wendin, *Quantum information processing with superconducting circuits: a review,* Rep. Prog. Phys. **80**, 106001 (2017).

[11] E. Togan, Y. Chu, A. Trifonov, L. Jiang, J. Maze, L. Childress, M. G. Dutt, A. S. Sørensen, P. Hemmer, A. S. Zibrov *et al.*, *Quantum entanglement between an optical photon and a solid-state spin qubit,* Nature **466**, 730 (2010).

[12] C. Monroe, *Quantum information processing with atoms and photons,* Nature **416**, 238 (2002).

[13] A. Wallraff, D. I. Schuster, A. Blais, L. Frunzio, R.-S. Huang, J. Majer, S. Kumar, S. M. Girvin, and R. J. Schoelkopf, *Strong coupling of a single photon to a superconducting qubit using circuit quantum electrodynamics,* Nature **431**, 162 (2004).

[14] F. Flamini, N. Spagnolo, and F. Sciarrino, *Photonic quantum information processing: a review,* Rep. Prog. Phys. **82**, 016001 (2018).

[15] S. L. Braunstein and P. van Loock, *Quantum information with continuous variables,* Rev. Mod. Phys. **77**, 513–577 (2005).

[16] E. Knill, R. Laflamme, and G. J. Milburn, *A scheme for efficient quantum computation with linear optics,* Nature **409**, 46 (2001).

[17] P. Kok, W. J. Munro, K. Nemoto, T. C. Ralph, J. P. Dowling, and G. J. Milburn, *Linear optical quantum computing with photonic qubits,* Rev. Mod. Phys. **79**, 135–174 (2007).

[18] J. Wrachtrup and F. Jelezko, *Processing quantum information in diamond,* J. Phys. - Condens. Mat. **18**, S807–S824 (2006).

[19] S. Prawer and I. Aharonovich, *Quantum information processing with diamond: Principles and applications* (Elsevier, 2014).

[20] J. Claudon, J. Bleuse, N. S. Malik, M. Bazin, P. Jaffrennou, N. Gregersen, C. Sauvan, P. Lalanne, and J.-M. Gérard, *A highly efficient single-photon source based on a quantum dot in a photonic nanowire,* Nat. Photonics **4**, 174 (2010).

[21] A. Kiraz, M. Atatüre, and A. Imamoğlu, *Quantum-dot single-photon sources: Prospects for applications in linear optics quantum-information processing,* Phys. Rev. A **69**, 032305 (2004).

[22] D. J. Wineland, M. Barrett, J. Britton, J. Chiaverini, B. DeMarco, W. M. Itano, B. Jelenković, C. Langer, D. Leibfried, V. Meyer *et al.*, *Quantum information processing with trapped ions,* Phil. T. Roy. Soc. A **361**, 1349–1361 (2003).

[23] R. Blatt and C. F. Roos, *Quantum simulations with trapped ions,* Nat. Phys. **8**, 277–284 (2012).

[24] C. Gross and I. Bloch, *Quantum simulations with ultracold atoms in optical lattices,* Science **357**, 995–1001 (2017).

[25] I. Bloch, *Quantum coherence and entanglement with ultracold atoms in optical lattices,* Nature **453**, 1016 (2008).

[26] S. Yelin, K. Kirby, and R. Côté, *Schemes for robust quantum computation with polar molecules,* Phys. Rev. A **74**, 050301 (2006).

[27] L. Mandel and E. Wolf, *Optical coherence and quantum optics* (Cambridge university press, 1995).

[28] M. Fox, *Quantum optics: an introduction*, vol. 15 (OUP Oxford, 2006).

[29] S. V. Polyakov and A. L. Migdall, *High accuracy verification of a correlated-photon-based method for determining photon-counting detection efficiency,* Optics express **15**, 1390–1407 (2007).

[30] I. R. Berchera and I. P. Degiovanni, *Quantum imaging with sub-poissonian light: challenges and perspectives in optical metrology,* Metrologia **56**, 024001 (2019).

[31] J. F. Clauser, *Experimental distinction between the quantum and classical field-theoretic predictions for the photoelectric effect,* Phys. Rev. D **9**, 853–860 (1974).

[32] D. C. Burnham and D. L. Weinberg, *Observation of simultaneity in parametric production of optical photon pairs,* Phys. Rev. Lett. **25**, 84–87 (1970).

[33] C. K. Hong and L. Mandel, *Experimental realization of a localized one-photon state,* Phys. Rev. Lett. **56**, 58–60 (1986).

[34] V. G. Dmitriev, G. G. Gurzadyan, and D. N. Nikogosyan, *Handbook of nonlinear optical crystals*, vol. 64 (Springer, 2013).

[35] L. Allen, M. W. Beijersbergen, R. J. C. Spreeuw, and J. P. Woerdman, *Orbital angular momentum of light and the transformation of laguerre-gaussian laser modes,* Phys. Rev. A **45**, 8185–8189 (1992).

[36] J. F. Nye, M. V. Berry, and F. C. Frank, *Dislocations in wave trains,* Proc. R. Soc. Lond. A **336**, 165–190 (1974).

[37] P. Vaity, J. Banerji, and R. Singh, *Measuring the topological charge of an optical vortex by using a tilted convex lens,* Phys. Lett. A **377**, 1154 – 1156 (2013).

[38] J. Leach, M. J. Padgett, S. M. Barnett, S. Franke-Arnold, and J. Courtial, *Measuring the orbital angular momentum of a single photon,* Phys. Rev. Lett. **88**, 257901 (2002).

[39] S. Slussarenko, V. D'Ambrosio, B. Piccirillo, L. Marrucci, and E. Santamato, *The polarizing sagnac interferometer: a tool for light orbital angular momentum sorting and spin-orbit photon processing,* Opt. Express **18**, 27205–27216 (2010).

[40] R. Horodecki, P. Horodecki, M. Horodecki, and K. Horodecki, *Quantum entanglement,* Rev. Mod. Phys. **81**, 865–942 (2009).

[41] M. Horodecki, P. Horodecki, and R. Horodecki, *On the necessary and sufficient conditions for separability of mixed quantum states,* Phys. Lett. A **223**, 1 (1996).

[42] A. Einstein, B. Podolsky, and N. Rosen, *Can quantum-mechanical description of physical reality be considered complete?* Phys. Rev. **47**, 777–780 (1935).

[43] N. Bohr, *Discussion with Einstein on epistemological problems in atomic physics,* in "Albert Einstein: Philosopher-Scientist," , P. A. Schilpp, ed. (MJF Books, New York, 1969), chap. 7, pp. 199–241, 3rd ed.

[44] J. S. Bell, *On the Einstein Podolsky Rosen paradox,* Physics Physique Fizika **1**, 195 (1964).

[45] J. F. Clauser, M. A. Horne, A. Shimony, and R. A. Holt, *Proposed experiment to test local hidden-variable theories,* Phys. Rev. Lett. **23**, 880–884 (1969).

[46] S. J. Freedman and J. F. Clauser, *Experimental test of local hidden-variable theories,* Phys. Rev. Lett. **28**, 938–941 (1972).

[47] J. F. Clauser and M. A. Horne, *Experimental consequences of objective local theories,* Phys. Rev. D **10**, 526 (1974).

[48] J. F. Clauser and A. Shimony, *Bell's theorem. experimental tests and implications,* Rep. Prog. Phys. **41**, 1881 (1978).

[49] A. Aspect, P. Grangier, and G. Roger, *Experimental tests of realistic local theories via bell's theorem,* Phys. Rev. Lett. **47**, 460–463 (1981).

[50] Y. Nambu, K. Usami, Y. Tsuda, K. Matsumoto, and K. Nakamura, *Generation of polarization-entangled photon pairs in a cascade of two type-i crystals pumped by femtosecond pulses,* Phys. Rev. A **66**, 033816 (2002).

[51] Y. Shih, A. Sergienko, M. H. Rubin, T. Kiess, and C. Alley, *Two-photon entanglement in type-ii parametric down-conversion,* Phys. Rev. A **50**, 23 (1994).

[52] A. Mair, A. Vaziri, G. Weihs, and A. Zeilinger, *Entanglement of the orbital angular momentum states of photons,* Nature **412**, 313 (2001).

[53] R. J. C. Spreeuw, *A classical analogy of entanglement,* Found. Phys. **28**, 361–374 (1998).

[54] R. J. C. Spreeuw, *Classical wave-optics analogy of quantum-information processing,* Phys. Rev. A **63**, 062302 (2001).

[55] M. McLaren, T. Konrad, and A. Forbes, *Measuring the nonseparability of vector vortex beams,* Phys. Rev. A **92**, 023833 (2015).

[56] L. J. Pereira, A. Z. Khoury, and K. Dechoum, *Quantum and classical separability of spin-orbit laser modes,* Phys. Rev. A **90**, 053842 (2014).

[57] P. Chowdhury, A. S. Majumdar, and G. S. Agarwal, *Nonlocal continuous-variable correlations and violation of bell's inequality for light beams with topological singularities,* Phys. Rev. A **88**, 013830 (2013).

[58] P. Chithrabhanu, S. G. Reddy, N. Lal, A. Anwar, A. Aadhi, and R. P. Singh, *Pancharatnam phase in non-separable states of light,* J. Opt. Soc. Am. B **33**, 2093–2098 (2016).

[59] M. Jabir, N. A. Chaitanya, M. Mathew, and G. Samanta, *Direct transfer of classical non-separable states into hybrid entangled two photon states,* Sci. Rep. **7**, 7331 (2017).

[60] S. Bose and D. Home, *Duality in entanglement enabling a test of quantum indistinguishability unaffected by interactions,* Phys. Rev. Lett. **110**, 140404 (2013).

[61] R. Short and L. Mandel, *Observation of sub-Poissonian photon statistics,* Phys. Rev. Lett. **51**, 384 (1983).

[62] P. Tapster, J. Rarity, and J. Satchell, *Use of parametric down-conversion to generate sub-Poissonian light,* Phys. Rev. A **37**, 2963 (1988).

[63] J. Laurat, T. Coudreau, N. Treps, A. Maître, and C. Fabre, *Conditional preparation of a quantum state in the continuous variable regime: generation of a sub-Poissonian state from twin beams,* Phys. Rev. Lett. **91**, 213601 (2003).

[64] J. Peřina, O. Haderka, and V. Michálek, *Sub-Poissonian-light generation by postselection from twin beams,* Opt. Express **21**, 19387–19394 (2013).

[65] S. Singh, *Antibunching, sub-Poissonian photon statistics and finite bandwidth effects in resonance fluorescence,* Opt. Commun. **44**, 254–258 (1983).

[66] X. Zou and L. Mandel, *Photon-antibunching and sub-Poissonian photon statistics,* Phys. Rev. A **41**, 475 (1990).

[67] M. Mirhosseini, O. S. Magaña-Loaiza, M. N. O'Sullivan, B. Rodenburg, M. Malik, M. P. Lavery, M. J. Padgett, D. J. Gauthier, and R. W. Boyd, *High-dimensional quantum cryptography with twisted light,* New J. Phys. **17**, 033033 (2015).

[68] J. T. Barreiro, T.-C. Wei, and P. G. Kwiat, *Beating the channel capacity limit for linear photonic superdense coding,* Nat. Phys. **4**, 282 (2008).

[69] C. Gerry, P. Knight, and P. L. Knight, *Introductory quantum optics* (Cambridge university press, 2005).

[70] R. J. Glauber, *Coherent and incoherent states of the radiation field,* Phys. Rev. **131**, 2766 (1963).

[71] L. Mandel and E. Wolf, *Optical coherence and quantum optics* (Cambridge university press, 1995).

[72] L. Mandel, *Sub-Poissonian photon statistics in resonance fluorescence,* Opt. Lett. **4**, 205–207 (1979).

[73] M. Lamperti, A. Allevi, M. Bondani, R. Machulka, V. Michálek, O. Haderka, and J. Peřina, *Optimal sub-Poissonian light generation from twin beams by photon-number resolving detectors,* J. Opt. Soc. Am. B **31**, 20–25 (2014).

[74] B. Blauensteiner, I. Herbauts, S. Bettelli, A. Poppe, and H. Hübel, *Photon bunching in parametric down-conversion with continuous-wave excitation,* Phys. Rev. A **79**, 063846 (2009).

[75] The source code is available via https://github.com/njlal/Photon_stat-Oscilloscope (Matlab).

[76] N. Lal, B. Shajilal, A. Anwar, C. Perumangatt, and R. Singh, *Observing sub-Poissonian statistics of heralded single photons using an oscilloscope,* in "International Conference on Fibre Optics and Photonics," (Optical Society of America, 2016), pp. Th3A–72.

[77] B. I. Cantor and M. C. Teich, *Dead-time-corrected photocounting distributions for laser radiation,* J. Opt. Soc. Am. **65**, 786–791 (1975).

[78] E. Jakeman and J. J. H., *Antibunching and sub-Poissonian statistics in photoelectron-triggered optical dead-time experiments,* Opt. Acta **33**, 557–576 (1986).

[79] M. Razavi, I. Söllner, E. Bocquillon, C. Couteau, R. Laflamme, and G. Weihs, *Characterizing heralded single-photon sources with imperfect measurement devices,* J. Phys. B: At. Mol. Opt. Phys. **42**, 114013 (2009).

[80] X. Guo, C.-l. Zou, C. Schuck, H. Jung, R. Cheng, and H. X. Tang, *Parametric down-conversion photon-pair source on a nanophotonic chip,* Light Sci. Appl. **6**, e16249 (2017).

[81] M. Avenhaus, H. B. Coldenstrodt-Ronge, K. Laiho, W. Mauerer, I. A. Walmsley, and C. Silberhorn, *Photon number statistics of multimode parametric down-conversion,* Phys. Rev. Lett. **101**, 053601 (2008).

[82] A. M. Yao, *Angular momentum decomposition of entangled photons with an arbitrary pump,* New J. Phys. **13**, 053048 (2011).

[83] A. Banerji, A. Anwar, H. Sable, N. Lal, and R. P. Singh, *Engineering of orbital angular momentum spectrum of down-converted photons with mode-invariant pump,* arXiv e-prints arXiv:1905.02554 (2019).

[84] R. W. Boyd, *Nonlinear optics* (Elsevier, 2003).

[85] G. S. Agarwal, *Quantum optics* (Cambridge University Press, 2012).

[86] C. Hong and L. Mandel, *Experimental realization of a localized one-photon state,* Phys. Rev. Lett. **56**, 58 (1986).

[87] P. Grangier, G. Roger, and A. Aspect, *Experimental evidence for a photon anti-correlation effect on a beam splitter: a new light on single-photon interferences,* Europhys. Lett. **1**, 173 (1986).

[88] A. B. U'Ren, C. Silberhorn, J. L. Ball, K. Banaszek, and I. A. Walmsley, *Characterization of the nonclassical nature of conditionally prepared single photons,* Phys. Rev. A **72**, 021802 (2005).

[89] A. M. Yao and M. J. Padgett, *Orbital angular momentum: origins, behavior and applications,* Adv. Opt. Photon. **3**, 161–204 (2011).

[90] P. Vaity, J. Banerji, and R. Singh, *Measuring the topological charge of an optical vortex by using a tilted convex lens,* Phys. Lett. A **377**, 1154–1156 (2013).

[91] S. Prabhakar, A. Kumar, J. Banerji, and R. Singh, *Revealing the order of a vortex through its intensity record,* Opt. Lett. **36**, 4398–4400 (2011).

[92] A. Kumar, J. Banerji, and R. Singh, *Intensity correlation properties of high-order optical vortices passing through a rotating ground-glass plate,* Opt. Lett. **35**, 3841–3843 (2010).

[93] A. Kumar, S. Prabhakar, P. Vaity, and R. Singh, *Information content of optical vortex fields,* Opt. Lett. **36**, 1161–1163 (2011).

[94] S. G. Reddy, S. Prabhakar, A. Kumar, J. Banerji, and R. Singh, *Higher order optical vortices and formation of speckles,* Opt. Lett. **39**, 4364–4367 (2014).

[95] S. G. Reddy, C. Permangatt, S. Prabhakar, A. Anwar, J. Banerji, and R. Singh, *Divergence of optical vortex beams,* Appl. Optics **54**, 6690–6693 (2015).

[96] P. Lochab, P. Senthilkumaran, and K. Khare, *Near-core structure of a propagating optical vortex,* J. Opt. Soc. Am. A **33**, 2485–2490 (2016).

[97] A. Kumar, J. Banerji, and R. Singh, *Hanbury brown–twiss-type experiments with optical vortices and observation of modulated intensity correlation on scattering from rotating ground glass,* Phys. Rev. A **86**, 013825 (2012).

[98] L. Mandel and E. Wolf, *Optical coherence and quantum optics* (Cambridge university press, 1995).

[99] H. J. Kimble, M. Dagenais, and L. Mandel, *Photon antibunching in resonance fluorescence,* Phys. Rev. Lett. **39**, 691 (1977).

[100] M. Beck, *Comparing measurements of g (2)(0) performed with different coincidence detection techniques,* J. Opt. Soc. Am. B **24**, 2972–2978 (2007).

[101] P. G. Kwiat, K. Mattle, H. Weinfurter, A. Zeilinger, A. V. Sergienko, and Y. Shih, *New high-intensity source of polarization-entangled photon pairs,* Phys. Rev. Lett. **75**, 4337 (1995).

[102] C. Hong and L. Mandel, *Theory of parametric down conversion of light,* Phys. Rev. A **31**, 2409 (1985).

[103] S. P. Walborn, C. H. Monken, S. Padua, and P. H. S. Ribeiro, *Spatial correlations in parametric down-converison,* Phys. Rep. **495**, 87 (2010).

[104] R. Ghosh and L. Mandel, *Observation of nonclassical effects in the interference of two photons,* Phys. Rev. Lett. **59**, 1903 (1987).

[105] Z. Y. Ou and L. Mandel, *Violation of bell's inequality and classical probability in a two photon correlation experiment,* Phys. Rev. Lett. **61**, 50 (1988).

[106] A. C. Dada, J. Leach, G. S. Buller, M. J. Padgett, and E. Andersson, *Experimental high-dimensional two-photon entanglement and violations of generalized bell inequalities,* Nat. Phys. **7**, 677 (2011).

[107] J. T. Barreiro, N. K. Langford, N. A. Peters, and P. G. Kwiat, *Generation of hyper-entangled photon pairs,* Phys. Rev. Lett. **95**, 260501 (2005).

[108] M. Barbieri, C. Cinelli, P. Mataloni, and F. D. Martini, *Polarization-momentum hyperentangled states: Realization and characterization,* Phys. Rev. A **72**, 052110 (2005).

[109] L. Neves, G. Lima, A. Delgado, and C. Saavedra, *Hybrid photonic entanglement: Realization, characterization and applications,* Phys. Rev. A **80**, 042322 (2009).

[110] D. L. Andrews and M. Babiker, eds., *The Angular Momentum of Light* (Cambridge, Cambridge University Press, 2012).

[111] M. Krenn, M. Malik, M. Erhard, and A. Zeilinger, *Orbital angular momentum*

of photons and the entanglement of laguerre-gaussian modes, Phil. Trans. R. Soc. A **375**, 20150442 (2017).

[112] A. Vaziri, G. Weihs, and A. Zeilinger, *Experimental two-photon, three-dimensional entanglement for quantum communication,* Phys. Rev. Lett. **89**, 240401 (2002).

[113] B. C. Heismayr, M. J. A. de Dood, and W. L"ofler, *Observation of four-photon orbital angular momentum entanglement,* Phys. Rev. Lett. **116**, 073601 (2016).

[114] F. M. Miatto, A. M. Yao, and S. M. Barnett, *Full characterization of the quantum spiral bandwidth of entangled biphotons,* Phys. Rev. A **83**, 033816 (2011).

[115] H. H. Arnaut and G. A. Barbosa, *Orbital and intrinsic angular momentum of single photons and entangled pairs of photons generated by parametric down-conversion,* Phys. Rev. Lett. **85**, 286 (2000).

[116] C. L. Osorio, G. Molina-Terriza, and J. P. Torres, *Orbital angular momentum correlations of entangled paired photons,* J. Opt. A: Pure Appl. Opt. **11**, 094013 (2009).

[117] V. Vicu na-Hernández, H. Cruz-Ramírez, R. Ramírez-Alarcón, and A. B. U'Ren, *Classical to quantum transfer of optical vortices,* Opt. Exp. **22**, 20027 (2014).

[118] A. Anwar, P. Vaity, C. Perumangatt, and R. Singh, *Direct transfer of pump amplitude to parametric down-converted photons,* Opt. Lett. **43**, 1155–1158 (2018).

[119] P. Vaity and L. Rusch, *Perfect vortex beam: Fourier transformation of a bessel beam,* Opt. Lett. **40**, 597 (2015).

[120] P. Vaity and L. Rusch, *Perfect vortex beam: Fourier transformation of a bessel beam,* Opt. Lett. **40**, 597–600 (2015).

[121] V. V. Kotlyar, A. A. Kovalev, and A. P. Porfirev, *Optimal phase element for generating a perfect optical vortex,* J. Opt. Soc. Am. A **33**, 2376–2384 (2016).

[122] J. V. Neumann, *Mathematical Foundations of Quantum Mechanics* (Princeton University Press, 1955).

[123] M. A. Nielsen and I. L. Chuang, *Quantum Computation and Quantum Information* (New Delhi, Cambridge University Press, 2010).

[124] J. Sperling and W. Vogel, *The schmidt number as a universal entanglement measure,* Phys. Scrip. **83**, 045002 (2011).

[125] N. Bohr, *The quantum postulate and the recent development of atomic theory,* Nature **121**, 580–590 (1928).

[126] D. M. Greenberger and A. Yasin, *Simultaneous wave and particle knowledge in a neutron interferometer,* Phys. Lett. A **128**, 391–394 (1988).

[127] T. J. Herzog, P. G. Kwiat, H. Weinfurter, and A. Zeilinger, *Complementarity and the quantum eraser,* Phys. Rev. Lett. **75**, 3034–3037 (1995).

[128] G. Björk and A. Karlsson, *Complementarity and quantum erasure in welcher weg experiments,* Phys. Rev. A **58**, 3477 (1998).

[129] D. Branning, W. Grice, R. Erdmann, and I. Walmsley, *Engineering the indistinguishability and entanglement of two photons,* Phys. Rev. Lett. **83**, 955 (1999).

[130] J. P. Torres, M. W. Mitchell, and M. Hendrych, *Indistinguishability of entangled photons generated with achromatic phase matching,* Phys. Rev. A **71**, 022320 (2005).

[131] T. Pittman, D. Strekalov, A. Migdall, M. Rubin, A. Sergienko, and Y. Shih, *Can two-photon interference be considered the interference of two photons?* Phys. Rev. Lett. **77**, 1917 (1996).

[132] D. Bouwmeester, J.-W. Pan, K. Mattle, M. Eibl, H. Weinfurter, and A. Zeilinger, *Experimental quantum teleportation,* Nature **390**, 575 (1997).

[133] M. Müller, S. Bounouar, K. D. Jöns, M. Glässl, and P. Michler, *On-demand generation of indistinguishable polarization-entangled photon pairs,* Nat. Photonics **8**, 224 (2014).

[134] Y.-M. He, Y. He, Y.-J. Wei, D. Wu, M. Atatüre, C. Schneider, S. Höfling, M. Kamp, C.-Y. Lu, and J.-W. Pan, *On-demand semiconductor single-photon source with near-unity indistinguishability,* Nat. Nanotechnol. **8**, 213 (2013).

[135] D. Bhatti, J. von Zanthier, and G. S. Agarwal, *Entanglement of polarization and orbital angular momentum,* Phys. Rev. A **91**, 062303 (2015).

[136] A. E. Willner, H. Huang, Y. Yan, Y. Ren, N. Ahmed, G. Xie, C. Bao, L. Li, Y. Cao, Z. Zhao *et al.*, *Optical communications using orbital angular momentum beams,* Adv. Opt. Photonics **7**, 66–106 (2015).

[137] J. P. Torres, *Optical communications: Multiplexing twisted light,* Nat. Photonics **6**, 420 (2012).

[138] G. Molina-Terriza, J. P. Torres, and L. Torner, *Twisted photons,* Nat. Phys. **3**, 305 (2007).

[139] J. Leach, E. Bolduc, D. J. Gauthier, and R. W. Boyd, *Secure information capacity of photons entangled in many dimensions,* Phys. Rev. A **85**, 060304 (2012).

[140] G. Vallone, V. D'Ambrosio, A. Sponselli, S. Slussarenko, L. Marrucci, F. Sciarrino, and P. Villoresi, *Free-space quantum key distribution by rotation-invariant twisted photons,* Phys. Rev. Lett. **113**, 060503 (2014).

[141] M. Mafu, A. Dudley, S. Goyal, D. Giovannini, M. McLaren, M. J. Padgett, T. Konrad, F. Petruccione, N. Lütkenhaus, and A. Forbes, *Higher-dimensional orbital-angular-momentum-based quantum key distribution with mutually unbiased bases,* Phys. Rev. A **88**, 032305 (2013).

[142] H. Qassim, F. M. Miatto, J. P. Torres, M. J. Padgett, E. Karimi, and R. W. Boyd, *Limitations to the determination of a laguerre–gauss spectrum via projective, phase-flattening measurement,* J. Opt. Soc. Am. B **31**, A20–A23 (2014).

[143] C. Perumangatt, N. Lal, A. Anwar, S. G. Reddy, and R. Singh, *Quantum information with even and odd states of orbital angular momentum of light,* Phys. Lett. A **381**, 1858–1865 (2017).

[144] W. Peeters and M. van Exter, *Optical characterization of periodically-poled ktiopo 4,* Opt. Express **16**, 7344–7360 (2008).

[145] G. A. Tyler and R. W. Boyd, *Influence of atmospheric turbulence on the propagation of quantum states of light carrying orbital angular momentum,* Opt. Lett. **34**, 142–144 (2009).

[146] J. R. Gonzalez Alonso and T. A. Brun, *Protecting orbital-angular-momentum photons from decoherence in a turbulent atmosphere,* Phys. Rev. A **88**, 022326 (2013).

[147] G. R. Salla, C. Perumangattu, S. Prabhakar, A. Anwar, and R. P. Singh, *Recovering the vorticity of a light beam after scattering,* Appl. Phys. Lett. **107**, 021104 (2015).

[148] C. Perumangatt, G. R. Salla, A. Anwar, A. Aadhi, S. Prabhakar, and R. Singh, *Scattering of non-separable states of light,* Opt. Commun. **355**, 301–305 (2015).

[149] M. Krenn, J. Handsteiner, M. Fink, R. Fickler, and A. Zeilinger, *Twisted photon entanglement through turbulent air across vienna,* P. Natl. Acad. Sci. USA **112**, 14197–14201 (2015).

[150] A. Hamadou Ibrahim, F. S. Roux, M. McLaren, T. Konrad, and A. Forbes, *Orbital-angular-momentum entanglement in turbulence,* Phys. Rev. A **88**, 012312 (2013).

List of Publications

Thesis related Publications

1. **Nijil Lal**, Anindya Banerji, Ayan Biswas, Ali Anwar, and R. P. Singh, "Photon statistics of twisted heralded single photons", *J. Mod. Opt. 67 (2), 126-132 (2020)*.

2. **Nijil Lal**, Biveen Shajilal, Ali Anwar, Chithrabhanu Perumangatt, and R. P. Singh, "Observing sub-Poissonian statistics of twisted single photons using oscilloscope", *Rev. Sci. Instr. 90 (11), 113104 (2019)*.

3. Anindya Banerji, Ali Anwar, Hrushikesh Sable, **Nijil Lal**, R. P. Singh, "Engineering of orbital angular momentum spectrum of down-converted photons with mode-invariant pump", under review in *Physical Review A*; arXiv e-prints arXiv: 1905.02554 [quant-ph] (2019).

Other Publications

4. Chithrabhanu Perumangatt, **Nijil Lal**, Ali Anwar, S. G. Reddy, R. P. Singh, "Quantum Information with Even/Odd States of Orbital Angular Momentum of Light", *Phys. Lett. A 381(22), 1858-1865 (2017)*.

5. Chithrabhanu Perumangatt, S. G. Reddy, **Nijil Lal**, Ali Anwar, R. P. Singh, "Pancharatnam phase in non-separable states of light", *J. Opt. Soc. Am. B 33, 10 (2016).*

6. Ali Anwar, Chithrabhanu P, Salla Gangi Reddy, **Nijil Lal**, R. P. Singh, "Selecting the pre- detection characteristics for effective fiber coupling of entangled photon sources", *Opt. Comm. 382, 219-224 (2017).*

7. Pachava Srinivas, C. Perumangatt, **Nijil Lal**, R. P. Singh, and B. Srinivasan, "Investigation of propagation dynamics of truncated vector vortex beams", *Opt. Lett. 43, 2579-2582 (2018).*

JOURNAL OF MODERN OPTICS
2020, VOL. 67, NO. 2, 126–132
https://doi.org/10.1080/09500340.2019.1699180

Taylor & Francis
Taylor & Francis Group

Photon statistics of twisted heralded single photons

Nijil Lal [a,b], Anindya Banerji [a], Ayan Biswas [a,b], Ali Anwar [a†] and R. P. Singh[a]

[a]Physical Research Laboratory, Ahmedabad 380009, India; [b]Indian Institute of Technology, Gandhinagar 382355, India

ABSTRACT

We study the correlation properties of single photons carrying orbital angular momentum (OAM) in a Hanbury Brown and Twiss (HBT) type experiment. We have characterized single photon sources obtained by pumping a nonlinear crystal with a laser beam carrying different OAM under same experimental conditions. For twisted heralded single photons carrying OAM, we calculate $g^{(2)}(0)$, a measurable parameter characterizing the quality of a single photon source, and observe an increment with the OAM of the single photon. The single photon behaviour of the heralded photons is observed to be reducing with higher orders of their OAM. An OAM-dependent variation of the photon statistics will be relevant to quantum information experiments involving twisted heralded single photons.

ARTICLE HISTORY
Received 12 April 2019
Accepted 18 November 2019

KEYWORDS
Optical vortices; spatial modes of light; intensity correlation; single photon sources

1. Introduction

Single photon sources are one of the most important quantum sources of light finding applications in quantum key distribution, random number generation, quantum computing with photons and quantum metrology (*1*–*4*). One of the most popular technique to produce a single photon source is to use the spontaneous parametric down conversion (SPDC) process in a $\chi^{(2)}$ nonlinear crystal (*5*, *6*). In this process, one photon of the pump is converted to two photons of lower energies, which propagate in a certain direction following the conservation laws of energy and momentum. Since the two down converted photons are generated at the same time, detection of one photon heralds the presence of the other (*7*, *8*). Therefore, single photon sources obtained by using this technique are generally called as heralded single photon sources. Optical vortices or Laguerre Gaussian (LG) beams with zero radial index are gaining popularity in implementing various quantum information protocols (*9*, *10*) as they provide an extra degree of freedom in the form of orbital angular momentum (OAM) (*11*, *12*) that can be measured using standard experimental techniques (*13*–*15*). Optical vortices of different orders or azimuthal indices form different spatial modes of light with their characteristic properties (*16*–*20*). Intensity correlations of classical optical vortices are found to have dependence on the order of the vortex while scattered from a rotating ground-glass plate (*16*). Such studies evoke interest in the correlation properties of single photons carrying OAM generated in spontaneous processes such as parametric down conversion. In the present work, starting with the Gaussian mode, we take different orders of vortices as a pump to the nonlinear crystal and study the intensity correlations of down converted photons to characterize them for single photon sources of light including twisted single photons.

2. Theory

The measurement of second-order correlation ($g^{(2)}(\tau)$) has been important in quantum optics, especially in observing antibunching which is a purely quantum mechanical behaviour. The normalized second-order correlation function (*21*), for a fixed position, is given as

$$g^{(2)}(\tau) = \frac{\langle \hat{E}^{(-)}(t)\hat{E}^{(-)}(t+\tau)\hat{E}^{(+)}(t+\tau)\hat{E}^{(+)}(\tau)\rangle}{\langle \hat{E}^{(-)}(t)\hat{E}^{(+)}(t)\rangle \langle \hat{E}^{(-)}(t+\tau)\hat{E}^{(+)}(t+\tau)\rangle} \quad (1)$$

and is usually measured in a Hanbury Brown–Twiss (HBT) experiment (*22*, *23*), which gives the correlation between two photons separated by a time delay, τ. For an ideal single photon source from which individual photons are emitted one after another as given in Figure 1(a), a photon either gets transmitted (along arm ***1***) at the beam splitter or gets reflected (along arm ***2***). There are no simultaneous incidences at the detectors D_1 and D_2 when there is no delay between the paths ***1*** and ***2*** ($\tau = 0$).

CONTACT Nijil Lal nijil@prl.res.in, nijillalck@gmail.com
†Currently at Centre for Quantum Technologies, National University of Singapore, 3 Science Drive 2, Singapore 117543, Singapore.

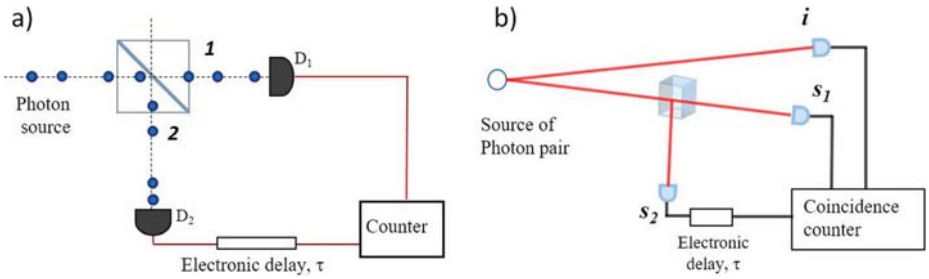

Figure 1. A simplified illustration of the HBT experiment for (a) an ideal single photon source where photons reaching the beam splitter through the input port will choose any of the paths 1 or 2 without resulting in any coincidence detection between the detectors D_1 and D_2 and (b) a heralded single photon source.

For heralded single photon sources generated by spontaneous parametric down conversion (SPDC), the photon correlation in the HBT experiment has to be done in the signal ($\boldsymbol{s}$) with the conditioned detection of idler ($\boldsymbol{i}$) (Figure 1(b)). For the ideal case of a single photon source when the delays between i, s_1 and s_2 are zero, the three fold detection probability between these arms would be zero. This probability, P_{i,s_1,s_2} when normalized with respect to the corresponding two-fold coincidences gives the second-order correlation (for zero delay)

$$g^{(2)}(0) = \frac{P_{i,s_1,s_2}}{P_{i,s_1}P_{i,s_2}} \tag{2}$$

where P_{i,s_1} and P_{i,s_2} are the two-fold coincidence probabilities between $i - s_1$ and $i - s_2$. The conditioned probability of coincidence detection can be expressed as $P_{i,j} = R_{i,j}/R_i$ where $R_{i,j}$ corresponds to the coincidence rate between the respective arms and R_i is the count rate of the heralding arm. Substituting for different probabilities in Equation (2), $g^{(2)}(0)$ in terms of experimentally measured rates will take the form (*23*, *24*)

$$g^{(2)}(0) = \frac{R_{i,s_1,s_2}R_i}{R_{i,s_1}R_{i,s_2}}. \tag{3}$$

This involves the calculation of $g^{(2)}(0)$ from the direct measurement of the three fold coincidences between the heralding idler mode and two signal modes.

The non-zero values for three-fold coincidence rate R_{i,s_1,s_2} could be attributed to accidental coincidences due to the finite width of our coincidence window. Assuming the probability of completely uncorrelated photons reaching all three detectors simultaneously as zero (for practical purposes), we can attribute the accidental coincidences to the occurrence of a random detection along with a coincidence detection. Rewriting the three-fold coincidence in terms of two-fold coincidence and a probabilistic detection at the third detector, i.e. $P_{i,s_1,s_2} = P_{i,s_1}R_{s_2}\Delta t + P_{i,s_2}R_{s_1}\Delta t$ where Δt is the coincidence window, a modified expression for $g^{(2)}(0)$ is obtained as (*25*)

$$g^{(2)}(0) = R_i\Delta t(R_{s_1}/R_{i,s_1} + R_{s_2}/R_{i,s_2}). \tag{4}$$

In order to study the effect of OAM on the second-order correlation function of SPDC photons, we need a more generic expression which clearly establishes the connection between the two. As is well known, OAM forms a complete basis and any state can be expanded in terms of it. The two photon down converted state can be written as

$$|\psi\rangle = \sum_{l_s,l_i} C_{l_s,l_i}\,|l_s\rangle\,|l_i\rangle \tag{5}$$

where $l_k \in \{-\infty, \infty\}$ is the OAM of the kth mode and $k \in \{s, i\}$. The normalized $|C_{l_s,l_i}|^2$ is the probability of the signal and idler photons having OAM l_s and l_i, respectively. This OAM of the signal and idler modes are constrained by the conservation relation $l_s + l_i = l_p$ where l_p is the OAM of the pump photon. To see how the OAM affects the second-order correlation function, we consider the case where the idler photon is in the 0 OAM state such that $l_i = 0$ and $l_s = l_p - l_i = l_p$. The corresponding coefficient $C_{l_p,0}$ can be calculated from the mode overlap integral as follows:

$$C_{l_p,0} = \int \mathrm{d}\boldsymbol{r}\Phi_p\left(l_p,\boldsymbol{r}\right)\Phi_s^*\left(l_p,\boldsymbol{r}\right)\Phi_i^*\left(0,\boldsymbol{r}\right) \tag{6}$$

where $\Phi_k(l_k,\boldsymbol{r})$ is the spatial mode function of the kth mode with normalized beam waist, $\bar{w_k} = w_k/\sqrt{\lambda_p L}$ (where L is the crystal length). In the paraxial regime, the beam waists of the pump and down-converted signal/idler arms can be taken to be equal in the generation plane. In the calculation of the overlap integral in Equation (6), we have assumed $\bar{w_p} = \bar{w_i} = \bar{w_s} = 1$. For the pump wavelength of 405 nm and a crystal length of 2 mm, a pump beam waist of $w_p = 30\,\mu$m corresponds to a normalized value of $\bar{w_p} \approx 1$.

In case the pump, signal and idler are all written in terms of LG modes with radial indices taken as zero,

Equation (6) is evaluated to have the following closed form (*26*):

$$C_{l_p,0} = \frac{1}{3}\sqrt{\frac{8}{\pi}}\left(\frac{2}{3}\right)^{|l_p|} \tag{7}$$

The coincidence probability, or probability of the idler and signal photon being in 0 and l_p OAM state respectively, is then calculated simply by taking the square of Equation (7). These are the probabilities P_{i,s_1} and P_{i,s_2}. Equation (2) can be rewritten in terms of these probabilities as follows:

$$g^{(2)}(0) = \frac{P_{i,s_2}R_{s_1}\Delta t + P_{i,s_1}R_{s_2}\Delta t}{P_{i,s_1}P_{i,s_2}} \tag{8}$$

where we have assumed that all triple coincidence events happen only due to accidents resulting from finite coincidence window, following the prescription of (*25*). This can be further simplified to

$$g^{(2)}(0) = \left(\frac{R_{s_1}}{P_{i,s_1}} + \frac{R_{s_2}}{P_{i,s_2}}\right)\Delta t \tag{9}$$

It can be seen numerically that the summation of $|C_{l_s,l_i}|^2$ for all l_i gives $R_{s_1} + R_{s_2}$, which would be the total count rate of both of the signal arms. Experimentally, we have multi-mode fibres in the two signal arms which ensures we couple almost all the photons independent of their modes, preserving the total count rate and making R_{s_1} and R_{s_2} essentially constants. In an ideal situation, the rate of singles R_{s_1} and R_{s_2} should be equal to each other. Also, from Equation (7), it can be easily seen that the coincidence probabilities P_{i,s_1} and P_{i,s_2} only depend on the pump OAM and therefore should be equal to each other. With these considerations, we can arrive at the following simplified form of the second-order correlation function:

$$g^{(2)}(0) = 2\left(\frac{R_s}{P_{i,s}}\right)\Delta t \tag{10}$$

Since the quantity R_s is a constant with change in OAM of the twisted photon, the second-order correlation function varies as the inverse of the coincidence probability, $P_{i,s} = |C_{l_s,l_i}|^2$. The value of R_s is taken to be equal to the experimentally observed count rate of either of the signal arms ($R_s = R_{s_1} = R_{s_2}$), while $P_{i,s}$ is determined theoretically from Equation (7).

3. Experiment

Experimental set-up for studying the correlation of heralded signal photons from the SPDC is given in Figure 2. A diode laser (Toptica Topmode) of wavelength 405 nm is used as a pump. Optical vortices of different orders, generated using spiral phase plates (SPP) (Holo/Or) are incident on a $\chi^{(2)}$ non-linear crystal (β-barium borate or BBO, $5 \times 5 \times 2$ mm), which generates a cone of correlated pairs of down-converted photons at phase-matching conditions. Degenerate signal–idler pairs are selected using interference filters. The pump polarization is adjusted along the crystal optic axis using a half wave plate ensuring maximum down-conversion. The idler photons are coupled to a single-mode fibre due to which only photons with OAM, $l_i = 0$ are selected in the idler arm. This ensures that the corresponding signal photons are carrying the same OAM as the pump photon following the OAM conservation. The signal is equally split using a 50:50 beam splitter and each portion is coupled to a multimode fibre. The idler and signals from the two ports of the beam splitter are then guided to single photon counting modules (Excelitas SPCM-AQRH-16-FC, dark counts $\sim$ 25 cps). The interference filters (IF) of pass band 810 5 nm cut the undesired light at detection. Optimizing fibre coupling using fibre collimators, maximum coincidences are achieved between signal and idler arms. The coincident photons are counted using a time to digital converter (ID800 TDC, IDQuantique). The coincidence window (Δt) for heralding is kept as 810 ps. The detector position, length of fibres and BNC connectors from SPCM to TDC are optimally matched such that the relative delays between all three detectors are zero. This is ensured by obtaining maximum two fold coincidences between $i - s_1$ and $i - s_2$.

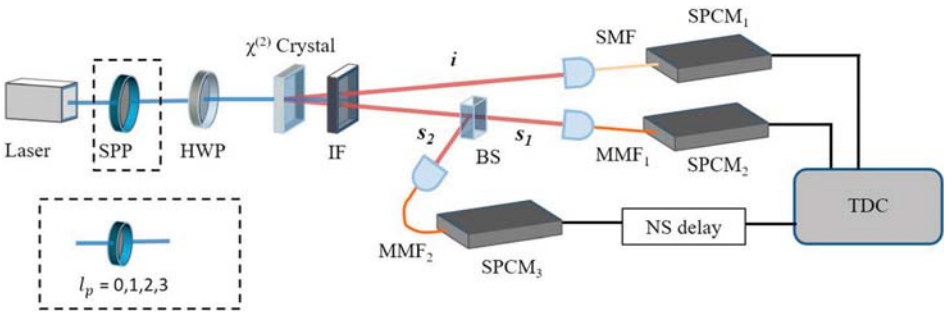

Figure 2. HBT-like set-up to determine the second-order correlation for a heralded single photon source. The delay generator (NS delay) introduces electronic delay in steps of 0.5 ns between the two output ports of the beam splitter (BS) in the signal arm.

4. Results and discussion

The second-order coherence function, $g^{(2)}(\tau)$, is calculated from Equation (3) as a function of the time delay between photons reaching the beam splitter for a Gaussian pump. A delay generator introduces electronic delay in steps of 0.5 ns between the two output ports of the beam splitter (s_1 and s_2) in the signal arm. Coincidence measurements recorded for pair of detectors $SPCM_1$ and $SPCM_2$ kept in these two arms are heralded by the detection of a photon in the idler arm, $\boldsymbol{i}$. Antibunching (for $\tau = 0$) is observed by varying the temporal delay between arms s_1 and s_2 as given in Figure 3.

While the expected value of $g^{(2)}(0)$ for a true single photon source is zero, the non-zero values in a heralded detection can be attributed to accidental coincidences between the three detectors which can arise from simultaneous generation of multiple photon pairs, dark counts, background fluorescence, etc. We have studied $g^{(2)}(0)$ by increasing the pump power and observed an increase with power (Figure 4). The steady increment in $g^{(2)}(0)$ with pump power is due to the fact that the rate of pair production and hence the probability of simultaneous creation of multiple photon pairs are proportional to the pump power (*27*). This results in more than two photons reaching together at the beam splitter leading to coincidences between the two signal arms. A higher $g^{(2)}(0)$ shows a reduced non-classical behaviour. Hence, it is crucial for quantum optical experiments using heralded single photon sources to be done in the lower pump power regime.

As discussed before, the orbital angular momentum is conserved in parametric down conversion (*15*) such that

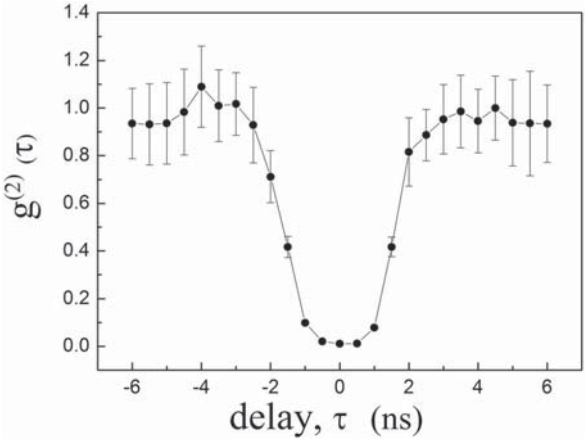

Figure 3. The variation of second-order correlation function with delay, τ, for a fundamental Gaussian mode as pump ($l_p = 0$). The error bar corresponds to the standard deviation obtained from the measured count rate uncertainties. Coincidence window, $\Delta t =$ 810 ps.

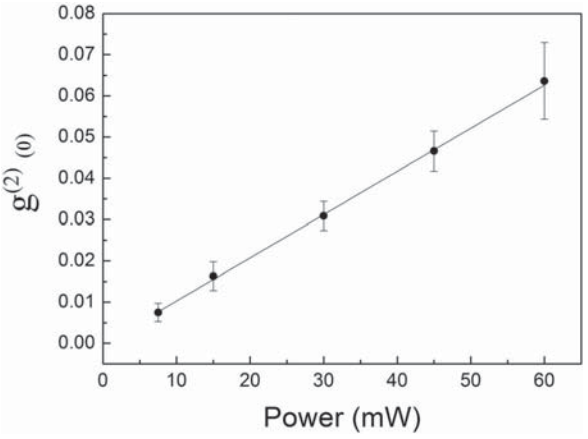

Figure 4. The variation of $g^{(2)}(0)$ with increasing pump power. A linear fit (line) to the experimental points (symbols) extrapolates to the origin, suggesting that multi-pairs from the down-converted output are the dominant contributors to a non-zero $g^{(2)}(0)$. Pump is a fundamental Gaussian mode. Error bar corresponds to standard deviation obtained from count rate uncertainties.

the sum of the orbital angular momenta of the down converted photons equals the pump OAM. While the output beams of the parametric down conversion are incoherent sum of multiple spatial modes, the signal–idler photon pairs will have OAM l_s and l_i respectively, restricted by the OAM conservation $l_i + l_s = l_p$, where l_p is the pump OAM. *By coupling the idler into a single mode fibre, we restrict the idler spatial mode to be Gaussian*, (i.e. $l_i = 0$), *and thereby selecting the signal OAM to be the same as that of the pump*. Hence, the heralded correlation measurements done in the signal arm give the statistics of twisted photons whose OAM is defined by that of the pump. The pump OAM is varied using SPPs of different orders to study the statistics of generated twisted single photons. Heralded second-order correlation is measured for each order of pump OAM.

The second-order correlation function for $= 0, g^{(2)}(0)$, measured in the low power regime (*pumppower7mW*) for different OAM values of single photons is given in Table 1. For a single photon with $\boldsymbol{l} = 0$, we have obtained 0.00820.00430.00820.0043 from Equation (3). As the probability of detection of three-fold coincidences is very low, the statistical error in such measurements can be relatively high. Hence, we have also calculated $g^{(2)}(0)$ using Equation (4), where the direct measurements of three-fold coincidences are not used. Here, $g^{(2)}(0)$ is calculated with the assumption that three-fold coincidences result from the simultaneous occurrence of a two-fold coincidence (between the heralding photon and one of the signal photons) and an accidental coincidence in the

Table 1. Second-order correlation, $g^{(2)}(0)$, for a single photon source calculated (a) directly from the measured three-fold coincidences using Equation (3) and (b) indirectly from the two-fold coincidences by considering the three-fold detection as probabilistic accidental coincidences with the heralding arm using Equation (4).

Twisted photon OAM, $l = l_p$	**0**	**1**	**2**	**3**
(a) $g^{(2)}(0)$: direct	0.0082 ± 0.0043	0.015 ± 0.011	0.030 ± 0.057	0.045 ± 0.17
(b) $g^{(2)}(0)$: indirect	0.0047 ± 0.00013	0.0094 ± 0.00028	0.021 ± 0.00094	0.042 ± 0.0016

third detector. In both cases, an increment in $g^{(2)}(0)$ has been observed with the increasing orders of the OAM.

We have calculated the two-fold detection probability, $P_{i,s_j} = R_{i,s_j}/R_i$ from experimentally observed rates and studied the variation for photons carrying different OAM. This is calculated for both P_{i,s_1} and P_{i,s_2} and when normalized they are shown to be matching exactly with theoretically calculated values for normalized two-fold detection probability, $|C_{l_p,0}|^2$, for the down-converted pair of photons to have OAM, $(l_p, 0)$ (Figure 5). In obtaining Equation (7), we have assumed that normalized pump beam waist, $\bar{w_p} \approx 1$. Since we take the radial index of the LG modes to be zero, the OAM distribution depends only on $\bar{w_p}$ and gets flatter and wider with increase in $\bar{w_p}$ (*28*). This can further make the two-fold probability distribution in Figure 5 as well as the variation in the derived $g^{(2)}(0)$ in Figure 6 flatter. Hence, one can optimize $\bar{w_p}$ to control the dependence of $g^{(2)}(0)$ on OAM of twisted photons.

Second-order correlation parameter, $g^{(2)}(0)$, has been calculated for the heralded single photons corresponding to different orders of the twisted single photon. The top row in Table 1 lists $g^{(2)}(0)$ obtained through the direct measurement of triple coincidences between the three detectors using Equation (3) for different orders of OAM. It can be seen that the error is larger compared to the bottom row since very few triple coincidences are registered even for longer exposure times. This error corresponds to the statistical standard deviation determined using error propagation formula in Equation (3). The bottom row gives the same but the non-zero value of $g^{(2)}(0)$ is modelled to be due to potential accidental coincidences which arise when a random detection is recorded along with a true two-fold coincidence between the other two detectors (Equation (4)). This indirect method provides an better alternative as the two-fold coincidences are easier to measure and optimize compared to three-fold coincidences. Here, we obtain slightly lower value for $g^{(2)}(0)$ with reduced standard deviation compared to the direct measurement from three-fold coincidences. It is also observed that $g^{(2)}(0)$ is increasing with increasing order of OAM of twisted photons. It is shown in Figure 5 that the two-fold coincidence probability between the idler–signal arms decreases with pump OAM since the OAM content corresponding to $(0, l_p)$ modes in the down-converted output decreases. As a result, the relative probability of

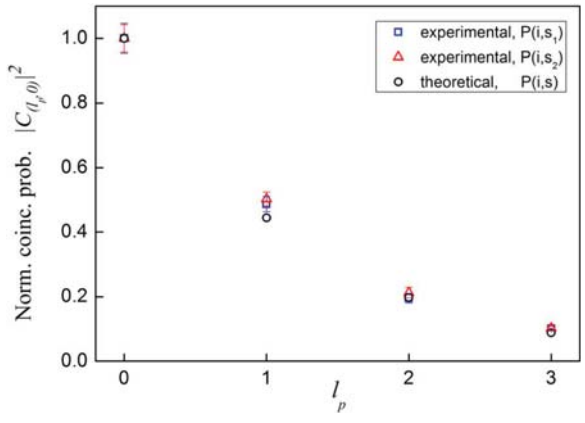

Figure 5. Variation of normalized probability $|C_{l_p,0}|^2$ (circle) and experimentally measured conditional probabilities $R_{i,s_1}/R_i$ (square) and $R_{i,s_2}/R_i$ (triangle), with l_p. Since the idler is selected as the Gaussian mode, the twisted single photon OAM, $l = l_p$. The experimental probabilities are normalized to unity at $l_p = 0$ (for $l_p = 0$, $R_i = 1.75 \times 10^4\ s^{-1}\ mW^{-1}$, $R_{i,s_1} = 408\ s^{-1}\ mW^{-1}$ and $R_{i,s_2} = 400\ s^{-1}\ mW^{-1}$).

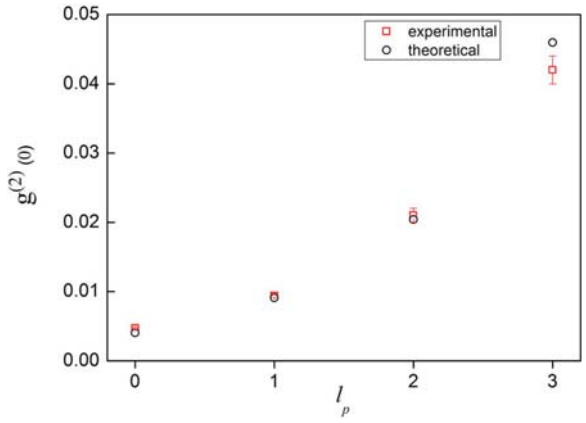

Figure 6. The variation of second-order correlation function with OAM of the heralded single photon, $l = l_p$. Experimental (squares) and theoretical (circles) values are in good agreement. The theoretical data correspond to Equation (10) where R_s is taken to be equal to the experimentally observed signal count rate, $R_s = 4.15 \times 10^4\ s^{-1}\ mW^{-1}$.

accidental coincidences with respect to true two-fold coincidences increases and it is visible as an increment in $g^{(2)}(0)$ with OAM.

The experimentally calculated values for second-order correlation (Table 1(b)) obtained from the indirect method given in Equation (4) are plotted in Figure 6. The error bars correspond to the standard deviation obtained from uncertainties in count(and coincidence) rates. The theoretical plot for the OAM dependent $g^{(2)}(0)$ as calculated from the coincidence probability (Equation (10)) is also given. The coincidence window is taken to be 810 ps. The experimental values are in good agreement with the theoretical predictions. Orbital angular momentum of photons has emerged over years as a strong candidate for information encoding in quantum information protocols using heralded single photons. Variations in the statistics of twisted single photons will become relevant while dealing with OAM of photons generated in parametric down-conversion. The results are of greater importance since an intuitive guess does not associate a quantity like second-order correlation ($g^{(2)}(0)$) to be dependent on the OAM of the photon.

5. Conclusion

We have calculated the second-order coherence function with zero delay, $g^{(2)}(0)$ for different OAM values of heralded single photons. It was calculated from the direct measurement of the simultaneous detection between the three detectors in a heralded HBT experiment as well as through a model that accounts for the accidental three-fold coincidences. In both cases, $g^{(2)}(0)$ is found to be increasing with the increasing order of the OAM for the twisted photons. This suggests that the non-classicality of the twisted photons generated in parametric down-conversion deteriorates in terms of the second-order correlations, with higher orders of their OAM. In experiments related to quantum information using OAM of photons, it is a general technique to generate single photons carrying OAM by pumping an SPDC crystal using vortex beams of different order and post-selecting the idler photon to a single mode fibre ($l_i = 0$). The results can be significant while using such OAM states of single photons for quantum information applications.

Disclosure statement

No potential conflict of interest was reported by the authors.

ORCID

Nijil Lal http://orcid.org/0000-0002-6517-7283
Anindya Banerji http://orcid.org/0000-0001-6926-706X
Ayan Biswas http://orcid.org/0000-0002-7500-145X
Ali Anwar http://orcid.org/0000-0002-7454-1059

References

(1) Lo H.K.; Curty M.; Tamaki K. Secure Quantum Key Distribution. *Nat. Photonics* **2014,** *8* (8), 595–604.
(2) Herrero-Collantes M.; Garcia-Escartin J.C. Quantum Random Number Generators. *Rev. Mod. Phys.***2017,** *89* (1), 015004.
(3) Northup T.; Blatt R. Quantum Information Transfer Using Photons. *Nat. Photonics* **2014,** *8* (5), 356–363.
(4) Giovannetti V.; Lloyd S.; Maccone L. Advances in Quantum Metrology. *Nat. Photonics* **2011,** *5* (4), 222–229.
(5) Boyd R.W. *Nonlinear Optics*; Elsevier: Amsterdam, 2003.
(6) Agarwal G.S. *Quantum Optics*; Cambridge University Press: Cambridge, 2012.
(7) Burnham D.C.; Weinberg D.L. Observation of Simultaneity in Parametric Production of Optical Photon Pairs. *Phys. Rev. Lett.* **1970,** *25* (2), 84–87.
(8) Hong C.; Mandel L. Experimental Realization of a Localized One-photon State. *Phys. Rev. Lett.* **1986,** *56* (1), 58–60.
(9) Mirhosseini M.; Magaña-Loaiza O.S.; O'Sullivan M.N.; Rodenburg B.; Malik M.; Lavery M.P.; Padgett M.J.; Gauthier D.J.; Boyd R.W. High-dimensional Quantum Cryptography With Twisted Light. *New J. Phys.* **2015,** *17* (3), 033033.
(10) Barreiro J.T.; Wei T.C.; Kwiat P.G. Beating the Channel Capacity Limit for Linear Photonic Superdense Coding. *Nat. Phys.* **2008,** *4* (4), 282–286.
(11) Allen L.; Beijersbergen M.W.; Spreeuw R.; Woerdman J. Orbital Angular Momentum of Light and the Transformation of Laguerre-Gaussian Laser Modes. *Phys. Rev. A* **1992,** *45* (11), 8185–8189.
(12) Yao A.M.; Padgett M.J. Orbital Angular Momentum: Origins, Behavior and Applications. *Adv. Opt. Photonics* **2011,** *3* (2), 161–204.
(13) Vaity P.; Banerji J.; Singh R. Measuring the Topological Charge of an Optical Vortex by Using a Tilted Convex Lens. *Phys. Lett. A* **2013,** *377* (15), 1154–1156.
(14) Prabhakar S.; Kumar A.; Banerji J.; Singh R. Revealing the Order of a Vortex Through Its Intensity Record. *Opt. Lett.* **2011,** *36* (22), 4398–4400.
(15) Mair A.; Vaziri A.; Weihs G.; Zeilinger A. Entanglement of the Orbital Angular Momentum States of Photons. *Nature* **2001,** *412* (6844), 313–316.
(16) Kumar A.; Banerji J.; Singh R. Hanbury Brown–Twiss-type Experiments with Optical Vortices and Observation of Modulated Intensity Correlation on Scattering From Rotating Ground Glass. *Phys. Rev. A* **2012,** *86* (1), 013825.
(17) Kumar A.; Prabhakar S.; Vaity P.; Singh R. Information Content of Optical Vortex Fields. *Opt. Lett.***2011,** *36* (7), 1161–1163.
(18) Reddy S.G.; Prabhakar S.; Kumar A.; Banerji J.; Singh R. Higher Order Optical Vortices and Formation of Speckles. *Opt. Lett.* **2014,** *39* (15), 4364–4367.
(19) Reddy S.G.; Permangatt C.; Prabhakar S.; Anwar A.; Banerji J.; Singh R. Divergence of Optical Vortex Beams. *Appl. Optics* **2015,** *54* (22), 6690–6693.

(20) Lochab P.; Senthilkumaran P.; Khare K. Near-core Structure of a Propagating Optical Vortex. *J. Opt. Soc. Am. A* **2016,** *33* (12), 2485–2490.
(21) Mandel L.; Wolf E. *Optical Coherence and Quantum Optics*; Cambridge University Press: Cambridge, 1995.
(22) Kimble H.J.; Dagenais M.; Mandel L. Photon Antibunching in Resonance Fluorescence. *Phys. Rev. Lett.* **1977,** *39* (11), 691–695.
(23) U'Ren A.B.; Silberhorn C.; Ball J.L.; Banaszek K.; Walmsley I.A. Characterization of the Nonclassical Nature of Conditionally Prepared Single Photons. *Phys. Rev. A* **2005,** *72* (2), 021802.
(24) Grangier P.; Roger G.; Aspect A. Experimental Evidence for a Photon Anticorrelation Effect on a Beam Splitter: A New Light on Single-photon Interferences. *Europhys. Lett.* **1986,** *1* (4), 173–179.
(25) Beck M. Comparing Measurements of G (2)(0) Performed with Different Coincidence Detection Techniques. *J. Opt. Soc. Am. B* **2007,** *24* (12), 2972–2978.
(26) Banerji A.; Anwar A.; Sable H.; Lal N.; Singh R.P.. Engineering of Orbital Angular Momentum Spectrum of Down-Converted Photons with Mode-Invariant Pump. 2019, arXiv:1905.02554.
(27) Razavi M.; Söllner I.; Bocquillon E.; Couteau C.; Laflamme R.; Weihs G. Characterizing Heralded Single-photon Sources with Imperfect Measurement Devices. *J. Phys. B – At. Mol. Opt.* **2009,** *42* (11), 114013.
(28) Torres J.; Alexandrescu A.; Torner L. Quantum Spiral Bandwidth of Entangled Two-photon States. *Phys. Rev. A* **2003,** *68* (5), 050301.

Review of Scientific Instruments ARTICLE scitation.org/journal/rsi

Observing sub-Poissonian statistics of twisted single photons using oscilloscope

Cite as: Rev. Sci. Instrum. 90, 113104 (2019); doi: 10.1063/1.5109544
Submitted: 9 May 2019 • Accepted: 3 November 2019 •
Published Online: 21 November 2019

Nijil Lal,[1,2,a] Biveen Shajilal,[3,b] Ali Anwar,[1,c] Chithrabhanu Perumangatt,[1,c] and R. P. Singh[1]

AFFILIATIONS

[1]Physical Research Laboratory, Ahmedabad 380009, India
[2]Indian Institute of Technology, Gandhinagar 382355, India
[3]Cochin University of Science and Technology, Kochi 682022, India

[a]**Electronic mail:** nijil@prl.res.in
[b]**Present address:** Centre for Quantum Computation & Communication Technology, Department of Quantum Science, The Australian National University, Canberra, ACT 2601, Australia.
[c]**Present address:** Centre for Quantum Technologies, National University of Singapore, 3 Science Drive 2, 117543, Singapore.

ABSTRACT

Heralded single photon sources (HSPSs) from spontaneous parametric down-conversion are widely used as single photon sources. We study the photon number statistics of an HSPS carrying orbital angular momentum in our laboratory and observe the sub-Poissonian statistics using only photodetectors and an oscilloscope.

I. INTRODUCTION

The photon is a prominent qubit candidate in quantum information processing (QIP). Most of these applications require a single photon source (SPS) which will provide an "on-demand," deterministic supply of photons. Such ideal SPSs can be realized in crystal color centers,[1] quantum dots,[2] single atoms,[3] single ions,[4] and single molecules.[5] The photon being an indivisible quantum of energy and the consequent impossibility of copying associated information from an unknown arbitrary state makes single photon sources an ideal choice for quantum information processing, secure communication, and metrology. Spontaneous parametric down-conversion (SPDC) is one of the most widely used processes to generate single photon sources as it provides a robust and bright source at room temperature.[6] In this process, a pump photon is down-converted in frequency in a $\chi^{(2)}$ nonlinear crystal to a pair of photons, conventionally called the signal (s) and the idler (i). The detection of one photon from the pair heralds the presence of another, and this conditioned detection serves as a technique for generating single photon sources. SPDC is also important in QIP as a bright source of entangled photon pairs[7] and thus finds applications in quantum teleportation,[8] quantum cryptography,[9] and quantum dense coding.[10]

A single photon source shows nonclassical properties such as sub-Poissonian photon number distribution and antibunching. The inherent thermal nature of the photon distribution in the individual arms (i.e., signal or idler) evokes the possibility of occurrences of multiple photons and hence would qualify the source as less quantum than it is expected to be. The occurrence of multiple photon pairs and consequent photon bunching threatens the security in cryptography related applications. Thus, it is important to study and quantify the nonclassicality of the single photon sources being used. A general classification puts the sources into three categories, super-Poissonian, Poissonian, and sub-Poissonian, according to the photon number distribution. Classical sources, such as thermal and coherent radiation, show super-Poissonian and Poissonian statistics, respectively, while certain nonclassical sources, such as a single photon source, show sub-Poissonian distribution. Violations of bounds defined for the number statistics of classical sources imply the nonclassical behavior of single photon sources.[11–14] Photon antibunching is another manifestation of the nonclassical behavior of the source and can be observed through the measurement of the degree of second-order coherence, $g^{(2)}(\tau)$. Single photon sources show antibunching, and hence, $g^{(2)}(0)$ falls to zero. Although antibunching and sub-Poissonian statistics are completely nonclassical

effects and tend to occur together in many systems, they are distinct effects and need not necessarily be associated with one another.[15,16] For a heralded SPS, antibunching can be observed using a heralded Hanbury Brown-Twiss (HBT) type experiment.[17,18] Twisted single photons carrying orbital angular momentum (OAM) are gaining interest in quantum information processing as they provide infinite number of orthogonal states to encode information.[19,20] The statistical second order correlation of classical beams[21,22] as well as photons[23] carrying OAM has already been studied. In the present work, we verify the sub-Poissonian nature of heralded single photons generated in parametric down-conversion having Gaussian as well as higher order OAM using a simple setup consisting of photodetectors and an oscilloscope.

II. THEORY

One can define an ideal single photon source as a Fock state for which the number statistics gives mean, $\mu = 1$, and variance, $\sigma^2 = 0$. Treatment of the electromagnetic field as a quantum harmonic oscillator allows us to define quadrature field operators, $\hat{X}_1$ and $\hat{X}_2$, which can be shown to follow the uncertainty relation,[24] $\langle \Delta\hat{X}_1^2 \rangle \langle \Delta\hat{X}_2^2 \rangle \geq 1/16$. The minimum uncertainty state, with $\langle \Delta\hat{X}_1^2 \rangle = \langle \Delta\hat{X}_2^2 \rangle$, is the coherent state,

$$|\alpha\rangle = \exp^{\frac{-|\alpha|^2}{2}} \sum_{n=0}^{\infty} \frac{\alpha^n}{\sqrt{n!}} |n\rangle, \tag{1}$$

which defines a Poissonian distribution of photon number,[25] n, with $\langle (\Delta\hat{n})^2 \rangle = \langle \hat{n} \rangle$. Squeezing these states in terms of number or phase is achieved when the respective variance is less than that corresponding to the coherent state. The photon number variance can be written as

$$\langle \Delta\hat{n}^2 \rangle = \langle \hat{n} \rangle + \langle \hat{a}^\dagger \hat{a}^\dagger \hat{a}\hat{a} - \langle \hat{a}^\dagger \hat{a} \rangle^2 \rangle, \tag{2}$$

where $\hat{a}$ and $\hat{a}^\dagger$ are the annihilation and creation operators. Based on the variance, the Mandel Q-parameter[26] is defined by

$$Q \equiv \frac{\langle \hat{a}^\dagger \hat{a}^\dagger \hat{a}\hat{a} - \langle \hat{a}^\dagger \hat{a} \rangle^2 \rangle}{\langle \hat{a}^\dagger \hat{a} \rangle} = \frac{\langle (\Delta\hat{n})^2 \rangle - \langle \hat{n} \rangle}{\langle \hat{n} \rangle}. \tag{3}$$

It classifies light sources on the basis of photon number fluctuations. $Q \geq 0$ for coherent and all other classical sources of light, while sub-Poissonian light is identified with $Q < 0$.[26,27]

The detected photoelectron statistics and the statistics of the incident photons can be different depending upon various factors such as the coherence time of the incident light, detector dead-time, and efficiency of detection. The first two are taken care of while setting the binning window and pump intensity, respectively. This is discussed in detail in Sec. III. Correcting for the efficiency, the mean and standard deviation for the detected-photon distribution can be written as[28]

$$\langle m \rangle = \eta \langle n \rangle, \tag{4}$$

$$\sigma^2(m) = \eta^2 \sigma^2(n) + \eta(1-\eta)\langle n \rangle, \tag{5}$$

where m is the detected photocounts, n is the actual photocounts, η is the detector quantum efficiency, and σ^2 is the variance. Hence, the expression for the Fano factor will be

$$F_n = (F_m - (1-\eta))/\eta. \tag{6}$$

Correcting for the efficiency of detection, the Q-parameter will be

$$Q_n = Q_m/\eta. \tag{7}$$

III. EXPERIMENT

The experimental setup used for building the statistics of the heralded single photon source is given in Fig. 1.[29] A 405 nm diode laser (Toptica TopMode) is used as a pump to generate photon pairs from a Type-I BiBO crystal (Castech, 5 mm thickness). The polarization of the pump is oriented along the crystal axis using a half-wave plate. The output pairs are spectrally filtered using interference filters of passband of 810 ± 5 nm to rule out the nondegenerate pairs. Two diametrically opposite regions are selected from the cone of correlated pairs of photons generated in the Type-I SPDC. These individual arms (signal and idler) are then collimated and coupled to a single mode fiber (SMF, *idler*) and a multimode fiber (MMF, *signal*) through a fiber coupler (CFC-5X-B).

The individual signal and idler photons are detected using single photon detectors. We have used two single photon counting modules (SPCMs, Excelitas SPCM-AQRH-16-FC) placed in both signal and idler arms for the detection of the photon pairs. Photomultiplier tubes (PMTs), which will be more common in laboratories than an SPCM can also be used for the detection. The coincidences are maximized by optimizing the coupling to the fiber. The

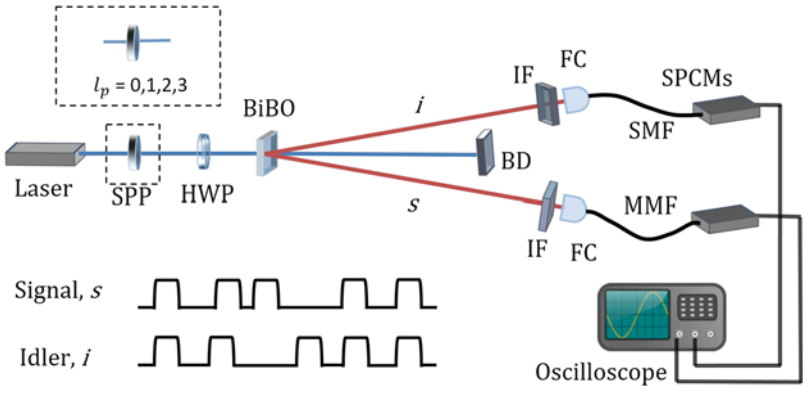

FIG. 1. Experimental setup to determine the photon number statistics of the heralded PDC source. HWP—half wave plate, BiBO—nonlinear crystal, BD—beam dump, IF—interference filters, FC—fiber couplers, and SPCMs—single photon counting modules. Different OAM orders can be imparted to the heralded single photon by placing SPPs of different orders in pump and projecting the idler photon in a single mode fiber.

SPCM (or PMT) generates a TTL pulse in response to each photon incidence. However, the total number of photon incidences that can be recorded by a detector is limited by the detector dead time. If more than two photon incidences occur at the detector within the dead-time, the detector will not be able to register the second detection and the number statistics will not give the correct distribution.[30,31] Therefore, it is important to verify that the probability of such multiple detection within the dead-time is negligible. The individual count rates are $\sim 10^4/s$ for the single mode fiber and $\sim 10^5/s$ for the multimode fiber (MMF). The detector dead time is 27 ns (t_d) for the SPCMs used in the setup. If n is the total count rate in the detector associated with MMF (being larger in value compared to the SMF) and t_d is the dead time corresponding to the detector, then $n \ll 1/t_d$ ensures that the probability that more than two photons arriving within the dead time interval is very less. Our count rates are such that this probability is negligible and dead time effects on the total counts can be ignored. In addition to this, since the detectors being used are not photon number-resolving, the output pulses can correspond to the incidence of one or more photons. The pump power is kept in the low power regime (1 mW) in order to avoid such scenarios due to the possible multiple photon generations.[32]

The output waveform from each arm of the SPDC is recorded using a digital oscilloscope (Infiniium 90000A series) for an exposure time of 20.5 ms. Ten iterations of such time series have been recorded to calculate the Q-parameter. Each iteration records a time series of 20.5 Mpts and a resolution of 1 ns. Oscilloscopes with lower specifications can also be used but with compromising the length of the time series to be captured and time resolution. In order to build the statistics, the detection events at the photodiodes are counted within a defined time interval (binning window) and the distribution of the number of such occurrences is obtained. This is done by converting the analog output from the oscilloscope into a series of 1's and 0's which corresponds to the presence or absence of a detection, respectively. We built a MATLAB code which identifies an event pulse in the oscilloscope output time series and labels its onset as 1 and the rest of the series as 0. This generates a binary time series of events in terms of the occurrences or nonoccurrences of photon detection (Fig. 2). A probability distribution of events is built from this generated time series.

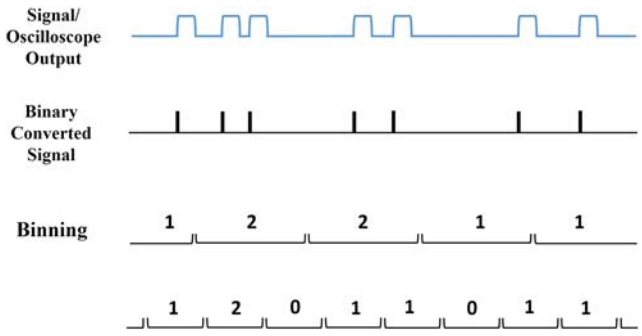

FIG. 2. Building the number statistics from the recorded time series. The oscilloscope output is converted into binary time series of 0's and 1's that represent the presence (1) or absence (0) of a detected photon. Corresponding probability distributions are built from this series by defining an appropriate binning window size.

The time series of binaries generated for both the signal and idler are then sliced into smaller binning windows in such a way that statistically one detection falls in a bin. The number distribution is developed for these individual arms. A new time series corresponding to the coincidences of photon pairs is developed from the time series corresponding to the signal and idler, in a way that a count is observed in one arm (within the coincidence window, τ_c = 10 ns), given a detection in the other arm. The number distribution of this new time series corresponds to the statistics of the heralded single photon source from SPDC. Another important factor to be taken care of is the coherence time of the input pump field. If the binning window is considerably larger than the coherence time, the statistics of the photoelectrons will result in a Poissonian distribution independent of the inherent photon statistics.[33] Since we are taking two photon coincidence here, the coherence of the pump will determine the coherence of paired down-converted photons. The pump coherence time is 80 ns, which in turn results in a coherence time of ~80 ns for the biphoton output of the SPDC. The binning window (20 ns) defined for building the coincidence series during postprocessing is much within this two photon coherence time. The MATLAB code to build the statistics from the recorded time series is shared in the GitHub repository for open access.[34]

Twisted single photons of different orders are obtained in SPDC by pumping with optical vortices of different orders and projecting the idler photon in a single mode fiber and hence selecting only those with OAM, $l = 0$. Due to OAM conservation in SPDC, this will result in only those signal photons which have the same OAM as the pump contributing to the coincidence counts.[35] Hence, a photon number distribution obtained for the coincidence events will correspond to the number statistics of single photons carrying OAM.

IV. RESULTS AND DISCUSSION

Initially, to see the photon number distribution for a classical coherent source, we select a coherent laser source (Thorlabs 2 mW HeNe, 632.8 nm). The intensity is attenuated such that the detected photocounts are below the saturation level of the detectors. The time series of events recorded using an oscilloscope was converted into a binary series of photon incidence events. A counting histogram that gives the probability of detection of n events within the corresponding time bin is generated for this time series that shows Poissonian distribution (Fig. 3). For a time bin width such that an average number of less than one photon falls within the bin ($\mu = 0.1$), the variance (σ^2) is determined to be 0.103. The Q-parameter is calculated to be 0.045 ± 0.03 [for net efficiency, $\eta = 0.66$ in Eq. (7)] which is close to a Poissonian distribution of photon numbers.

For the heralded single photon source, the number statistics is built from the binary series of coincidences generated by postprocessing the recorded events of individual signal and idler photons (Fig. 4). For $\mu = 0.1$, the variance (σ^2) for this source is calculated to be 0.0901. The Mandel Q-parameter comes out to be −0.099. The negative value of Q is an indication of the sub-Poissonian behavior of the source. The detectors that are used in the experiments have a quantum efficiency of 0.6 at the spectral region in which the experiment has been undertaken. Along with this, taking the coupling efficiency of the fiber and other losses into account, the net efficiency

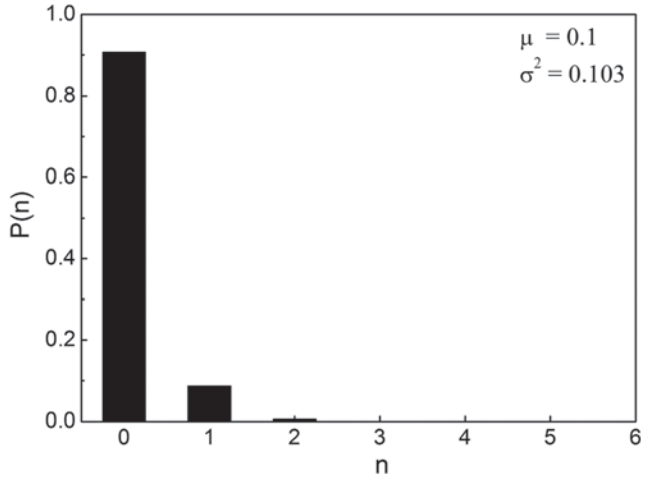

FIG. 3. Detected photon number distribution for a coherent source. Here, n corresponds to the number of detected photons within a binning window, and P(n) is the probability of obtaining n detection events per bin. The mean photon number is approximately equal to the variance.

of detection is determined to be $\eta = 0.3$. Incorporating this value, the Q-parameter for the heralded photon source is determined as −0.33 for the heralded single photons. A set of repeated measurements reveals the average value, $Q = -0.331 \pm 0.004$, for a heralded SPS generated using a Gaussian pump profile. $Q = -1$ implies an ideal single photon source where photons come out in order with a variance that equals to zero in their temporal distribution. Intuitively, Q is expected to be less negative (i.e., reduced nonclassicality) for the case of heralded SPS as the pair generation is a spontaneous process and it would result in a nonzero variance. In addition to this, various losses randomize the detection of a HSPS and hence result in a reduced nonclassicality in measurement. While the intention of this work is not to formulate a rigorous theoretical model for the number statistics of heralded photons, we matched the experimentally observed data with the statistics of a simulated coincidence series. A coincidence series is generated from two correlated time series consisting only 0 and 1 which correspond to the individual idler and signal series. The correlated time series can be generated by randomly distributing 1's in a time series (such that the sum of 1's is matched with the experimentally observed single counts) and duplicating it. The random distribution of 1's replicates the spontaneous nature of the pair generation process. However, the actual scenario would differ from this as losses in the system would individually randomize these series further. After incorporating a loss of $\eta = 0.3$ in each time series separately by randomly erasing 30% of 1's, we build the coincidence series the same way we did during postprocessing of the experimental data 2. For parameters such as efficiency, binning window, coincidence window, total counts, and time series length

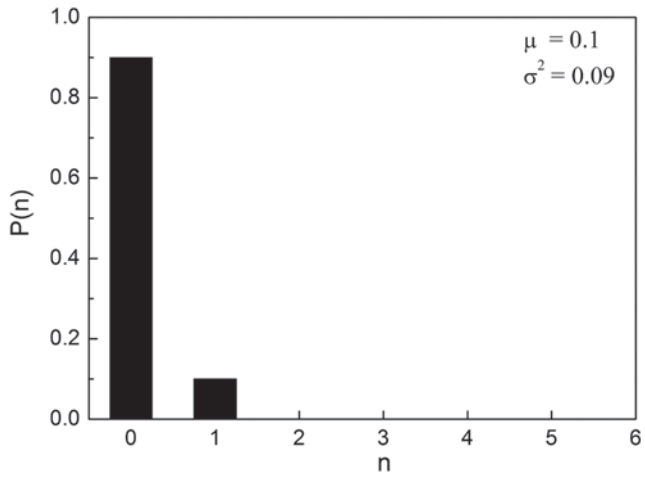

FIG. 4. Detected photon number distribution for a heralded single photon source. Here, n corresponds to the number of coincidence detection within a binning window, and P(n) is the probability of obtaining n coincidence events per bin.

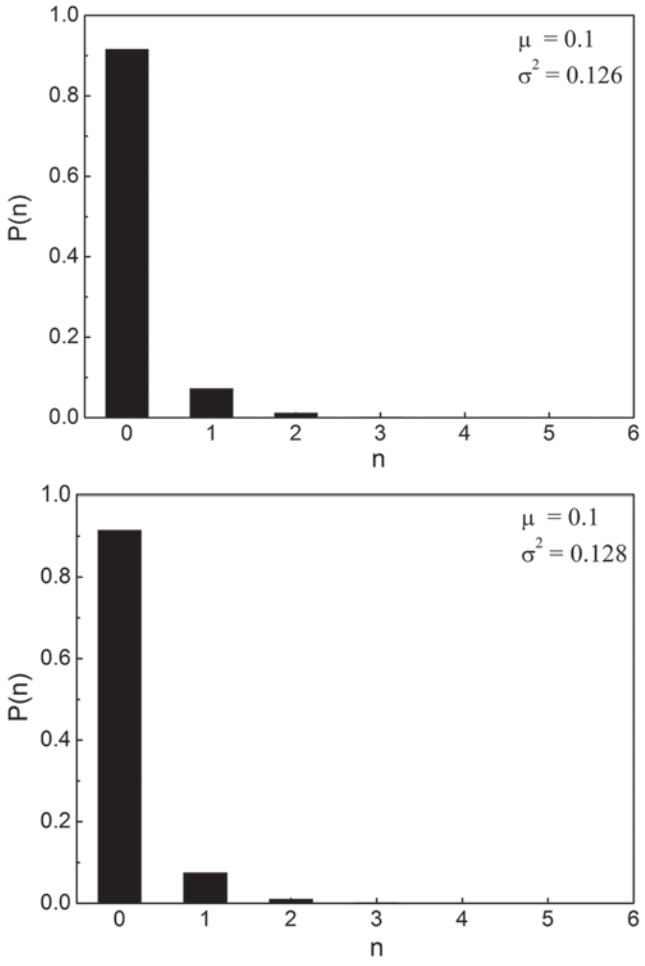

FIG. 5. Detected photon number distribution for thermal photons in the individual idler (top) and signal (bottom) arms of the downconverted pairs. Here, n corresponds to the number of single arm (idler/signal) photons within a binning window, and P(n) is the probability of obtaining n detection events per bin.

matched with the corresponding experimentally observed values, the Q-parameter turns out to be −0.3. Hence, the experimentally observed value of Q for HSPS is reasonable with the predictions from a lossy model for spontaneously generated correlated pairs of photons.

In the same way, photon number histograms are generated for the individual arms of the down-converted pairs of photons (Fig. 5). For an average photon number $\mu = 0.1$, the variances were 0.126 and 0.128, respectively, for the signal and idler arms which are significantly apart from that corresponds to a Poissonian distribution. With $\eta = 0.3$, the Q-parameter is calculated to be 0.87 and 0.93 for the idler and signal arms, respectively, with statistical errors of the order of 10^{-3}. This super-Poissonian behavior is expected since the individual signal and idler photons from the down-conversion process are in a thermal state.[33,36,37] Being thermal in nature, the single arm statistics is expected to be such that $Q = 1$.

The Q-parameter for the heralded single photons having different OAM, obtained by pumping with an optical vortex and projecting the idler arm to $l = 0$, are given in Table I. The time series of photon detection events of 20.5 ms length are recorded using the oscilloscope. 10 such iterations are recorded to determine the Q-parameter within statistical errors. For heralded single photons, it is found to violate the classical bounds of number statistics (i.e., $Q \geq 0$) by ~10 standard deviations for photons carrying different OAM. The Q-parameter is observed to decrease with the increasing order of twisted photon OAM. This can be attributed to the reduction in the number of coincidence events with higher order pump as the singles in the idler arm (with $l = 0$) decrease with pump order. The effects on the probability amplitude of the two photon coincidences and spectral bandwidth when pumped with different Laguerre-Gaussian modes is already discussed in the literature.[38,39]

The background counts due to ambient stray light (<100 cps) has been measured and subtracted from the detected counts. Afterpulsing probability for the detectors that are used is about 0.5% and is negligible. Ringing is taken care of by appropriately terminating the output pulse into a 50 Ω load at the oscilloscope. Triggering from noise signals is also taken care of during postprocessing. This is done by keeping a threshold of 1.0 V while doing the conversion of the time series to binary series since the output TTL levels after BNC couplers are >1.5 V.

TABLE I. Mandel Q-parameter obtained for the photon number distributions of twisted single photons having different orders generated in parametric down conversion.

Twisted photon OAM, l	Q-parameter
0	−0.331 ±0.002
1	−0.336 ±0.003
2	−0.343 ±0.005
3	−0.353 ±0.008

V. CONCLUSIONS

Conventional quantum optics experiments to determine the nonclassical statistical behavior of single photon sources involve time-to-digital converters along with associated postprocessing. Here, we introduce a simple technique to build the number statistics of a heralded single photon source using a digital oscilloscope. The signal and idler in the SPDC output are detected and registered in the oscilloscope. From the recorded data, a time series corresponding to the coincident detection and the corresponding number distribution are obtained. In this way, one can observe the sub-Poissonian behavior of the photon number statistics of the source using a set of detectors and an oscilloscope available in almost all the optics laboratories. We also show that in this way we can determine the number statistics of heralded single photons carrying OAM and thus can characterize them for further applications involving OAM of single photons.

REFERENCES

[1]T. Gaebel, I. Popa, A. Gruber, M. Domhan, F. Jelezko, and J. Wrachtrup, "Stable single-photon source in the near infrared," New J. Phys. **6**, 98 (2004).
[2]A. J. Shields, "Semiconductor quantum light sources," Nat. Photonics **1**, 215–223 (2007).
[3]M. Hennrich, T. Legero, A. Kuhn, and G. Rempe, "Photon statistics of a non-stationary periodically driven single-photon source," New J. Phys. **6**, 86 (2004).
[4]C. Maurer, C. Becher, C. Russo, J. Eschner, and R. Blatt, "A single-photon source based on a single Ca+ ion," New J. Phys. **6**, 94 (2004).
[5]M. Steiner, A. Hartschuh, R. Korlacki, and A. J. Meixner, "Highly efficient, tunable single photon source based on single molecules," Appl. Phys. Lett. **90**, 183122 (2007).
[6]S. Fasel, O. Alibart, S. Tanzilli, P. Baldi, A. Beveratos, N. Gisin, and H. Zbinden, "High-quality asynchronous heralded single-photon source at telecom wavelength," New J. Phys. **6**, 163 (2004).
[7]M. V. Jabir and G. K. Samanta, "Robust, high brightness, degenerate entangled photon source at room temperature," Sci. Rep. **7**, 12613 (2017).
[8]D. Boschi, S. Branca, F. De Martini, L. Hardy, and S. Popescu, "Experimental realization of teleporting an unknown pure quantum state via dual classical and Einstein-Podolsky-Rosen channels," Phys. Rev. Lett. **80**, 1121 (1998).
[9]N. Gisin, G. Ribordy, W. Tittel, and H. Zbinden, "Quantum cryptography," Rev. Mod. Phys. **74**, 145 (2002).
[10]K. Mattle, H. Weinfurter, P. G. Kwiat, and A. Zeilinger, "Dense coding in experimental quantum communication," Phys. Rev. Lett. **76**, 4656 (1996).
[11]R. Short and L. Mandel, "Observation of sub-Poissonian photon statistics," Phys. Rev. Lett. **51**, 384 (1983).
[12]P. Tapster, J. Rarity, and J. Satchell, "Use of parametric down-conversion to generate sub-Poissonian light," Phys. Rev. A **37**, 2963 (1988).
[13]J. Laurat, T. Coudreau, N. Treps, A. Maître, and C. Fabre, "Conditional preparation of a quantum state in the continuous variable regime: Generation of a sub-Poissonian state from twin beams," Phys. Rev. Lett. **91**, 213601 (2003).
[14]J. Peřina, O. Haderka, and V. Michálek, "Sub-Poissonian-light generation by postselection from twin beams," Opt. Express **21**, 19387–19394 (2013).
[15]S. Singh, "Antibunching, sub-Poissonian photon statistics and finite bandwidth effects in resonance fluorescence," Opt. Commun. **44**, 254–258 (1983).
[16]X. Zou and L. Mandel, "Photon-antibunching and sub-Poissonian photon statistics," Phys. Rev. A **41**, 475 (1990).
[17]P. Grangier, G. Roger, and A. Aspect, "Experimental evidence for a photon anticorrelation effect on a beam splitter: A new light on single-photon interferences," Europhys. Lett. **1**, 173 (1986).
[18]A. B. U'Ren, C. Silberhorn, J. L. Ball, K. Banaszek, and I. A. Walmsley, "Characterization of the nonclassical nature of conditionally prepared single photons," Phys. Rev. A **72**, 021802 (2005).

[19]M. Mirhosseini, O. S. Magaña-Loaiza, M. N. O'Sullivan, B. Rodenburg, M. Malik, M. P. Lavery, M. J. Padgett, D. J. Gauthier, and R. W. Boyd, "High-dimensional quantum cryptography with twisted light," New J. Phys. **17**, 033033 (2015).
[20]J. T. Barreiro, T.-C. Wei, and P. G. Kwiat, "Beating the channel capacity limit for linear photonic superdense coding," Nat. Phys. **4**, 282 (2008).
[21]A. Kumar, J. Banerji, and R. Singh, "Intensity correlation properties of high-order optical vortices passing through a rotating ground-glass plate," Opt. Lett. **35**, 3841–3843 (2010).
[22]A. Kumar, J. Banerji, and R. Singh, "Hanbury Brown–Twiss-type experiments with optical vortices and observation of modulated intensity correlation on scattering from rotating ground glass," Phys. Rev. A **86**, 013825 (2012).
[23]N. Lal, A. Banerji, A. Biswas, A. Anwar, and R. P. Singh, "Single photon sources with different spatial modes," e-print arXiv:1905.01089 [quant-ph] (2019).
[24]C. Gerry, P. Knight, and P. L. Knight, *Introductory Quantum Optics* (Cambridge University Press, 2005).
[25]R. J. Glauber, "Coherent and incoherent states of the radiation field," Phys. Rev. **131**, 2766 (1963).
[26]L. Mandel and E. Wolf, *Optical Coherence and Quantum Optics* (Cambridge University Press, 1995).
[27]L. Mandel, "Sub-Poissonian photon statistics in resonance fluorescence," Opt. Lett. **4**, 205–207 (1979).
[28]M. Lamperti, A. Allevi, M. Bondani, R. Machulka, V. Michálek, O. Haderka, and J. Peřina, "Optimal sub-Poissonian light generation from twin beams by photon-number resolving detectors," J. Opt. Soc. Am. B **31**, 20–25 (2014).
[29]N. Lal, B. Shajilal, A. Anwar, C. Perumangatt, and R. Singh, "Observing sub-Poissonian statistics of heralded single photons using an oscilloscope," in *International Conference on Fibre Optics and Photonics* (Optical Society of America, 2016), p. Th3A.72.
[30]B. I. Cantor and M. C. Teich, "Dead-time-corrected photocounting distributions for laser radiation," J. Opt. Soc. Am. **65**, 786–791 (1975).
[31]E. Jakeman and J. H. Jefferson, "Antibunching and sub-Poissonian statistics in photoelectron-triggered optical dead-time experiments," Opt. Acta **33**, 557–576 (1986).
[32]M. Razavi, I. Söllner, E. Bocquillon, C. Couteau, R. Laflamme, and G. Weihs, "Characterizing heralded single-photon sources with imperfect measurement devices," J. Phys. B: At., Mol. Opt. Phys. **42**, 114013 (2009).
[33]B. Blauensteiner, I. Herbauts, S. Bettelli, A. Poppe, and H. Hübel, "Photon bunching in parametric down-conversion with continuous-wave excitation," Phys. Rev. A **79**, 063846 (2009).
[34]The source code is available via https://github.com/njlal/Photon_stat-Oscilloscope (MATLAB).
[35]A. Mair, A. Vaziri, G. Weihs, and A. Zeilinger, "Entanglement of the orbital angular momentum states of photons," Nature **412**, 313 (2001).
[36]X. Guo, C.-l. Zou, C. Schuck, H. Jung, R. Cheng, and H. X. Tang, "Parametric down-conversion photon-pair source on a nanophotonic chip," Light Sci. Appl. **6**, e16249 (2017).
[37]M. Avenhaus, H. B. Coldenstrodt-Ronge, K. Laiho, W. Mauerer, I. A. Walmsley, and C. Silberhorn, "Photon number statistics of multimode parametric down-conversion," Phys. Rev. Lett. **101**, 053601 (2008).
[38]A. M. Yao, "Angular momentum decomposition of entangled photons with an arbitrary pump," New J. Phys. **13**, 053048 (2011).
[39]A. Banerji, A. Anwar, H. Sable, N. Lal, and R. P. Singh, "Engineering of orbital angular momentum spectrum of down-converted photons with mode-invariant pump," e-print arXiv:1905.02554 [quant-ph] (2019).